6-8-2017

Gold Nanoparticles and Quantum Dots: Their Optical Interaction and Application in A Hydrogel Modified Lateral Flow Sensing Device

Julie A. Jenkins
University of Connecticut - Storrs, julie.jenkins@uconn.edu

Gold Nanoparticles and Quantum Dots: Their Optical Interaction and Application in A Hydrogel Modified Lateral Flow Sensing Device

Julie Ann Jenkins, Ph.D.

University of Connecticut, 2017

The goal of this dissertation was to study the optical properties of gold nanoparticles (Au NP) and quantum dots (QD) and to use their unique properties in sensing applications. The first part of this dissertation focuses on studying the dipole coupling in a gold nanoparticle random array. A blue shift and narrowing of the extinction peak, when compared to the single particle and solution spectra, was observed when 120 nm Au NPs were randomly immobilized on a glass substrate. This was determined to be due to the long-range dipole coupling of the Au NPs in the array. The motivation behind the second project was to study the temperature dependent change in decay kinetics of aqueous phase quantum dots when in close proximity to 120 nm Au NP, using α-carboxy-ω-Thiol terminated Poly(N-isopropyl acrylamide) (PNIPAM) as a spacer. The structure of PNIPAM will expand or collapse based with a change in temperature, thus varying the interparticle distance between the QD and the Au NP. The temperature dependent decay kinetics of the system is studied by taking the fluorescence lifetime decay of the QD – PNIPAM – Au NP nanocomplex at different temperatures. The purpose of the third and final project was to develop of a novel lateral flow assay platform. In this work, Au NPs and QDs are captured by modifying the nitrocellulose membrane with a polymer hydrogel instead of using pre-printed biological probes. This unique modification of current lateral flow strips provides an alternate method of capturing the nanoparticle probes and introduces many possibilities to enhance the design of conventional lateral flow devices.

Gold Nanoparticles and Quantum Dots: Their Optical Interaction and Application in A Hydrogel Modified Lateral Flow Sensing Device

Julie Ann Jenkins

B.A., Augsburg College, 2009

A Dissertation

Submitted in Partial Fulfillment of the

Requirements for the Degree of

Doctor of Philosophy

at the

University of Connecticut

2017

APPROVAL PAGE

Doctor of Philosophy Dissertation

Gold Nanoparticles and Quantum Dots: Their Optical Interaction and Application in A Hydrogel Modified Lateral Flow Sensing Device

Presented by

Julie Ann Jenkins, B.A.

Major Advisor

_____

Dr. Jing Zhao

Associate Advisor

_____

Dr. Steven L. Suib

Associate Advisor

_____

Dr. Jessica L. Rouge

University of Connecticut

2017

Dedicated To

My parents, Mr. and Mrs. Jed and Cynthia Jenkins

Acknowledgments

There are so many people that have guided me to this point and for whom I am forever grateful. I would like to start off by thanking my research advisor, Dr. Jing Zhao, for her knowledge, understanding and support of everything I do, and for taking a chance on me as one of her first graduate students. I have thoroughly enjoyed every conversation we've had – whether it be about chemistry or life. Thank you for believing in me and sticking with me until the end. I am also grateful to Dr. Steve Suib for his guidance and wisdom, and for always siding with me in the "Great Jenkins-Dietz Debate." Since I first arrived at UCONN, he has helped instill in me a confidence that I will carry with me the rest of my life. I am equally appreciative to Dr. Jessica Rouge for always having an open door, and for all the valuable discussions we've had. I am thankful for Dr. Rebecca Quardokus for being on my committee and for always having a smile on her face. It makes graduate school less scary. I would also like thank Dr. Yu Lei for his guidance and patience through our collaboration. My sincerest gratitude to Dr. Edward Neth - for not only passing on his love of teaching, and for mentoring me during my time at UCONN, but for also helping me with every technical issue that came my way. I have yet to throw my laptop out a window because of him, and my bank account is thankful!

I want to thank all my friends and family for their encouragement and support during this journey. My sincerest thanks to Dr. Swayandipta Dey and Dr. Sravan Thota who took the leap with me into a new lab. Their endless assistance and our daily conversations are priceless. I would like to thank my roommate Kelli Rutledge for her friendship, support, and most importantly, for putting up with me for 4 years! Thank you, Dr. Jenn Satterwhite-Warden and Nicole Sassu, for making my time in Connecticut unforgettable and for always making me feel young. To all the rest of my friends and co-workers at UCONN, thank you for making this an

incredible experience and for teaching me how to be a New Englander! Thank you to my CT volleyball family, especially Megan Droesch, for not only being an amazing friend, but for working with my schedule so I was able to coach and get an education at the same time. I am grateful to Alain and Lynn Veilleux for being my east coast parents and for always being there for me, picking me up from the airport and for making sure I was always fed. A special shout out to my girls, who have always had my back and been there to lift me up when I fall. I could not do life without you and I love you all to pieces. I want to thank Dr. Vivian Feng from Augsburg for instilling in me a love of analytical chemistry. I am also appreciative of my SarTec family for their encouragement, understanding, and patience while I pursued this dream.

A special thank you goes to my little brother and sister, Jed and Jamie, and my sister-in-law Anne, for always being there for me, and for pushing me to be my best. You know I have the utmost respect for each of you, and am so proud of everything you have accomplished – but I now have back my throne as the highest degree holder! To my nephew, Harrison, and niece, Adeline, who have brought so much joy to my life: I want to thank you for always making me laugh. They have made these five years away from Minnesota bearable. An appreciation that words cannot describe goes to my parents, Jed and Cynthia Jenkins. Thank you for always believing in me, teaching me to never give up, and for showing me that I can do whatever I set my mind to. I promise to pay off my "tab" eventually, but there's no way I could ever fully repay you for everything you've done for me. I love you! Finally, my thanks and praise to God who has blessed me tremendously.

Table of Contents

List of Figures

List of Schemes

List of Tables

Chapter One :

Introduction

1.1 Part One: Optical Interactions of Gold Nanoparticles and Quantum Dots

1.1.1 Background and Significance

Nanomaterials have been investigated over the past few decades due their many unique features which are not observed on the bulk scale. The properties of these materials are highly dependent on their size, shape, surface area, porosity, structure, and are also heavily influenced by the environment surrounding the nanoparticle - including refractive index of the solvent, ligands, and their proximity to other nanoparticles. A change in any of these factors can alter the properties of the nanomaterials.

1.1.2 Gold Nanoparticles

Gold nanoparticle colloids (Au NP) have been used for centuries, dating as far back as the 4th or 5th century.[1] They were used for aesthetic purposes, and for coloring ceramics. The Roman Lycurgus Cup, which shows a green color in reflected light, and a ruby red color in transmitted light is one of the oldest and most famous examples of Au NP use in those early years.[2] Up until the Middle Ages, it was also believed that Au NPs held curative powers for diseases such as dysentery, epilepsy, and heart and venereal issues.[1, 3] The most common medical use of Au colloids through the Middle Ages was for the diagnosis of syphilis, which continued to be used until the 20th century. Today, Au NPs are still one of the most common probes used in diagnostic applications and continue to be investigated due to their fascinating features.

In addition to diagnostics, Au NPs have been utilized more recently in a variety of applications, largely driven by their unique plasmonic features,[4-6] which differ from those at the bulk scale. When the Au nanoparticles are excited by light of proper frequencies, the free electrons in the nanoparticle oscillate in unison, giving rise to the phenomenon of localized surface plasmon resonance (LSPR) as shown in **Figure 1.1A**. LSPR results in wavelength-dependent absorption, and scattering of photons by noble metal nanoparticles (**Figure 1.1B)** as well as greatly amplified electromagnetic field localized around the nanoparticles.[7-8] The LSPR peak wavelength (λ_{max}) is determined by the size, shape, composition of the nanoparticles, and also the dielectric environment around them.[7-13] Due to these phenomena, plasmonic nanostructures have been used in many applications such as plasmonic waveguides,[14-17] photovoltaic,[18-23] bio- or chemo-sensors,[7-8, 24-29] and surface-enhanced spectroscopies.[30-37]

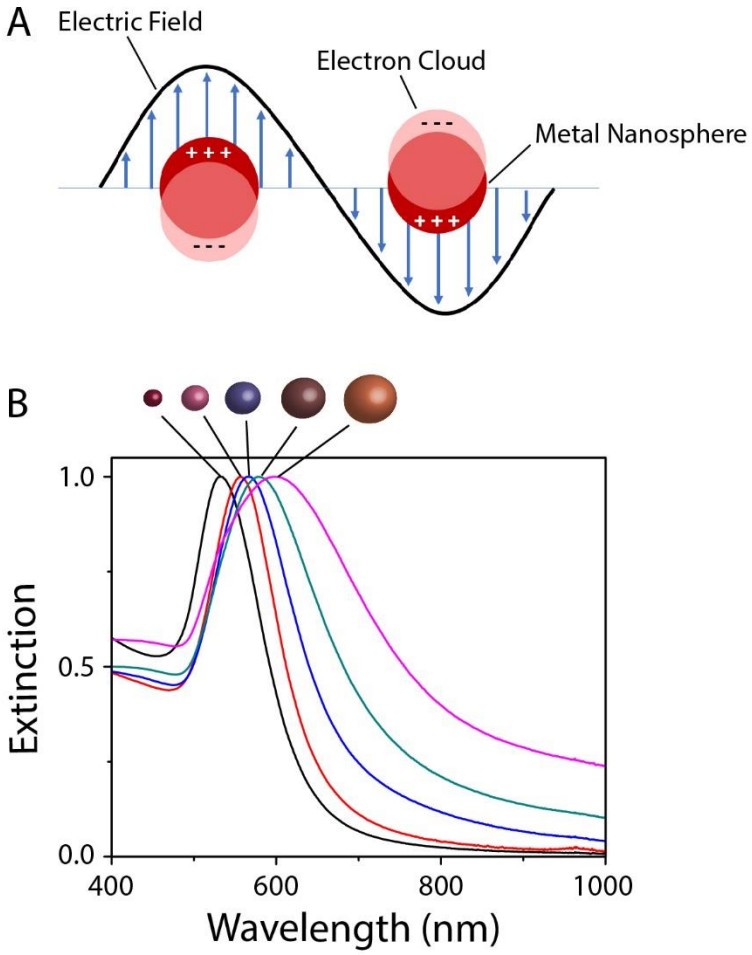

Figure 1.1. Localized surface plasmon resonance. (A) Scheme illustrating a localized surface plasmon (B) Wavelength dependent extinction of different sized gold nanoparticles. As the Au NPs increase in size, their color changes, and their LSPR peak wavelength max red shifts.

Various methods exist to synthesize gold nanoparticles.[38-40] One of the most common and simplest syntheses is the Frens' method[41], which was originally introduced by Turkevich.[42] This method uses sodium citrate to reduce a gold salt ($HAuCl_4$) in water where citrate acts as both the reducing and stabilizing (or capping) agent. Frens' modified Turkevich's method by introducing a way to control the size of the Au NPs by adjusting the trisodium citrate to gold ratio. As the ratio increases, the particle diameter will become smaller.[43-44] At low citrate concentrations, the particle

size distribution becomes larger and the results are less reproducible. Therefore, in order to achieve larger (>100 nm), more homogenous Au NPs, a seed mediated method is preferred. With seed mediated methods, a nanoparticle seed is prepared first. In the second step, more precursors are added to the seed solution, growing the seeds to a larger size. A seed-mediated synthesis provides greater control over the particle size, and also allows the creation of more versatile nanomaterials, such as core/shell and bimetallic nanoparticles.[45-47] The addition of hydroxylamine hydrochloride to colloidal gold is known to aid in the growth of the nanoparticles.[42, 47] In the synthetic procedure described in detail by Li et al., spherical gold nanoparticles of larger sizes (>120 nm) can be synthesized.[48]

1.1.3 Gold Nanoparticle Assembled Structures

Research advances over the past couple decades has led to many methods to synthesize noble metal nanoparticles and to fabricate patterned nanostructures as LSPR substrates. These efforts in developing patterned or assembled nanostructures have been promoted to tune the plasmonic interactions.[49-56]

1.1.3.1 Gold Nanoparticle Ordered Arrays

A widely-used method to create metal nanoparticle arrays includes lithographic nanopatterning followed by vacuum deposition of noble metals.[49, 57-60] Highly ordered nanostructures with well-controlled nanoparticle geometry and interparticle spacing can be developed using this method. The LSPR max peak wavelength of the nanoparticle arrays can be adjusted by simply changing the interparticle distance or shape of the particles. These highly ordered patterns with flexibility in the pattern design and narrow resonance peaks are a major

advantage to using lithography techniques,[61-63] but they are usually expensive and instrumentation heavy, therefore, not widely applicable.

1.1.3.2 Gold Nanoparticle Random Arrays

Another common method to produce LSPR substrate is self-assembly of colloidal nanoparticles on pretreated solid support such as glass. One common technique is self-assembled monolayer (SAM) which produces a monolayer or sub-monolayer of nanoparticles on the substrate.[64-69] The self-assembly method is simple, more cost effective, and broadly applicable when compared to lithographic techniques. The downfall of the self-assembly method is that it yields LSPR substrates with randomly distributed nanoparticles; therefore, they often have broad LSPR bands.

1.1.4 Quantum Dots

Quantum dots (QD) are another group of nanomaterials that have received much attention in recent years due to their unique optical and electronic properties. QDs are light-emitting semi-conductor nanomaterials that typically range between 2 – 10 nm in size. They have a broad absorption and very narrow, size-tunable emission spectra (**Figure 1.2**).[70-71] Smaller QDs exhibit larger band gaps and therefore have a higher energy emission. As a QD grows in size, the band gap decreases, red shifting its emission peak wavelength. The broad absorption and large stoke shifts of QDs also allow varying sizes of QDs to be excited by one wavelength of light that is far away from their emission peaks. These size tunable emission bands, coupled with a broad absorption are what make quantum dots so appealing in comparison to dyes.[72]

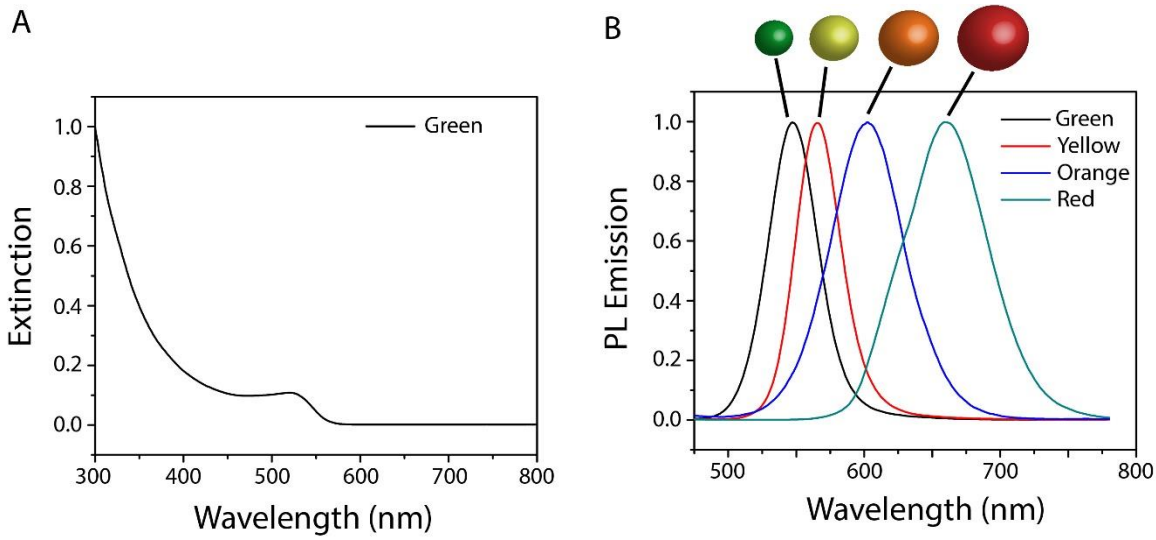

Figure 1.2. Broad absorption and narrow size-tunable emission of quantum dots. (A) Extinction spectrum of aqueous phase green quantum dots. (B) PL emission spectra of different sized QDs. The emission peak wavelength red shifts as the quantum dot size gets bigger.

In comparison to organic dyes or fluorescent proteins commonly used in sensing applications, QDs are also brighter and have higher stability against photo-bleaching.[71] They can exhibit high fluorescent quantum yield, and have large molar extinction coefficients which makes them beneficial for bioimaging and biosensing applications.[70-71, 73] Their high stability against photo- and chemical degradation, the ability to target a specific biomolecule via labelling the QD and their potential for water solubility, make them ideal candidates for use as probes in deep-tissue imaging, assay labelling, cellular labelling and as donors in fluorescence resonance energy transfer (FRET).

1.1.5 Förster Resonance Energy Transfer Between Gold Nanoparticles and Quantum Dots

The effect on the extinction of Au NP random arrays due to their dipole interactions has been discussed, but Au NPs also have the capability of interacting with the dipoles of other

nanomaterials. One way is by a non-radiative energy transfer process called Förster Resonance Energy Transfer (FRET)[74]. This process is driven by dipole-dipole interactions between an excited donor and a lower energy acceptor. QDs are fluorophores that once excited by a higher energy photon, can emit a lower energy photon in a radiative relaxation process. When in close proximity to an Au NP, an excited QD has the opportunity to transfer its energy non-radiatively to the Au NP. Two factors that will determine how efficiently this transfer process occurs are (1) the distance between the two particles and (2) the degree of spectral overlap between the photoluminescence (PL) of the donor and the absorption of the acceptor. In the case of QDs and Au NPs, the efficiency of energy transfer can be studied experimentally by monitoring changes in either the fluorescence intensity, or fluorescent lifetime of the QD, both of which will decrease when FRET is occurring[74]. There have been many attempts at controlling the distance between the donor and acceptor. Some of these studies use polymer or silica coatings around the nanoparticle[75-77], as well as DNA or other biological linkers[75, 78-82]. FRET has played a major role in biosensing applications. This technique can be used to image and measure changes in nucleic acid hybridization, enzyme activity, protein conformations and to monitor environmental changes, such as pH and temperature.[83]

1.2 Part Two: The Application of Nanoparticles in a Hydrogel Modified Lateral Flow Sensing Device

1.2.1 Background and Significance

Diagnosis and detection have become vital components of various industries including healthcare and agriculture.[84] In the healthcare field, proper diagnosis is important to eliminate illness and death due to improper treatment of a disease.[84] Rapid and sensitive diagnosis techniques are needed to properly care for, and treat a patient.[85] Point-of-care (POC) devices have become

common diagnostic tools due to their ease of use and low cost. POC devices can be used outside the laboratory, like in a hospital or even for personal use in one's own home.[86] These devices are cheaper than other detection methods because there is no need for expensive equipment and trained personnel for operation of the device[87].

1.2.2 Lateral Flow Assays

Lateral flow assays (LFA) are an example of a POC device.[86, 88] They have gained popularity in the field due to the simplicity of design, rapidity, portability and low cost, and are used to detect a large range of analytes. These targets could include anything from infectious disease and cancer biomarkers, to bio-toxins.[70, 85, 88-90] The most common LFA is the pregnancy stick, which detects the presence of human chorionic gonadotropin (hCG) in urine.[91] The LFA technique integrates two common detection techniques; chromatography and immunoassays.[86, 90] High performance liquid chromatography (HPLC) and gas chromatography (GS) are often used as separation methods for detection applications. These methods are highly selective and sensitive but they can be time consuming and laborious. They also require expensive equipment which is often unaffordable to those in third world countries, or certain industries like farming.[88] Thin-layer chromatography counteracts these negative aspects by being rather inexpensive and fast, but it suffers from high standard deviation of results.[92] Therefore, other detection techniques are needed for POC applications. A common immunoassay similar to LFAs is enzyme-linked immunosorbent assay (ELISA).[86] ELISA incorporates a sandwich assay protocol, and uses a color change for detection. ELISA requires washing steps, and can therefore be long and laborious testing procedure. In LFAs, a polymeric-based membrane pulls a liquid sample along the strip. The material in the sample passes various zones where molecules have been attached on the membrane that exhibit either more or less of an interaction with certain materials in the liquid sample[86]. A

scheme for the setup of a typical sandwich type LFA is shown in **Figure 1.3**. LFAs combine the benefits of both chromatography and immunoassays to create a rapid, inexpensive, and portable detection technique.

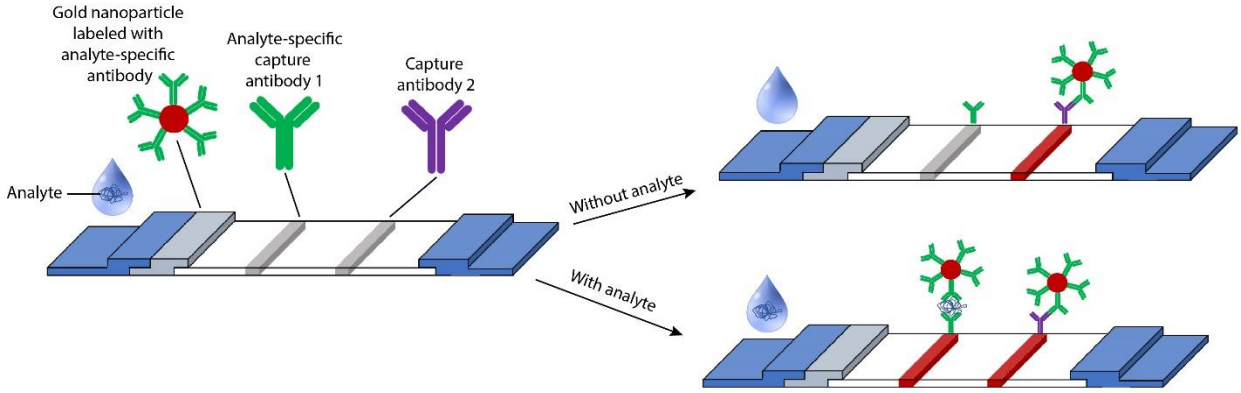

Figure 1.3. Scheme for a sandwich-type lateral flow assay. The gold nanoparticle detection probe is labeled with analyte specific antibodies. Pre-printed capture antibodies are placed at the test and control line. The antibody on the test line is specific to the analyte, and the antibody at the control line is specific for the antibody labeled on the detection probe. Without the analyte present, the gold nanoparticle is captured by the antibody on the control line, but not the one at the test line, forming one colored line. With the analyte present, the gold nanoparticle will be captured at both the test and control line forming two colored lines. Therefore, a positive result will have two lines, and a negative result will only have one.

1.2.3 Advantages and Disadvantages of Lateral Flow Assays

Lateral flow assays offer many advantages over current detection methods. LFA is a rapid, inexpensive, and easy to use technique for point-of-care diagnostics.[70, 84, 88, 90] They have an established technology where development of new devices can be brought to market fairly quickly due to their ease of design and manufacture.[87] This technique relies on detection by the naked eye

and thus does not need trained professionals to operate the device. They also use dry reagents, which do not need refrigeration and therefore have a longer shelf life than other solution based detection methods (~12-24 months).[87] This can be advantageous in third world countries where cheap devices with long shelf lives are needed for biomedical purposes.[86]

In addition to their advantages, LFA's have some disadvantages. Currently, commercial devices only provide a qualitative result (yes/no or positive/negative) or semi-quantitative results of the concentration of an analyte using a strip reader[70]. In order to visually detect the analyte, a high concentration of the colored nanoparticle is needed. Since biological probes are used to capture the nanoparticles, the device needs to allow for optimal reaction time between the probe and the analyte. This often leads to inefficient capture of labels at the test line, therefore LFA devices regularly exhibit low sensitivity.[70, 90] There are ways to increase the sensitivity of the technique, but many require additional instrumentation, sample pretreatment, or complex label design and are often cumbersome to use. A common way to improve sensitivity is by using a strip reader, or CCD camera to analyze results.[70, 93] These devices can aid in detection by taking an image of the strip and analyzing the intensity of the color, but fully quantitative results are still difficult to achieve due to the depth of the nitrocellulose membrane. Many gold nanoparticles are captured below the surface of the membrane and are not seen by the strip reader. Other ways to improve sensitivity are by enhancing the signal intensity, allowing for improved visual results[70]. These could include anything from dual nanoparticle probes[94], to enzyme enhanced particle labels.[95] Although these methods are successful in increasing sensitivity, they can increase cost by the addition of instrumentation and render the strip more complex.

The long-term goal of this project is to increase sensitivity and lower the cost of LFAs by eliminating the need for pre-printed biological probes on the nitrocellulose membrane. As an alternative, the detection probes will be captured by modifying the strip with a polymer hydrogel.

1.2.4 Polymer Hydrogels

A hydrogel is a polymer network that is formed by cross-linking one or more monomers where the polymer exists as a colloidal gel in a water-swollen state. They are also referred to as hydrophilic gels where the backbone is a polymeric chain with hydrophilic functional groups. The hydrophilicity of the functional groups, combined with the crosslinking of monomers forms a structure that retains a lot of water, but does not dissolve in it. Hydrogels have been used in many applications such as tissue engineering, separation of biomolecules, drug delivery, food additives, agriculture, pharmaceuticals, beauty products, and biosensors.[96] Polyacrylamide and agarose are two hydrogels that are often used in gel electrophoresis[97], affinity chromatography and ion-exchange chromatography due to their ability to maintain good flow after coupling, their ability to tolerate extreme pH and ionic strength conditions, and most importantly because they show minimal adsorption of molecules.[98]

When a hydrogel is added to the membrane of the lateral flow assay strip, we expect a size-selective capture of the nanoparticle probes. We believe the porosity and polymer structure of the hydrogel, as well as the specific hydrogel used all play an important role in the capture of the nanoparticles. This technique will revolutionize the way lateral flow assays are developed.

1.2.5 Overview of Dissertation

The goal of this dissertation was to study the optical properties of gold nanoparticles and quantum dots and to use their unique properties in sensing applications. The effects of a dielectric

environment change on the plasmonic properties of gold nanoparticles, as well as how gold nanoparticles can affect the optical properties of other nanomaterials, like quantum dots was studied. The distance between particles was observed to be a very important factor. The knowledge gained from that work was used to create a novel paper based sensing device using nanoparticles as optical detection probes.

Chapter one focuses on introducing the background, significance and important aspects of the work completed in this dissertation. The information presented allows for a basic understanding of the concepts behind the work and sets a concrete foundation for the comprehension of optical interactions between nanoparticles and how these properties can be used in sensing applications.

Chapter two focuses on the optical interactions of gold nanoparticles in a random array. A surprising blue shift and narrowing of the extinction peak was observed when 120 nm Au NPs were randomly immobilized on a glass substrate. This work focuses on the reasoning behind the observed blue shift, and looks into the effects of long range dipole coupling on these random arrays.

Chapter three focuses on studying the temperature dependent change in decay dynamics of aqueous phase quantum dots when in close proximity to 120 nm Au NP, using α-carboxy-ω-Thiol terminated Poly(N-isopropyl acrylamide) (PNIPAM) as a spacer. The structure of PNIPAM is affected by a temperature change, thus varying the interparticle distance between the QD and the Au NP. This process is monitored by comparing the fluorescence lifetime decay of the QD – PNIPAM – Au NP nanocomplex at different temperatures.

Chapter four focuses on the development of a novel lateral flow assay platform. This work provides an alternate method of capturing the detection probes by modifying the nitrocellulose

membrane with a polymer hydrogel. The hydrogel captures the nanoparticles on the strip instead of using pre-printed biological probes.

1.3 References

1. Daniel, M.-C.; Astruc, D., Gold Nanoparticles: Assembly, Supramolecular Chemistry, Quantum-Size-Related Properties, and Applications toward Biology, Catalysis, and Nanotechnology. *Chem. Rev.* **2004,** *104* (1), 293-346.
2. Freestone, I.; Meeks, N.; Sax, M.; Higgitt, C., The Lycurgus Cup—a Roman Nanotechnology. *Gold bulletin* **2007,** *40* (4), 270-277.
3. Antonii, F., Panacea Aurea-Auro Potabile. *Hamburg: Ex Bibliopolio Frobeniano 1618*, 250.
4. Bai, J.; Flowers, K.; Benegal, S.; Calizo, M.; Patel, V.; Bishnoi, S. W., Using the Enzymatic Growth of Nanoparticles to Create a Biosensor. An Undergraduate Quantitative Analysis Experiment. *J. Chem. Educ.* **2009,** *86* (6), 712.
5. Choi, H.; Chen, Y.-S.; Stamplecoskie, K. G.; Kamat, P. V., Boosting the Photovoltage of Dye-Sensitized Solar Cells with Thiolated Gold Nanoclusters. *J. Phys. Chem. Lett.* **2014,** *6* (1), 217-223.
6. Yang, X.; Yang, M.; Pang, B.; Vara, M.; Xia, Y., Gold Nanomaterials at Work in Biomedicine. *Chem. Rev.* **2015,** *115* (19), 10410-10488.
7. Mayer, K. M.; Hafner, J. H., Localized Surface Plasmon Resonance Sensors. *Chem. Rev.* **2011,** *111* (6), 3828-57.
8. Willets, K. A.; Van Duyne, R. P., Localized Surface Plasmon Resonance Spectroscopy and Sensing. *Annu. Rev. Phys. Chem.* **2007,** *58*, 267-97.
9. Henry, A.-I.; Bingham, J. M.; Ringe, E.; Marks, L. D.; Schatz, G. C.; Van Duyne, R. P., Correlated Structure and Optical Property Studies of Plasmonic Nanoparticles. *J. Phys. Chem. C* **2011,** *115* (19), 9291-9305.
10. McMahon, J. M.; Wang, Y.; Sherry, L. J.; Van Duyne, R. P.; Marks, L. D.; Gray, S. K.; Schatz, G. C., Correlating the Structure, Optical Spectra, and Electrodynamics of Single Silver Nanocubes. *J. Phys. Chem. C* **2009,** *113* (7), 2731-2735.
11. Brust, M.; Kiely, C. J., Some Recent Advances in Nanostructure Preparation from Gold and Silver Particles: A Short Topical Review. *Colloids and Surfaces A: Physicochemical and Engineering Aspects* **2002,** *202* (2), 175-186.
12. Willets, K. A.; Van Duyne, R. P., Localized Surface Plasmon Resonance Spectroscopy and Sensing. *Annu. Rev. Phys. Chem.* **2007,** *58*, 267-297.
13. Mayer, K. M.; Hafner, J. H., Localized Surface Plasmon Resonance Sensors. *Chem. Rev.* **2011,** *111* (6), 3828-3857.
14. Maier, S. A.; Kik, P. G.; Atwater, H. A., Observation of Coupled Plasmon-Polariton Modes in Au Nanoparticle Chain Waveguides of Different Lengths: Estimation of Waveguide Loss. *Appl. Phys. Lett.* **2002,** *81* (9), 1714-1716.
15. Zhang, J.; Cai, L. K.; Bai, W. L.; Xu, Y.; Song, G. F., Hybrid Plasmonic Waveguide with Gain Medium for Lossless Propagation with Nanoscale Confinement. *Opt Lett* **2011,** *36* (12), 2312-2314.
16. Oulton, R. F.; Sorger, V. J.; Genov, D. A.; Pile, D. F. P.; Zhang, X., A Hybrid Plasmonic Waveguide for Subwavelength Confinement and Long-Range Propagation. *Nat. Photonics* **2008,** *2* (8), 496-500.
17. Sun, M. T.; Hou, Y. X.; Li, Z. P.; Liu, L. W.; Xu, H. X., Remote Excitation Polarization-Dependent Surface Photochemical Reaction by Plasmonic Waveguide. *Plasmonics* **2011,** *6* (4), 681-687.

18. Choi, H.; Chen, W. T.; Kamat, P. V., Know Thy Nano Neighbor. Plasmonic Versus Electron Charging Effects of Metal Nanoparticles in Dye-Sensitized Solar Cells. *ACS Nano* **2012,** *6* (5), 4418-4427.
19. Spinelli, P.; Ferry, V. E.; van de Groep, J.; van Lare, M.; Verschuuren, M. A.; Schropp, R. E. I.; Atwater, H. A.; Polman, A., Plasmonic Light Trapping in Thin-Film Si Solar Cells. *J Optics-Uk* **2012,** *14* (2), 024002.
20. Munday, J. N.; Atwater, H. A., Large Integrated Absorption Enhancement in Plasmonic Solar Cells by Combining Metallic Gratings and Antireflection Coatings. *Nano Lett.* **2011,** *11* (6), 2195-2201.
21. Ferry, V. E.; Sweatlock, L. A.; Pacifici, D.; Atwater, H. A., Plasmonic Nanostructure Design for Efficient Light Coupling into Solar Cells. *Nano Lett.* **2008,** *8* (12), 4391-4397.
22. Mubeen, S.; Lee, J.; Lee, W. R.; Singh, N.; Stucky, G. D.; Moskovits, M., On the Plasmonic Photovoltaic. *ACS Nano* **2014,** *8* (6), 6066-6073.
23. Paci, B.; Bailo, D.; Albertini, V. R.; Wright, J.; Ferrero, C.; Spyropoulos, G. D.; Stratakis, E.; Kymakis, E., Spatially-Resolved in-Situ Structural Study of Organic Electronic Devices with Nanoscale Resolution: The Plasmonic Photovoltaic Case Study. *Adv. Mater.* **2013,** *25* (34), 4760-4765.
24. Bingham, J. M.; Anker, J. N.; Kreno, L. E.; Van Duyne, R. P., Gas Sensing with High-Resolution Localized Surface Plasmon Resonance Spectroscopy. *J. Am. Chem. Soc.* **2010,** *132* (49), 17358-17359.
25. Kreno, L. E.; Hupp, J. T.; Van Duyne, R. P., Metal-Organic Framework Thin Film for Enhanced Localized Surface Plasmon Resonance Gas Sensing. *Anal. Chem.* **2010,** *82* (19), 8042-8046.
26. Bendikov, T. A.; Rabinkov, A.; Karakouz, T.; Vaskevich, A.; Rubinstein, I., Biological Sensing and Interface Design in Gold Island Film Based Localized Plasmon Transducers. *Anal. Chem.* **2008,** *80* (19), 7487-7498.
27. Zhao, J.; Das, A.; Schatz, G. C.; Sligar, S. G.; Van Duyne, R. P., Resonance Localized Surface Plasmon Spectroscopy: Sensing Substrate and Inhibitor Binding to Cytochrome P450. *J. Phys. Chem. C* **2008,** *112* (34), 13084-13088.
28. Larsson, E. M.; Alegret, J.; Kall, M.; Sutherland, D. S., Sensing Characteristics of Nir Localized Surface Plasmon Resonances in Gold Nanorings for Application as Ultrasensitive Biosensors. *Nano Lett.* **2007,** *7* (5), 1256-1263.
29. Anker, J. N.; Hall, W. P.; Lyandres, O.; Shah, N. C.; Zhao, J.; Van Duyne, R. P., Biosensing with Plasmonic Nanosensors. *Nat. Mater.* **2008,** *7* (6), 442-453.
30. Aslan, K.; Lakowicz, J. R.; Geddes, C. D., Rapid Deposition of Triangular Silver Nanoplates on Planar Surfaces: Application to Metal-Enhanced Fluorescence. *J. Phys. Chem. B* **2005,** *109* (13), 6247-6251.
31. Brown, L. V.; Zhao, K.; King, N.; Sobhani, H.; Nordlander, P.; Halas, N. J., Surface-Enhanced Infrared Absorption Using Individual Cross Antennas Tailored to Chemical Moieties. *J. Am. Chem. Soc.* **2013,** *135* (9), 3688-3695.
32. Geddes, C. D.; Cao, H.; Gryczynski, I.; Gryczynski, Z.; Fang, J. Y.; Lakowicz, J. R., Metal-Enhanced Fluorescence (Mef) Due to Silver Colloids on a Planar Surface: Potential Applications of Indocyanine Green to in Vivo Imaging. *J. Phys. Chem. A* **2003,** *107* (18), 3443-3449.

33. Jeanmaire, D. L.; Van Duyne, R. P., Surface Raman Spectroelectrochemistry: Part I. Heterocyclic, Aromatic, and Aliphatic Amines Adsorbed on the Anodized Silver Electrode. *J. Electroanal. Chem. Interfac.* **1977,** *84* (1), 1-20.
34. Moskovits, M., Surface-Enhanced Spectroscopy. *Rev. Mod. Phys.* **1985,** *57* (3), 783-826.
35. Tian, X.-D.; Liu, B.-J.; Li, J.-F.; Yang, Z.-L.; Ren, B.; Tian, Z.-Q., Shiners and Plasmonic Properties of Au Core Sio2shell Nanoparticles with Optimal Core Size and Shell Thickness. *J Raman Spectrosc* **2013,** *44* (7), 994-998.
36. Tian, Z. Q., Surface-Enhanced Raman Spectroscopy: Advancements and Applications. *J Raman Spectrosc* **2005,** *36* (6-7), 466-470.
37. Ataka, K.; Giess, F.; Knoll, W.; Naumann, R.; Haber-Pohlmeier, S.; Richter, B.; Heberle, J., Oriented Attachment and Membrane Reconstitution of His-Tagged Cytochrome C Oxidase to a Gold Electrode: In Situ Monitoring by Surface-Enhanced Infrared Absorption Spectroscopy. *J. Am. Chem. Soc.* **2004,** *126* (49), 16199-16206.
38. Paluri, S. L.; Edwards, M. L.; Lam, N. H.; Williams, E. M.; Meyerhoefer, A.; Pavel Sizemore, I. E., Introducing "Green" and "Nongreen" Aspects of Noble Metal Nanoparticle Synthesis: An Inquiry-Based Laboratory Experiment for Chemistry and Engineering Students. *J. Chem. Educ* **2014,** *92* (2), 350-354.
39. Jenkins, S. V.; Gohman, T. D.; Miller, E. K.; Chen, J., Synthesis of Hollow Gold–Silver Alloyed Nanoparticles: A "Galvanic Replacement" Experiment for Chemistry and Engineering Students. *J. Chem. Educ.* **2015,** *92* (6), 1056-1060.
40. Sharma, R.; Gulati, S.; Mehta, S., Preparation of Gold Nanoparticles Using Tea: A Green Chemistry Experiment. *J. Chem. Educ* **2012,** *89* (10), 1316-1318.
41. Frens, G., Controlled Nucleation for the Regulation of the Particle Size in Monodisperse Gold Suspensions. *Nature* **1973,** *241* (105), 20-22.
42. Turkevich, J.; Stevenson, P. C.; Hillier, J., A Study of the Nucleation and Growth Processes in the Synthesis of Colloidal Gold. *Discuss. Faraday Soc.* **1951,** *11*, 55-75.
43. Ji, X.; Song, X.; Li, J.; Bai, Y.; Yang, W.; Peng, X., Size Control of Gold Nanocrystals in Citrate Reduction: The Third Role of Citrate. *J. Am. Chem. Soc.* **2007,** *129* (45), 13939-13948.
44. Thanh, N. T.; Maclean, N.; Mahiddine, S., Mechanisms of Nucleation and Growth of Nanoparticles in Solution. *Chem. Rev.* **2014,** *114* (15), 7610-7630.
45. McGilvray, K. L.; Fasciani, C.; Bueno-Alejo, C. J.; Schwartz-Narbonne, R.; Scaiano, J. C., Photochemical Strategies for the Seed-Mediated Growth of Gold and Gold–Silver Nanoparticles. *Langmuir* **2012,** *28* (46), 16148-16155.
46. Cargnello, M.; Agarwal, R.; Klein, D. R.; Diroll, B. T.; Agarwal, R.; Murray, C. B., Uniform Bimetallic Nanocrystals by High-Temperature Seed-Mediated Colloidal Synthesis and Their Catalytic Properties for Semiconducting Nanowire Growth. *Chem. Mater.* **2015,** *27* (16), 5833-5838.
47. Brown, K. R.; Natan, M. J., Hydroxylamine Seeding of Colloidal Au Nanoparticles in Solution and on Surfaces. *Langmuir* **1998,** *14* (4), 726-728.
48. Li, J. F.; Tian, X. D.; Li, S. B.; Anema, J. R.; Yang, Z. L.; Ding, Y.; Wu, Y. F.; Zeng, Y. M.; Chen, Q. Z.; Ren, B., Surface Analysis Using Shell-Isolated Nanoparticle-Enhanced Raman Spectroscopy. *Nat. Protoc.* **2013,** *8* (1), 52-65.
49. Hicks, E. M.; Zou, S. L.; Schatz, G. C.; Spears, K. G.; Van Duyne, R. P.; Gunnarsson, L.; Rindzevicius, T.; Kasemo, B.; Kall, M., Controlling Plasmon Line Shapes through Diffractive Coupling in Linear Arrays of Cylindrical Nanoparticles Fabricated by Electron Beam Lithography. *Nano Lett.* **2005,** *5* (6), 1065-1070.

50. Tian, X. D.; Zhou, Y. D.; Thota, S.; Zou, S. L.; Zhao, J., Plasmonic Coupling in Single Silver Nanosphere Assemblies by Polarization-Dependent Dark-Field Scattering Spectroscopy. *J. Phys. Chem. C* **2014,** *118* (25), 13801-13808.
51. Shegai, T.; Li, Z.; Dadosh, T.; Zhang, Z.; Xu, H.; Haran, G., Managing Light Polarization Via Plasmon-Molecule Interactions within an Asymmetric Metal Nanoparticle Trimer. *Proc Natl Acad Sci U S A* **2008,** *105* (43), 16448-53.
52. Halas, N. J.; Lal, S.; Chang, W. S.; Link, S.; Nordlander, P., Plasmons in Strongly Coupled Metallic Nanostructures. *Chem. Rev.* **2011,** *111* (6), 3913-61.
53. He, L.; Wang, M.; Ge, J.; Yin, Y., Magnetic Assembly Route to Colloidal Responsive Photonic Nanostructures. *Accounts Of Chemical Research* **2012,** *45* (9), 1431-1440.
54. Henzie, J.; Andrews, S. C.; Ling, X. Y.; Li, Z.; Yang, P., Oriented Assembly of Polyhedral Plasmonic Nanoparticle Clusters. *Proc Natl Acad Sci U S A* **2013,** *110* (17), 6640-5.
55. Fan, J. A.; Wu, C.; Bao, K.; Bao, J.; Bardhan, R.; Halas, N. J.; Manoharan, V. N.; Nordlander, P.; Shvets, G.; Capasso, F., Self-Assembled Plasmonic Nanoparticle Clusters. *Science* **2010,** *328* (5982), 1135-8.
56. Wustholz, K. L.; Henry, A.-I.; McMahon, J. M.; Freeman, R. G.; Valley, N.; Piotti, M. E.; Natan, M. J.; Schatz, G. C.; Van Duyne, R. P., Structure-Activity Relationships in Gold Nanoparticle Dimers and Trimers for Surface-Enhanced Raman Spectroscopy. *J. Am. Chem. Soc.* **2010,** *132* (31), 10903-10910.
57. Hicks, E. M.; Zhang, X.; Zou, S.; Lyandres, O.; Spears, K. G.; Schatz, G. C.; Van Duyne, R. P., Plasmonic Properties of Film over Nanowell Surfaces Fabricated by Nanosphere Lithography. *J Phys Chem B* **2005,** *109* (47), 22351-8.
58. Zhang, X.; Hicks, E. M.; Zhao, J.; Schatz, G. C.; Van Duyne, R. P., Electrochemical Tuning of Silver Nanoparticles Fabricated by Nanosphere Lithography. *Nano Lett* **2005,** *5* (7), 1503-7.
59. Ormonde, A. D.; Hicks, E. C.; Castillo, J.; Van Duyne, R. P., Nanosphere Lithography: Fabrication of Large-Area Ag Nanoparticle Arrays by Convective Self-Assembly and Their Characterization by Scanning Uv-Visible Extinction Spectroscopy. *Langmuir : the ACS journal of surfaces and colloids* **2004,** *20* (16), 6927-31.
60. Kim, S.; Marelli, B.; Brenckle, M. A.; Mitropoulos, A. N.; Gil, E. S.; Tsioris, K.; Tao, H.; Kaplan, D. L.; Omenetto, F. G., All-Water-Based Electron-Beam Lithography Using Silk as a Resist. *Nat Nanotechnology* **2014,** *9* (4), 306-310.
61. Kravets, V. G.; Schedin, F.; Grigorenko, A. N., Extremely Narrow Plasmon Resonances Based on Diffraction Coupling of Localized Plasmons in Arrays of Metallic Nanoparticles. *Phys. Rev. Lett.* **2008,** *101* (8).
62. Auguie, B.; Barnes, W. L., Collective Resonances in Gold Nanoparticle Arrays. *Phys. Rev. Lett.* **2008,** *101* (14).
63. Chu, Y. Z.; Schonbrun, E.; Yang, T.; Crozier, K. B., Experimental Observation of Narrow Surface Plasmon Resonances in Gold Nanoparticle Arrays. *Appl. Phys. Lett.* **2008,** *93* (18).
64. Feichtenschlager, B.; Pabisch, S.; Peterlik, H.; Kickelbick, G., Nanoparticle Assemblies as Probes for Self-Assembled Monolayer Characterization: Correlation between Surface Functionalization and Agglomeration Behavior. *Langmuir : the ACS journal of surfaces and colloids* **2012,** *28* (1), 741-750.
65. Feichtenschlager, B.; Lornoschitz, C. J.; Kickelbick, G., Tuning the Self-Assembled Monolayer Formation on Nanoparticle Surfaces with Different Curvatures: Investigations on

Spherical Silica Particles and Plane-Crystal-Shaped Zirconia Particles. *J Colloid Interf Sci* **2011,** *360* (1), 15-25.
66. Chen, H. J.; Wang, Y. L.; Qu, J. Y.; Dong, S. J., Self-Assembled Silver Nanoparticle Monolayer on Glassy Carbon: An Approach to Sers Substrate. *J Raman Spectrosc* **2007,** *38* (11), 1444-1448.
67. Peng, Z. Q.; Qu, X. H.; Dong, S. J., Immobilization of the Nanoparticle Monolayer onto Self-Assembled Monolayers by Combined Sterically Enhanced Hydrophobic and Electrophoretic Forces. *Langmuir : the ACS journal of surfaces and colloids* **2004,** *20* (1), 5-10.
68. Nakanishi, T.; Ohtani, B.; Uosaki, K., Fabrication and Characterization of Cds-Nanoparticle Mono- and Multilayers on a Self-Assembled Monolayer of Alkanedithiols on Gold. *J. Phys. Chem. B* **1998,** *102* (9), 1571-1577.
69. Freeman, R. G.; Grabar, K. C.; Allison, K. J.; Bright, R. M.; Davis, J. A.; Guthrie, A. P.; Hommer, M. B.; Jackson, M. A.; Smith, P. C.; Walter, D. G.; Natan, M. J., Self-Assembled Metal Colloid Monolayers - an Approach to Sers Substrates. *Science* **1995,** *267* (5204), 1629-1632.
70. Huang, X.; Aguilar, Z. P.; Xu, H.; Lai, W.; Xiong, Y., Membrane-Based Lateral Flow Immunochromatographic Strip with Nanoparticles as Reporters for Detection: A Review. *Biosens. Bioelectron.* **2016,** *75*, 166-180.
71. Kairdolf, B. A.; Smith, A. M.; Stokes, T. H.; Wang, M. D.; Young, A. N.; Nie, S., Semiconductor Quantum Dots for Bioimaging and Biodiagnostic Applications. *Annu. Rev. Anal. Chem.* **2013,** *6*, 143-162.
72. Medintz, I. L.; Uyeda, H. T.; Goldman, E. R.; Mattoussi, H., Quantum Dot Bioconjugates for Imaging, Labelling and Sensing. *Nat Mater* **2005,** *4* (6), 435-446.
73. Alivisatos, P., The Use of Nanocrystals in Biological Detection. *Nat. Biotechnol.* **2004,** *22* (1), 47-52.
74. Clapp, A. R.; Medintz, I. L.; Mattoussi, H., Förster Resonance Energy Transfer Investigations Using Quantum-Dot Fluorophores. *ChemPhysChem* **2006,** *7* (1), 47-57.
75. Yu, X.; Lei, D. Y.; Amin, F.; Hartmann, R.; Acuna, G. P.; Guerrero-Martínez, A.; Maier, S. A.; Tinnefeld, P.; Carregal-Romero, S.; Parak, W. J., Distance Control in-between Plasmonic Nanoparticles Via Biological and Polymeric Spacers. *Nano Today* **2013,** *8* (5), 480-493.
76. Dey, S.; Zhou, Y.; Tian, X.; Jenkins, J. A.; Chen, O.; Zou, S.; Zhao, J., An Experimental and Theoretical Mechanistic Study of Biexciton Quantum Yield Enhancement in Single Quantum Dots near Gold Nanoparticles. *Nanoscale* **2015,** *7* (15), 6851-6858.
77. Ma, X.; Fletcher, K.; Kipp, T.; Grzelczak, M. P.; Wang, Z.; Guerrero-Martínez, A.; Pastoriza-Santos, I.; Kornowski, A.; Liz-Marzán, L. M.; Mews, A., Photoluminescence of Individual Au/Cdse Nanocrystal Complexes with Variable Interparticle Distances. *The Journal of Physical Chemistry Letters* **2011,** *2* (19), 2466-2471.
78. Loweth, C. J.; Caldwell, W. B.; Peng, X.; Alivisatos, A. P.; Schultz, P. G., DNA-Based Assembly of Gold Nanocrystals. *Angew. Chem. Int. Ed.* **1999,** *38* (12), 1808-1812.
79. Claridge, S. A.; Goh, S. L.; Frechet, J. M.; Williams, S. C.; Micheel, C. M.; Alivisatos, A. P., Directed Assembly of Discrete Gold Nanoparticle Groupings Using Branched DNA Scaffolds. *Chem. Mater.* **2005,** *17* (7), 1628-1635.
80. Mastroianni, A. J.; Claridge, S. A.; Alivisatos, A. P., Pyramidal and Chiral Groupings of Gold Nanocrystals Assembled Using DNA Scaffolds. *J. Am. Chem. Soc.* **2009,** *131* (24), 8455-8459.

81. Aldaye, F. A.; Sleiman, H. F., Dynamic DNA Templates for Discrete Gold Nanoparticle Assemblies: Control of Geometry, Modularity, Write/Erase and Structural Switching. *J. Am. Chem. Soc.* **2007,** *129* (14), 4130-4131.
82. Zanchet, D.; Micheel, C. M.; Parak, W. J.; Gerion, D.; Williams, S. C.; Alivisatos, A. P., Electrophoretic and Structural Studies of DNA-Directed Au Nanoparticle Groupings. *The Journal of Physical Chemistry B* **2002,** *106* (45), 11758-11763.
83. Chou, K. F.; Dennis, A. M., Förster Resonance Energy Transfer between Quantum Dot Donors and Quantum Dot Acceptors. *Sensors* **2015,** *15* (6), 13288-13325.
84. Ang, G. Y.; Yu, C. Y.; Chan, K. G.; Singh, K. K. B.; Chan Yean, Y., Development of a Dry-Reagent-Based Nucleic Acid-Sensing Platform by Coupling Thermostabilised Late-Pcr Assay to an Oligonucleotide-Modified Lateral Flow Biosensor. *J. Microbiol. Methods* **2015,** *118*, 99-105.
85. Li, Z.; Wang, Y.; Wang, J.; Tang, Z.; Pounds, J. G.; Lin, Y., Rapid and Sensitive Detection of Protein Biomarker Using a Portable Fluorescence Biosensor Based on Quantum Dots and a Lateral Flow Test Strip. *Anal. Chem.* **2010,** *82* (16), 7008-7014.
86. Posthuma-Trumpie, G. A.; Korf, J.; van Amerongen, A., Lateral Flow (Immuno) Assay: Its Strengths, Weaknesses, Opportunities and Threats. A Literature Survey. *Anal. Bioanal. Chem.* **2009,** *393* (2), 569-582.
87. Wong, R.; Tse, H., *Lateral Flow Immunoassay*. Humana Press: New York, NY, 2009.
88. Ngom, B.; Guo, Y.; Wang, X.; Bi, D., Development and Application of Lateral Flow Test Strip Technology for Detection of Infectious Agents and Chemical Contaminants: A Review. *Anal. Bioanal. Chem.* **2010,** *397* (3), 1113-1135.
89. Chin, C. D.; Linder, V.; Sia, S. K., Commercialization of Microfluidic Point-of-Care Diagnostic Devices. *Lab Chip* **2012,** *12* (12), 2118-2134.
90. Li, X.; Lu, D.; Sheng, Z.; Chen, K.; Guo, X.; Jin, M.; Han, H., A Fast and Sensitive Immunoassay of Avian Influenza Virus Based on Label-Free Quantum Dot Probe and Lateral Flow Test Strip. *Talanta* **2012,** *100*, 1-6.
91. Leuvering, J. H.; Thal, P. J.; Van der Waart, M.; Schuurs, A. H., A Sol Particle Agglutination Assay for Human Chorionic Gonadotrophin. *J. Immunol. Methods* **1981,** *45* (2), 183-194.
92. Cserháti, T.; Forgács, E., Trends in Thin-Layer Chromatography: 1997. *J. Chromatogr. Sci.* **1997,** *35* (8), 383-391.
93. Yu, L.; Shi, Z.; Fang, C.; Zhang, Y.; Liu, Y.; Li, C., Disposable Lateral Flow-through Strip for Smartphone-Camera to Quantitatively Detect Alkaline Phosphatase Activity in Milk. *Biosens. Bioelectron.* **2015,** *69*, 307-315.
94. Zhu, M.; Wang, Y.; Deng, Y.; Yao, L.; B. Adeloju, S.; Pan, D.; Xue, F.; Wu, Y.; Zheng, L.; Chen, W., Ultrasensitive Detection of Mercury with a Novel One-Step Signal Amplified Lateral Flow Strip Based on Gold Nanoparticle-Labeled Ssdna Recognition and Enhancement Probes. *Biosens. Bioelectron.* **2014,** *61*, 14-20.
95. He, Y.; Zhang, S.; Zhang, X.; Baloda, M.; Gurung, A. S.; Xu, H.; Zhang, X.; Liu, G., Ultrasensitive Nucleic Acid Biosensor Based on Enzyme–Gold Nanoparticle Dual Label and Lateral Flow Strip Biosensor. *Biosens. Bioelectron.* **2011,** *26* (5), 2018-2024.
96. Ahmed, E. M., Hydrogel: Preparation, Characterization, and Applications: A Review. *Journal of Advanced Research* **2015,** *6* (2), 105-121.
97. Hames, B. D., Gel Electrophoresis of Proteins: A Practical Approach. OUP Oxford: 1998; Vol. 197.

98. Freifelder, D., Physical Biochemistry: Applications to Biochemistry and Molecular Biology. Macmillan: 1982.

Chapter Two :

Blue Shifted Narrow Localized Surface Plasmon Resonance from Dipole Coupling in Gold Nanoparticle Random Arrays

2.1 Abstract

In this work, we develop a simple method to produce highly uniform localized surface plasmon resonance (LSPR) substrates based on self-assembly of colloidal gold nanoparticles onto pretreated glass substrate. The LSPR wavelength of the gold nanoparticle arrays is blue shifted from that of the gold nanoparticles in solution, and the single gold nanoparticles on glass substrates. The LSPR width is narrower than that of the single gold nanoparticles. The blue-shifted LSPR is due to the long-range dipole coupling in the gold nanoparticle random arrays indicated from simulations using T-matrix method. In addition to the popularly used LSPR wavelength dependence on the dielectric environment, we have found that the LSPR width of the gold nanoparticle random arrays is also sensitive to the change in the dielectric environment. The LSPR substrates are reproducible, uniform and robust with potential applications in LSPR sensing and imaging.

2.2 Introduction

The optical coupling in noble metal nanoparticle assemblies and patterned nanostructures gives rise to interesting new optical phenomena, which can be controlled by factors such as the geometry and interparticle distances of the nanoparticles.[1-13] Research efforts in developing patterned or assembled nanostructures have been promoted to tune the plasmonic interactions.[1, 8, 10-11, 13-16] Localized surface plasmon resonance (LSPR) of noble metal nanoparticles is the collective oscillation of electrons in the nanoparticles induced by the electromagnetic radiation of light.[17-18] LSPR results in wavelength-dependent absorption, and scattering of photons by noble metal nanoparticles as well as greatly amplified electromagnetic field localized around the nanoparticles.[17-18] The LSPR peak wavelength (λ_{max}) is determined by the size, shape, composition of the nanoparticles, and also the dielectric environment around them.[17-20] Due to these phenomena, plasmonic nanostructures have been used in many applications such as plasmonic waveguides,[21-24] photovoltaic,[25-30] bio- or chemo-sensors,[17-18, 31-36] and surface-enhanced spectroscopies.[37-44]

Research advances over the past couple of decades has led to many methods to synthesize noble metal nanoparticles and to fabricate patterned nanostructures as LSPR substrates. A widely used method to create metal nanoparticle arrays includes lithographic nanopatterning followed by vacuum deposition of noble metals.[10, 45-48] The method yields highly ordered nanostructures with well-controlled nanoparticle geometry and interparticle spacing. Dipole coupling in these patterned nanostructures causes the LSPR λ_{max} to shift depending on the distance between nanoparticles. Studies show that in both 1D and 2D metal nanoparticle arrays, the λ_{max} shifts when the distance between metal nanoparticles are changed or the environmental dielectric constant is varied.[49-52]

Most of the LSPR sensing methods rely on the resonance wavelength shift of the system upon analyte binding. For a high sensitivity of the detection, narrow resonance peaks are desirable to better determine the LSPR wavelength. Although the lithographic techniques are capable of producing highly ordered patterns with flexibility in the pattern design and narrow resonance peaks,[53-55] they are usually expensive and instrumentation heavy, therefore, not widely applicable. Another common method to produce LSPR substrate is self-assembly of colloidal nanoparticles on pretreated solid support such as glass. One self-assembly technique is self-assembled monolayer (SAM) which produces a monolayer or sub-monolayer of nanoparticles on the substrate.[56-61] Layer-by-layer assembly is another self-assembly method used to create multi-layer thin films of nanoparticles, where every other layer is composed of oppositely charged nanoparticles and molecules.[62-67] Compared to the lithographic techniques, the self-assembly method is simple, more cost effective, and broadly applicable. But usually the self-assembly method yields LSPR substrates with randomly distributed nanoparticles; therefore, they often have broad LSPR bands, which makes them not ideal for sensing applications. Moreover, from a fundamental point of view, the optical interactions in these random arrays of nanoparticles are not well understood, limiting the development of the self-assembly LSPR substrate.

In this work, a simple and reproducible method to fabricate a uniform film of 120 nm Au nanoparticles (NPs) on 3-aminopropyltriethoxysilane coated glass substrates based on electrostatic interactions is presented. The Au NP random arrays exhibit a blue-shifted narrow LSPR band, compared to the LSPR of Au NPs in water, and also the LSPR of single Au NPs on glass. Theoretical studies using T-matrix method[68] reveal that the long-range dipole coupling in the Au NP random arrays leads to the blue shifted narrow LSPR band. The studies also demonstrate that not only the LSPR λ_{max}, but also the LSPR width of the Au NP arrays is sensitive to changes in the

dielectric media of the nanoparticles. The LSPR substrates are reproducible, uniform and robust against high electrolyte concentration, therefore, may be used for LSPR width based sensing and imaging applications.

2.3 Experimental Methods

2.3.1 Chemicals and Materials

Gold (III) chloride trihydrate ($HAuCl_4$), hydroxylamine hydrochloride ($NH_2OH{\cdot}HCl$), and 3-aminopropyltriethoxysilane (APTES) were purchased from Sigma-Aldrich. Sodium citrate, methanol, ethanol, hydrochloric acid, acetone, benzene, cyclohexane and glass coverslips (22x22mm, #2) were purchased from Fisher Scientific.

2.3.2 Methods

2.3.2.1 Synthesis of Au Nanoparticles

A two-step seed mediated process was used to prepare 120 nm gold colloids, as previously reported.[42] The first step involves the reduction of $HAuCl_4$ with sodium citrate by the Frens' Method.[69] Briefly, 1060 μL of $HAuCl_4$ (0.0254 M) solution was brought to a boil in 99 mL of deionized (DI) water while stirring. Once boiling, 1000 μL of sodium citrate (0.0388 M) solution was added. After 15 minutes, the solution was allowed to cool to room temperature. 4 mL of the as-made nanoparticle solution synthesized in step one was added to 52 mL of DI water. The seeds were stirred at room temperature for one hour with 1000 μL sodium citrate (0.0388 M), 900 μL $HAuCl_4$ (0.0254 M), and 1400 μL hydroxylamine hydrochloride (0.0101 M). The nanoparticles were used directly from the growth solution.

2.3.2.2 Glass Substrate Preparation

The glass substrates were prepared using commercially available glass coverslips. The glass coverslips were cleaned by sonication in a dilute alkaline detergent for 15 minutes. They were sonicated in DI water several times to completely remove the detergent. The coverslips were further cleaned by immersing into a 1:1 (v/v) solution of hydrochloric acid and methanol for 30 minutes. They were thoroughly rinsed with DI water until a neutral pH was obtained. After cleaning, the glass coverslips were immersed in a 10% (v/v) solution of APTES in ethanol for 20 minutes to silanize the surface. The coverslips were sonicated in ethanol several times and annealed in the oven at 120°C for 3 hours.

2.3.2.3 Gold Nanoparticle Adsorption

The silanized glass substrates were immersed in the Au NP solution with a concentration of 5×10^9 particles/mL overnight so that the nanoparticles were adsorbed to the glass substrate, as illustrated in **Figure 2.1A**. After immobilization of the gold NPs on glass, the substrate was rinsed with DI water to remove any excess gold nanoparticles, and then dried in air.

2.3.2.4 Optical and Structural Characterization

A UV-vis spectrometer (Cary 60, Agilent Technologies) was used to determine the extinction spectrum of the gold nanoparticles in solution. A home-built LSPR setup was used to measure the UV-vis extinction spectra of the immobilized Au NPs on the glass substrate. In this setup, a halogen light source was fiber coupled and focused with convex lens on the Au NPs to a spot of ~ 0.5 cm diameter. The transmitted light after passing through the Au NPs was focused onto a fiber coupled spectrometer (QE65 Pro, Ocean Optics). The Au NP substrate was placed in

a home-built flow cell to allow incubation in various solvents. The scanning electron microscopy (SEM) image of the Au NPs on glass was obtained with JEOL JSM-6330F.

For comparison with the Au NP random arrays on glass, scattering spectra of single Au NPs was acquired with dark-field scattering microscope. To prepare the sample for single particle study, a highly diluted solution of the Au NPs was dropped on a piece of No. 1 coverglass (Fisher Scientific) and dried in air. The scattering spectra of single Au NPs were taken using a Nikon Ti-u microscope, where the light from a halogen lamp was focused on the Au NPs through a dark-field condenser (NA 0.85). The scattered light by the nanoparticles was collected with a 100× NA 0.8 objective (variable NA 0.8-1.3), and directed to the entrance slit of a spectrograph (IsoPlane SCT 320, Princeton Instruments) equipped with a CCD camera (PIXIS 1024BR, Princeton Instruments). Scattering spectra were corrected by signal collected from a nearby region without nanoparticles and normalized by the lamp intensity profile.

2.4 Results and Discussion

2.4.1 LSPR of Gold Nanoparticles on Glass

Adsorption of Au NPs to silanized glass was confirmed by both SEM imaging and optical measurements. From the SEM image of Au NPs on glass shown in **Figure 2.1B**, the NPs randomly distributed on the glass substrate. The diameter of the Au NPs was determined to be 116±13 nm. Atomic force microscopy measurements (**Figure 2.1C**) revealed that the height of the Au NP was about 120 nm, consistent with that from the SEM studies, and demonstrated that a sub-monolayer of the Au NPs was formed on glass. From the SEM image, the average center-to-center distance between the nanoparticles was 226±92 nm, which was determined from analysis on several substrates.

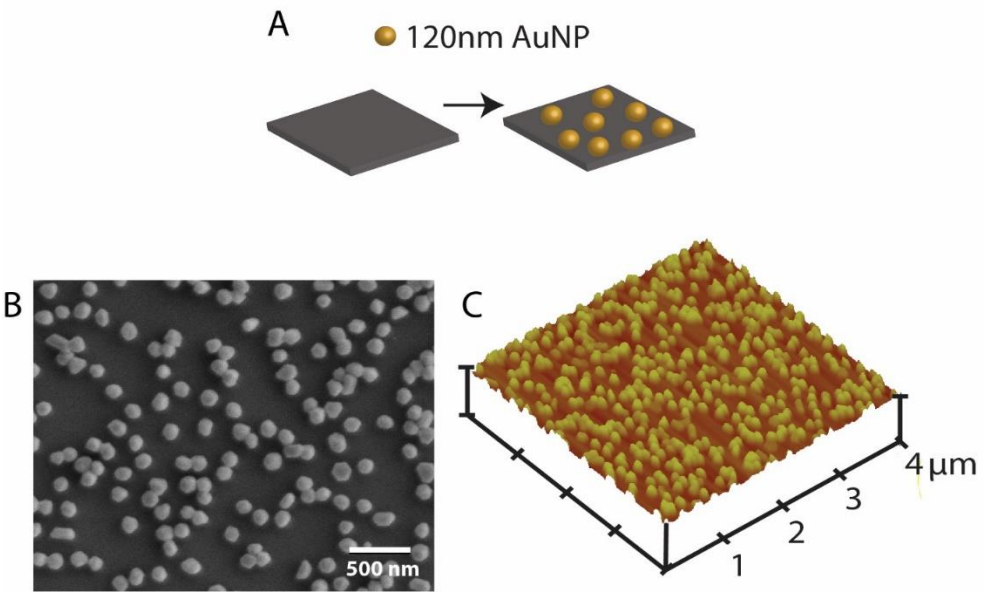

Figure 2.1. (A) Scheme of the immobilization of gold nanoparticle on silanized glass coverslip. (B) SEM and (C) AFM images of 120nm gold spheres immobilized on glass coverslip in a random array.

The extinction spectrum of 120 nm Au nanoparticles in solution is shown in **Figure 2.2**, red dashed line. The LSPR band is broad with a peak at a wavelength of 600 nm and a FWHM (full width at half maximum) of 174 nm (0.61 eV). When the Au nanoparticles are immobilized on APTES treated glass, a narrow, blue-shifted LSPR spectrum was observed with a peak at 530 nm and the FWHM of the LSPR band is 84 ± 4 nm (0.36 ± 0.02 eV), 52% decreased from the solution LSPR band (shown in **Figure 2.2**, black solid curve). The blue-shifted narrow LSPR is different from previous studies of the LSPR of 10-80 nm Au NPs adsorbed on silanized glass where a LSPR band at ~520 nm was observed for the varying nanoparticle sizes and surface coverages.[70-73]

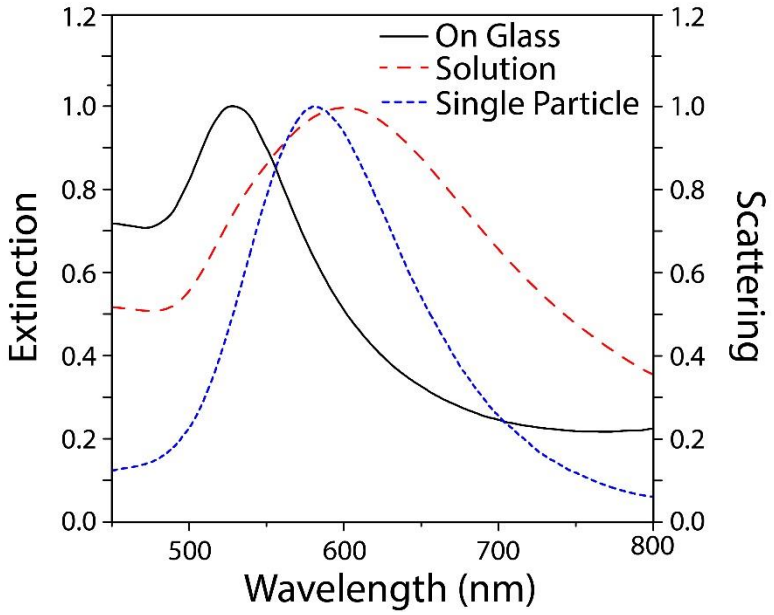

Figure 2.2. The extinction spectra of 120 nm gold nanoparticles in solution (red dashed) and immobilized on glass (black solid) as well as the scattering spectra of 120nm single gold nanoparticles (blue dashed). The extinction values are found on the left y-axis and the scattering values are located on the right y-axis.

We further compare the LSPR of the nanoparticles with dark-field scattering of single 120 nm Au NPs on glass. Ideally, the extinction of the Au NP arrays should be compared to the extinction of single NPs instead of scattering. But it is extremely difficult to measure the extinction of single NPs experimentally. To examine the difference between the extinction and scattering of single NPs, theoretical modeling was performed on an Au NP of 120 nm diameter and it revealed a small difference in the scattering and extinction spectra of single NP, as shown in **Figure 2.3**. Therefore, we compare the extinction of the randomly distributed Au NPs on glass with the scattering of single NPs. **Figure 2.2**, blue dashed line shows a representative scattering spectrum of a single Au NP. From the dark-field scattering spectra of 19 Au NPs, the average peak wavelength is at 571 ± 14 nm, and the average peak width is 103 ± 12 nm (0.38 ± 0.04 eV). It is

unexpected that the LSPR peak width of the random array of Au NPs is comparable with and even slightly smaller than that of the single NPs because typically, ensemble LSPR peak width of metal NPs is much larger than that of single NPs due to inhomogeneous broadening.

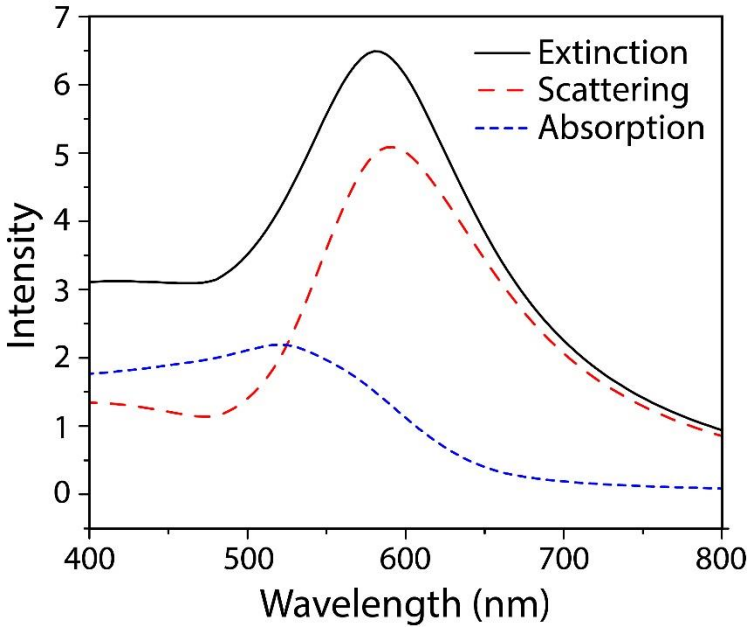

Figure 2.3. The theoretical extinction (black), scattering (red) and absorption (blue) of a single gold nanoparticle.

2.4.2 Theoretical Modeling of Gold Nanoparticle Random Arrays

In order to understand the origin of the narrow and blue-shifted LSPR band of the Au NP random arrays, theoretical studies using T-matrix method[68] are performed. The dielectric constant of Au is obtained from Palik's handbook.[74] Since there is no analytical formula to explicitly include substrate effect for arrays of particles and numerically including the substrate requires calculation power beyond the currently available resource,[75] the dielectric constant of the environment is determined using effective medium theory, similar to previous work.[11, 76] The comparison between

the calculated and experimental scattering spectra of a single NP with/without the substrate effect is shown in **Figure 2.4**.

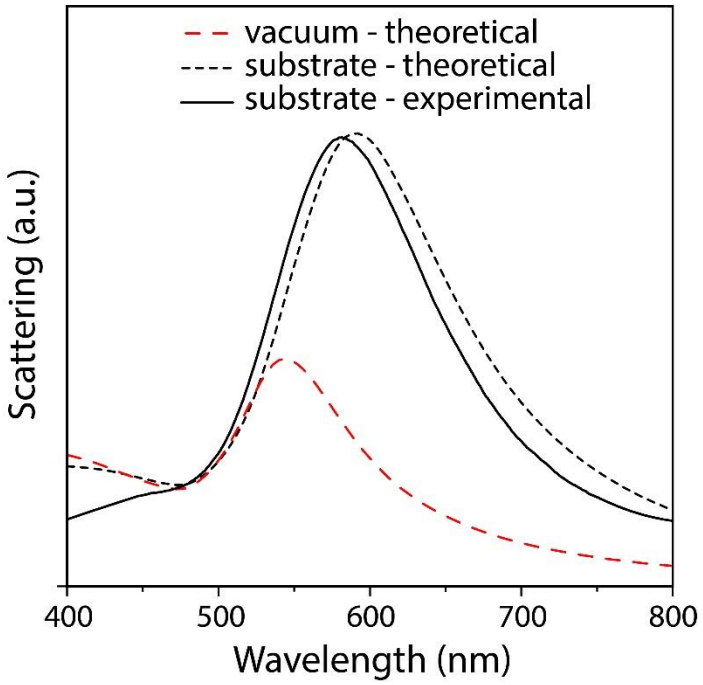

Figure 2.4. The substrate effect in scattering spectra of a 120nm single gold nanoparticle. The theoretical (black dashed) and experimental (black solid) scattering spectra of the gold nanoparticle on substrate both show a red shift from the theoretical scattering spectra of a single nanoparticle in a vacuum (red).

As illustrated in **Figure 2.6A**, Au nanoparticles of 120 nm diameter are arranged in a hexagonal lattice, and the distance between nanoparticles is set to be 226 nm, as determined by the experiment. To reproduce the randomness of the array, we randomly displace the particles from its lattice position with a maximum displacement of 45 nm (20% of the interparticle distance) in either of the two perpendicular directions of the hexagonal arrays. We chose 45 nm to be maximum displacement to avoid the overlap of the nanoparticle in the calculations. We also calculated the spectra using the maximum displacement of 40 nm and the results are very similar to those

presented here. Furthermore, we considered the effect of polarization of the incident light on the LSPR of the Au NP random arrays. The calculated spectra were almost identical for varying polarizations, shown in **Figure 2.5**.

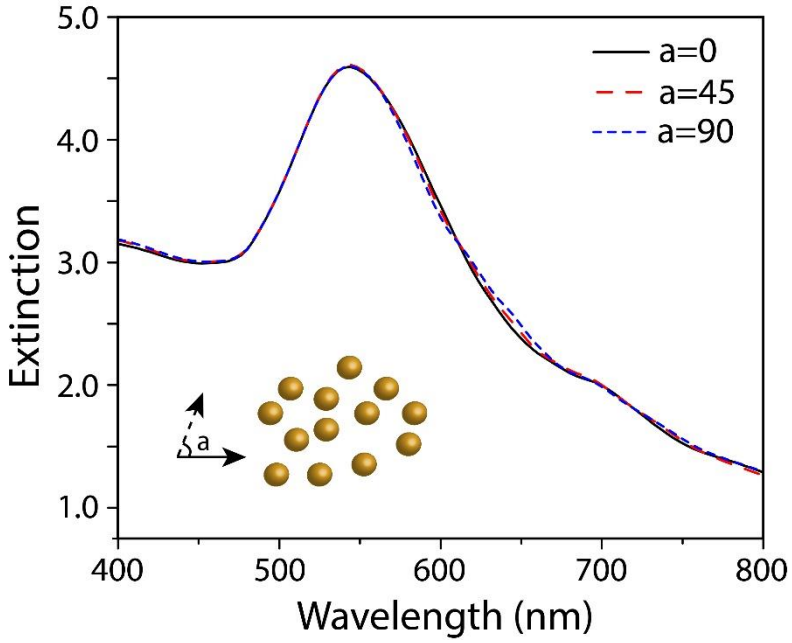

Figure 2.5. The theoretical extinction results of 120nm gold nanoparticle random arrays on a glass substrate with different incident polarizations. The angle, a, is varied relative to the X axis. The extinction spectra when a=0 (black), a=45 (red) and a=90 (blue) are the same.

The calculated LSPR spectra of a single Au NP and Au NP random arrays are shown in **Figure 2.6B**. The black solid line shows the scattering spectrum of a single 120 nm Au NP on glass. The spectrum matches well with the measured scattering spectrum of a single Au NP as shown in **Figure 2.2**, blue dashed line. To understand the origin of the blue shift and narrowing of the LSPR peak, we calculate the extinction spectra of the nanoparticle arrays by the exact method (**Figure 2.6B**, blue dashed line) or including dipole excitation only (**Figure 2.6B**, red dashed line). The two spectra are similar where the spectrum calculated by the exact method is slightly blue

shifted and broader than that from the calculation including the dipoles only. The calculations also agree well with the measured LSPR of the Au NP arrays as shown in **Figure 2.2**, black solid line. The results indicate that the higher order excitation of nanoparticles slightly broadens the resonance peak but the spectral change in the nanoparticle arrays compared to the nanoparticles in solution or single nanoparticles on glass is mainly due to the dipole coupling between the nanoparticles in the array. Previous studies on ordered nanoparticle arrays have demonstrated that dipole coupling between the nanoparticles lead to shifts in the resonance wavelength and also changes in the linewidth.[50] In this study, even though the nanoparticles are randomly distributed, an average interparticle distance that is about twice the nanoparticle diameter gives rise to the blue-shifted narrow plasmon band. We varied the interparticle distance in the calculations from 140 nm to 420 nm. The resulting LSPR wavelengths were plotted in **Figure 2.6C**. The peak wavelength blue-shifts as the interparticle distance increases from 140 nm to 180 nm, and then it starts to redshift as the interparticle distance continues to increase up to 420 nm. Notice that the scattering spectrum of a single Au NP has a peak at ~ 600 nm. For all the random arrays we calculated with varying interparticle distances, the LSPR wavelengths are bluer than the single particle scattering due to the long-range dipole coupling. Notice that a lot of previous work has revealed that near-field coupling between nanoparticle dimers or small aggregates results in a red-shift of the LSPR compared to that of single nanoparticles.[77-79] In those studies, the distances between the nanoparticles are usually quite small compared to the size of the nanoparticles. In this work, the average interparticle distance is much larger than the diameter of the nanoparticles. There is strong coherent dipole coupling between the nanoparticles from the far-field interaction of the dipoles. And this long-range interaction results in the blue-shift of the LSPR band and it is more often observed in nanoparticle arrays, instead of small aggregates. We expect that in experiments, by

tuning the nanoparticle solution concentration, the interparticle distance can be varied to obtain LSPR substrates with desired resonance wavelength and width.

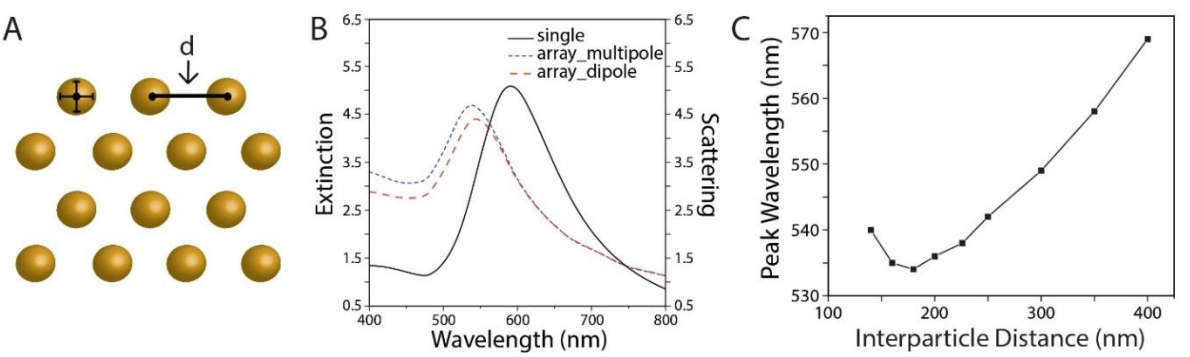

Figure 2.6. Theoretical extinction spectra of 120 nm gold nanoparticles random arrays. (A) Schematic illustration of the Au nanoparticle arrays in the theoretical study. The interparticle distance (d) from center to center is 226 nm for the spectra in Figure (B) and it is varied to calculate the extinction peaks in Figure (C). The centers of the nanoparticles were allowed to move 0-45 nm randomly in both the x and y directions. (B) The scattering spectrum of a single nanoparticle (black line), extinction spectra of random array using the exact method (blue dashed), and random array considering the dipoles only (red dashed). (C) The extinction peak wavelength of the nanoparticle random arrays while varying the interparticle distance. The peak wavelength blue-shifts as the interparticle distance increases from 140 nm to 180 nm, and then it starts to redshift as the interparticle distance continues to increase.

Previous studies show that long range plasmon coupling in ordered nanoparticle arrays resulted in narrow and interparticle-distance dependent plasmon resonance.[53-55] Here, we compare the difference in plasmon coupling of ordered and random nanoparticle arrays. From the theoretical calculations, the major difference in the ordered and random array is that the range of

plasmon coupling between nanoparticles is much longer in the ordered array than in the random array.

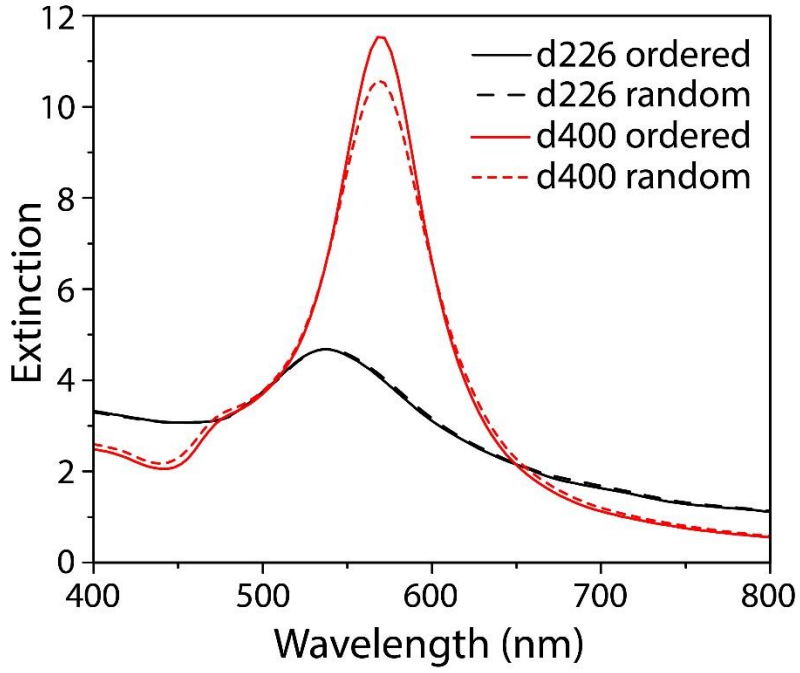

Figure 2.7. Theoretical extinction spectra of 120nm gold nanoparticle ordered versus random arrays. At a particle center to center distance, d, of 226nm, the ordered array (black) and the random array (black dashed) are comparable. When increasing the particle center to center distance to 400nm, the ordered array (red) and random array (red dashed) differ. The intensity of the ordered array is greater than that of the random array, and the FWHM is smaller in the ordered array.

The extinction of the ordered and random Au NP arrays with varying interparticle distance (d) is illustrated in **Figure 2.7**. When d = 226 nm, which is about twice of the diameter of the NPs, the plasmon coupling is dominated by neighboring nanoparticles in both the ordered and random arrays. Therefore, no difference is observed in the extinction spectra of them. When d is increased to 400 nm, plasmon coupling beyond neighboring nanoparticles starts to show effect in the ordered arrays. In other words, the periodic plasmon coupling in an ordered array have a much longer

range when d = 400 nm than the case where d = 226 nm. This long range coupling is due to the constructive interference between the scattered light from nanoparticles in the array. However, in the random array, this longer range coupling is canceled because of the randomness of the nanoparticles. The randomness shifts particles from their lattice position, changes the interparticle distance, and reduces the constructive interference between particles. Therefore, we observe a slightly broadened extinction spectrum with lower peak intensity of the random array than that of the ordered array with d = 400 nm. This difference becomes more prominent when d is further increased.

2.4.3 Refractive Sensitivity of the LSPR Peak Wavelength and Width

It has been demonstrated from extensive previous studies that LSPR of noble metal NPs is sensitive to the surroundings.[36, 80] Here, we examine both the resonance wavelength and the FWHM change of the Au NP arrays when the environmental dielectric constant is varied. Briefly, we assembled the glass substrate with Au NPs in a home-built flow cell and exposed the Au NPs to several media with varying refractive indices, including air, water, acetone, cyclohexane and benzene. After incubation in one solvent, the Au NPs were allowed to dry in N_2 completely before switching to a different solvent. The LSPR spectrum of the Au NPs in air was monitored throughout the whole process to ensure the solvents did not induce changes in the Au NPs arrangement, etc.

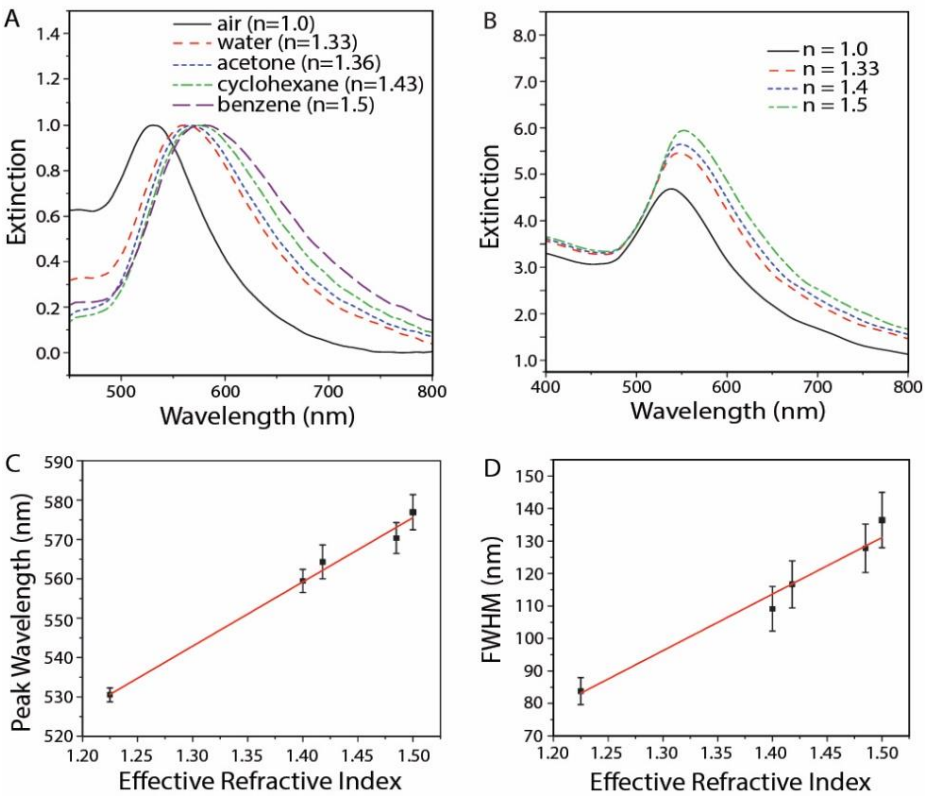

Figure 2.8. The variation of extinction spectra for the gold nanoparticle substrate with different refractive indices. (A) Experimental results of one slide when the environment is air (black), water (red), acetone (blue), cyclohexane (green), and benzene (purple) where the refractive index, n, equals 1.0, 1.33, 1.36, 1.43, and 1.5, respectively. (B) The theoretical results when n equals 1.0 (black), 1.33 (red), 1.4 (blue) and 1.5 (green). (C) Peak wavelength, λ_{max}, versus the effective refractive index (n_{eff}). A linear relationship between λ_{max} and n_{eff} is observed where $\lambda_{max} = 163.3\ n_{eff} + 330.0$. The error bars represent the standard deviation in λ_{max} calculated from nine total spots on three different substrates. (D) The full width at half-maximum (FWHM) versus refractive index with error bars. A linear relationship between FWHM and n_{eff} is observed where $FWHM = 174.1\ n_{eff} - 130.1$. The error bars represent the standard deviation in FWHM calculated from nine total spots on three different substrates.

The extinction spectra of the Au NP random arrays were taken in five media of different refractive indexes (RI), i.e. air (RI =1.0), water (RI =1.33), acetone (RI=1.36), cyclohexane (RI=1.43), and benzene (RI=1.50). As the RI of the medium increases, the extinction peak red shifts and becomes broader, as shown in **Figure 2.8A**. Same phenomena were observed in the theoretical studies using the exact method of 120 nm Au NPs random arrays on glass, with varying RI of the medium around the nanoparticles (shown in **Figure 2.8B**).

For quantitative analysis, we plotted the LSPR peak wavelength/FWHM versus the effective refractive index (n_{eff}), shown in **Figure 2.8C** and **Figure 2.8D**, respectively. Since the nanoparticles are partially immersed in solvents and partially on glass substrate, the effective refractive index is used in the plots instead of the refractive index of the solvents. The error bars were calculated from the standard deviation of LSPR wavelengths/FWHM measured at nine different spots of three Au NP substrates. From **Figure 2.8C**, there is a linear relationship between LSPR peak wavelength and the effective RI of the media, $\lambda_{max} = 163.3\ n_{eff} + 330.0$. The result is similar to previous work where many studies have revealed a linear relationship between the LSPR peak wavelengths of various nanostructures to refractive index of the surroundings.[20, 80-83] However, the sensitivity of LSPR peak width to the refractive index change is less discussed. LSPR peak width is an important factor that determines the figure of merit of plasmonic structures.[84] In our work, we observe a significant difference in the FWHM of the LSPR (from the spectra in **Figure 2.8A**) when the Au NPs were exposed to solvents with varying refractive indices. When calculating the FWHM, we subtracted the baseline. The plot in **Figure 2.8D** also reveals a linear relationship between LSPR FWHM and the effective RI, where $FWHM = 174.1 n_{eff} - 130.1$. There is also a linear relationship between FWHM and effective RI when the FWHM is calculated in eV unit (as shown in **Figure 2.9**). The study demonstrates that both the peak wavelength and

width change to refractive indices may be used as a measure for the dielectric media around the random array of the Au nanoparticles.

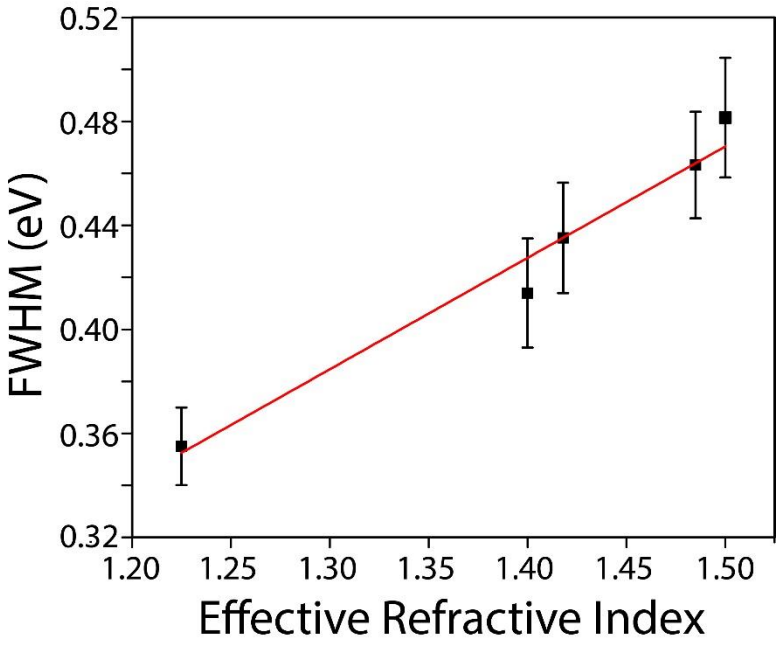

Figure 2.9. The full width at half-max (FWHM) in eV versus effective refractive index with error bars. A linear trendline (red) is shown with an equation of y = 0.428x – 0.172.

2.4.4 Uniformity, Reproducibility and Robustness of the LSPR Substrate

The self-assembly method of Au NPs produces uniform LSPR substrates over large area. The inset in **Figure 2.10A** is a picture of a LSPR substrate fabricated on a 22×22 mm glass. The LSPR substrate is visibly uniform with a dark red color across the entire substrate. The LSPR spectra taken at four randomly selected spots on the same substrate in air were plotted in **Figure 2.10A**. The four spectra largely overlapped indicating the LSPR substrate is uniform. In addition to the consistency of LSPR spectra within one LSPR substrate, it is important that the LSPR substrates need to be reproducible between different substrates. **Figure 2.10B** shows the distribution of LSPR λ_{max} of 37 substrates fabricated at different times with different batches of

nanoparticles. It is shown that LSPR peak wavelength changes slightly from substrate to substrate, and the majority of the substrates have a λ_{max} that falls between 520 and 530 nm.

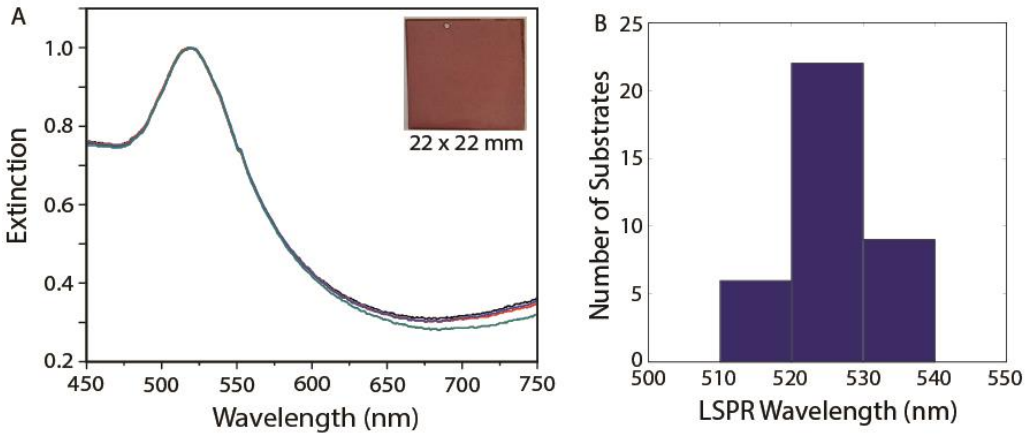

Figure 2.10. Uniformity and reproducibility of the gold nanoparticle substrates. (A) Extinction spectra of a substrate measured at four different spots after immobilization of gold nanoparticles almost completely overlap with each other. The inset is a picture of the 22×22 mm glass coverslip with a sub-monolayer of 120nm gold nanoparticles. The color of the substrate is uniform. (B) Peak wavelength, λ_{max}, of 37 substrates with the majority having λ_{max} between 520-530 nm.

In addition, in order to use the substrates for biological sensing applications, an important criterion is that the Au NPs should be stable in solutions with high electrolyte concentration. To test the robustness of the substrate, the Au NPs were incubated in 10 mM PBS buffer for one hour, rinsed several times to complete remove the electrolytes, and dried in N_2. The LSPR spectra of the Au NP substrate before and after incubation in PBS buffer were compared, and no change was observed. To summarize, the method presented in this work result in LSPR substrates that are highly uniform, reproducible and robust against high salt concentration, therefore, could be potentially use as a biosensing platform.

2.5 Conclusions

We have developed a simple self-assembly method to produce highly uniform, robust and reproducible LSPR substrates of randomly distributed gold nanoparticles on silanized glass. The long-range dipole coupling in the gold nanoparticle random array results in a blue-shifted narrow LSPR peak compared to the LSPR of the gold nanoparticles in solution. Theoretical studies by T-matrix method reveal that as the average interparticle distance varies in the random array, both the LSPR wavelength and width varies. Not only the LSPR wavelength, but also the LSPR FWHM of the nanoparticle substrates is sensitive to changes in the dielectric environments around the nanoparticles. Therefore, both the LSPR wavelength and width may be monitored for LSPR sensing applications. The LSPR substrate fabrication is cost-effective, and widely applicable. If combined with other technique such as photolithography, the method would produce multiplexed LSPR chips for sensing and imaging.

2.6 Acknowledgments

This work was funded by the UCONN Startup Fund, the Faculty Large Grant, the National Science Foundation (NSF ECCS-1238738) and the Office of Naval Research (ONR N00014-0-1-1118). We would like to thank Dr. Brunah Otieno for her help with AFM imaging.

2.7 References

1. Henzie, J.; Andrews, S. C.; Ling, X. Y.; Li, Z.; Yang, P., Oriented Assembly of Polyhedral Plasmonic Nanoparticle Clusters. *Proc Natl Acad Sci U S A* **2013,** *110* (17), 6640-5.
2. Henzie, J.; Grunwald, M.; Widmer-Cooper, A.; Geissler, P. L.; Yang, P. D., Self-Assembly of Uniform Polyhedral Silver Nanocrystals into Densest Packings and Exotic Superlattices. *Nat. Mater.* **2012,** *11* (2), 131-137.
3. Li, F.; Josephson, D. P.; Stein, A., Colloidal Assembly: The Road from Particles to Colloidal Molecules and Crystals. *Angew Chem Int Ed Engl* **2011,** *50* (2), 360-88.
4. Rycenga, M.; Cobley, C. M.; Zeng, J.; Li, W.; Moran, C. H.; Zhang, Q.; Qin, D.; Xia, Y., Controlling the Synthesis and Assembly of Silver Nanostructures for Plasmonic Applications. *Chem. Rev.* **2011,** *111* (6), 3669-712.
5. Chuntonov, L.; Haran, G., Trimeric Plasmonic Molecules: The Role of Symmetry. *Nano Lett* **2011,** *11* (6), 2440-2445.
6. Chuntonov, L.; Haran, G., Effect of Symmetry Breaking on the Mode Structure of Trimeric Plasmonic Molecules. *J. Phys. Chem. C* **2011,** *115* (40), 19488-19495.
7. Zou, S. L.; Schatz, G. C., Metal Nanoparticle Array Waveguides: Proposed Structures for Subwavelength Devices. *Phys. Rev. B* **2006,** *74* (12).
8. Halas, N. J.; Lal, S.; Chang, W. S.; Link, S.; Nordlander, P., Plasmons in Strongly Coupled Metallic Nanostructures. *Chem. Rev.* **2011,** *111* (6), 3913-61.
9. Prodan, E.; Radloff, C.; Halas, N. J.; Nordlander, P., A Hybridization Model for the Plasmon Response of Complex Nanostructures. *Science* **2003,** *302* (5644), 419-22.
10. Hicks, E. M.; Zou, S. L.; Schatz, G. C.; Spears, K. G.; Van Duyne, R. P.; Gunnarsson, L.; Rindzevicius, T.; Kasemo, B.; Kall, M., Controlling Plasmon Line Shapes through Diffractive Coupling in Linear Arrays of Cylindrical Nanoparticles Fabricated by Electron Beam Lithography. *Nano Lett.* **2005,** *5* (6), 1065-1070.
11. Tian, X. D.; Zhou, Y. D.; Thota, S.; Zou, S. L.; Zhao, J., Plasmonic Coupling in Single Silver Nanosphere Assemblies by Polarization-Dependent Dark-Field Scattering Spectroscopy. *J. Phys. Chem. C* **2014,** *118* (25), 13801-13808.
12. Hartland, G. V., Optical Studies of Dynamics in Noble Metal Nanostructures. *Chem Rev* **2011,** *111* (6), 3858-87.
13. Fan, J. A.; Wu, C.; Bao, K.; Bao, J.; Bardhan, R.; Halas, N. J.; Manoharan, V. N.; Nordlander, P.; Shvets, G.; Capasso, F., Self-Assembled Plasmonic Nanoparticle Clusters. *Science* **2010,** *328* (5982), 1135-8.
14. Shegai, T.; Li, Z.; Dadosh, T.; Zhang, Z.; Xu, H.; Haran, G., Managing Light Polarization Via Plasmon-Molecule Interactions within an Asymmetric Metal Nanoparticle Trimer. *Proc Natl Acad Sci U S A* **2008,** *105* (43), 16448-53.
15. He, L.; Wang, M.; Ge, J.; Yin, Y., Magnetic Assembly Route to Colloidal Responsive Photonic Nanostructures. *Accounts Of Chemical Research* **2012,** *45* (9), 1431-1440.
16. Wustholz, K. L.; Henry, A.-I.; McMahon, J. M.; Freeman, R. G.; Valley, N.; Piotti, M. E.; Natan, M. J.; Schatz, G. C.; Van Duyne, R. P., Structure-Activity Relationships in Gold Nanoparticle Dimers and Trimers for Surface-Enhanced Raman Spectroscopy. *J. Am. Chem. Soc.* **2010,** *132* (31), 10903-10910.
17. Mayer, K. M.; Hafner, J. H., Localized Surface Plasmon Resonance Sensors. *Chem. Rev.* **2011,** *111* (6), 3828-57.

18. Willets, K. A.; Van Duyne, R. P., Localized Surface Plasmon Resonance Spectroscopy and Sensing. *Annu. Rev. Phys. Chem.* **2007,** *58*, 267-97.
19. Henry, A.-I.; Bingham, J. M.; Ringe, E.; Marks, L. D.; Schatz, G. C.; Van Duyne, R. P., Correlated Structure and Optical Property Studies of Plasmonic Nanoparticles. *J. Phys. Chem. C* **2011,** *115* (19), 9291-9305.
20. McMahon, J. M.; Wang, Y.; Sherry, L. J.; Van Duyne, R. P.; Marks, L. D.; Gray, S. K.; Schatz, G. C., Correlating the Structure, Optical Spectra, and Electrodynamics of Single Silver Nanocubes. *J. Phys. Chem. C* **2009,** *113* (7), 2731-2735.
21. Maier, S. A.; Kik, P. G.; Atwater, H. A., Observation of Coupled Plasmon-Polariton Modes in Au Nanoparticle Chain Waveguides of Different Lengths: Estimation of Waveguide Loss. *Appl. Phys. Lett.* **2002,** *81* (9), 1714-1716.
22. Zhang, J.; Cai, L. K.; Bai, W. L.; Xu, Y.; Song, G. F., Hybrid Plasmonic Waveguide with Gain Medium for Lossless Propagation with Nanoscale Confinement. *Opt Lett* **2011,** *36* (12), 2312-2314.
23. Oulton, R. F.; Sorger, V. J.; Genov, D. A.; Pile, D. F. P.; Zhang, X., A Hybrid Plasmonic Waveguide for Subwavelength Confinement and Long-Range Propagation. *Nat. Photonics* **2008,** *2* (8), 496-500.
24. Sun, M. T.; Hou, Y. X.; Li, Z. P.; Liu, L. W.; Xu, H. X., Remote Excitation Polarization-Dependent Surface Photochemical Reaction by Plasmonic Waveguide. *Plasmonics* **2011,** *6* (4), 681-687.
25. Choi, H.; Chen, W. T.; Kamat, P. V., Know Thy Nano Neighbor. Plasmonic Versus Electron Charging Effects of Metal Nanoparticles in Dye-Sensitized Solar Cells. *ACS Nano* **2012,** *6* (5), 4418-4427.
26. Spinelli, P.; Ferry, V. E.; van de Groep, J.; van Lare, M.; Verschuuren, M. A.; Schropp, R. E. I.; Atwater, H. A.; Polman, A., Plasmonic Light Trapping in Thin-Film Si Solar Cells. *J Optics-Uk* **2012,** *14* (2), 024002.
27. Munday, J. N.; Atwater, H. A., Large Integrated Absorption Enhancement in Plasmonic Solar Cells by Combining Metallic Gratings and Antireflection Coatings. *Nano Lett.* **2011,** *11* (6), 2195-2201.
28. Ferry, V. E.; Sweatlock, L. A.; Pacifici, D.; Atwater, H. A., Plasmonic Nanostructure Design for Efficient Light Coupling into Solar Cells. *Nano Lett.* **2008,** *8* (12), 4391-4397.
29. Mubeen, S.; Lee, J.; Lee, W. R.; Singh, N.; Stucky, G. D.; Moskovits, M., On the Plasmonic Photovoltaic. *ACS Nano* **2014,** *8* (6), 6066-6073.
30. Paci, B.; Bailo, D.; Albertini, V. R.; Wright, J.; Ferrero, C.; Spyropoulos, G. D.; Stratakis, E.; Kymakis, E., Spatially-Resolved in-Situ Structural Study of Organic Electronic Devices with Nanoscale Resolution: The Plasmonic Photovoltaic Case Study. *Adv. Mater.* **2013,** *25* (34), 4760-4765.
31. Bingham, J. M.; Anker, J. N.; Kreno, L. E.; Van Duyne, R. P., Gas Sensing with High-Resolution Localized Surface Plasmon Resonance Spectroscopy. *J. Am. Chem. Soc.* **2010,** *132* (49), 17358-17359.
32. Kreno, L. E.; Hupp, J. T.; Van Duyne, R. P., Metal-Organic Framework Thin Film for Enhanced Localized Surface Plasmon Resonance Gas Sensing. *Anal. Chem.* **2010,** *82* (19), 8042-8046.
33. Bendikov, T. A.; Rabinkov, A.; Karakouz, T.; Vaskevich, A.; Rubinstein, I., Biological Sensing and Interface Design in Gold Island Film Based Localized Plasmon Transducers. *Anal. Chem.* **2008,** *80* (19), 7487-7498.

34. Zhao, J.; Das, A.; Schatz, G. C.; Sligar, S. G.; Van Duyne, R. P., Resonance Localized Surface Plasmon Spectroscopy: Sensing Substrate and Inhibitor Binding to Cytochrome P450. *J. Phys. Chem. C* **2008,** *112* (34), 13084-13088.
35. Larsson, E. M.; Alegret, J.; Kall, M.; Sutherland, D. S., Sensing Characteristics of Nir Localized Surface Plasmon Resonances in Gold Nanorings for Application as Ultrasensitive Biosensors. *Nano Lett.* **2007,** *7* (5), 1256-1263.
36. Anker, J. N.; Hall, W. P.; Lyandres, O.; Shah, N. C.; Zhao, J.; Van Duyne, R. P., Biosensing with Plasmonic Nanosensors. *Nat. Mater.* **2008,** *7* (6), 442-453.
37. Aslan, K.; Lakowicz, J. R.; Geddes, C. D., Rapid Deposition of Triangular Silver Nanoplates on Planar Surfaces: Application to Metal-Enhanced Fluorescence. *J. Phys. Chem. B* **2005,** *109* (13), 6247-6251.
38. Brown, L. V.; Zhao, K.; King, N.; Sobhani, H.; Nordlander, P.; Halas, N. J., Surface-Enhanced Infrared Absorption Using Individual Cross Antennas Tailored to Chemical Moieties. *J. Am. Chem. Soc.* **2013,** *135* (9), 3688-3695.
39. Geddes, C. D.; Cao, H.; Gryczynski, I.; Gryczynski, Z.; Fang, J. Y.; Lakowicz, J. R., Metal-Enhanced Fluorescence (Mef) Due to Silver Colloids on a Planar Surface: Potential Applications of Indocyanine Green to in Vivo Imaging. *J. Phys. Chem. A* **2003,** *107* (18), 3443-3449.
40. Jeanmaire, D. L.; Van Duyne, R. P., Surface Raman Spectroelectrochemistry: Part I. Heterocyclic, Aromatic, and Aliphatic Amines Adsorbed on the Anodized Silver Electrode. *J. Electroanal. Chem. Interfac.* **1977,** *84* (1), 1-20.
41. Moskovits, M., Surface-Enhanced Spectroscopy. *Rev. Mod. Phys.* **1985,** *57* (3), 783-826.
42. Tian, X.-D.; Liu, B.-J.; Li, J.-F.; Yang, Z.-L.; Ren, B.; Tian, Z.-Q., Shiners and Plasmonic Properties of Au Core Sio2shell Nanoparticles with Optimal Core Size and Shell Thickness. *J Raman Spectrosc* **2013,** *44* (7), 994-998.
43. Tian, Z. Q., Surface-Enhanced Raman Spectroscopy: Advancements and Applications. *J Raman Spectrosc* **2005,** *36* (6-7), 466-470.
44. Ataka, K.; Giess, F.; Knoll, W.; Naumann, R.; Haber-Pohlmeier, S.; Richter, B.; Heberle, J., Oriented Attachment and Membrane Reconstitution of His-Tagged Cytochrome C Oxidase to a Gold Electrode: In Situ Monitoring by Surface-Enhanced Infrared Absorption Spectroscopy. *J. Am. Chem. Soc.* **2004,** *126* (49), 16199-16206.
45. Hicks, E. M.; Zhang, X.; Zou, S.; Lyandres, O.; Spears, K. G.; Schatz, G. C.; Van Duyne, R. P., Plasmonic Properties of Film over Nanowell Surfaces Fabricated by Nanosphere Lithography. *J Phys Chem B* **2005,** *109* (47), 22351-8.
46. Zhang, X.; Hicks, E. M.; Zhao, J.; Schatz, G. C.; Van Duyne, R. P., Electrochemical Tuning of Silver Nanoparticles Fabricated by Nanosphere Lithography. *Nano Lett* **2005,** *5* (7), 1503-7.
47. Ormonde, A. D.; Hicks, E. C.; Castillo, J.; Van Duyne, R. P., Nanosphere Lithography: Fabrication of Large-Area Ag Nanoparticle Arrays by Convective Self-Assembly and Their Characterization by Scanning Uv-Visible Extinction Spectroscopy. *Langmuir : the ACS journal of surfaces and colloids* **2004,** *20* (16), 6927-31.
48. Kim, S.; Marelli, B.; Brenckle, M. A.; Mitropoulos, A. N.; Gil, E. S.; Tsioris, K.; Tao, H.; Kaplan, D. L.; Omenetto, F. G., All-Water-Based Electron-Beam Lithography Using Silk as a Resist. *Nat Nanotechnology* **2014,** *9* (4), 306-310.
49. Haynes, C. L.; McFarland, A. D.; Zhao, L. L.; Van Duyne, R. P.; Schatz, G. C.; Gunnarsson, L.; Prikulis, J.; Kasemo, B.; Kall, M., Nanoparticle Optics: The Importance of Radiative Dipole

Coupling in Two-Dimensional Nanoparticle Arrays. *J. Phys. Chem. B* **2003,** *107* (30), 7337-7342.
50. Zou, S. L.; Janel, N.; Schatz, G. C., Silver Nanoparticle Array Structures That Produce Remarkably Narrow Plasmon Lineshapes. *J. Chem. Phys.* **2004,** *120* (23), 10871-10875.
51. Wang, L.; Nishijima, Y.; Ueno, K.; Misawa, H.; Tamai, N., Effect of Dipole Coupling on near-Ir Lspr and Coherent Phonon Vibration of Periodic Gold Pair Nanocuboids. *J. Phys. Chem. C* **2012,** *116* (33), 17838-17846.
52. Weick, G.; Woollacott, C.; Barnes, W. L.; Hess, O.; Mariani, E., Dirac-Like Plasmons in Honeycomb Lattices of Metallic Nanoparticles. *Phys. Rev. Lett.* **2013,** *110* (10), 106801.
53. Kravets, V. G.; Schedin, F.; Grigorenko, A. N., Extremely Narrow Plasmon Resonances Based on Diffraction Coupling of Localized Plasmons in Arrays of Metallic Nanoparticles. *Phys. Rev. Lett.* **2008,** *101* (8).
54. Auguie, B.; Barnes, W. L., Collective Resonances in Gold Nanoparticle Arrays. *Phys. Rev. Lett.* **2008,** *101* (14).
55. Chu, Y. Z.; Schonbrun, E.; Yang, T.; Crozier, K. B., Experimental Observation of Narrow Surface Plasmon Resonances in Gold Nanoparticle Arrays. *Appl. Phys. Lett.* **2008,** *93* (18).
56. Feichtenschlager, B.; Pabisch, S.; Peterlik, H.; Kickelbick, G., Nanoparticle Assemblies as Probes for Self-Assembled Monolayer Characterization: Correlation between Surface Functionalization and Agglomeration Behavior. *Langmuir : the ACS journal of surfaces and colloids* **2012,** *28* (1), 741-750.
57. Feichtenschlager, B.; Lornoschitz, C. J.; Kickelbick, G., Tuning the Self-Assembled Monolayer Formation on Nanoparticle Surfaces with Different Curvatures: Investigations on Spherical Silica Particles and Plane-Crystal-Shaped Zirconia Particles. *J Colloid Interf Sci* **2011,** *360* (1), 15-25.
58. Chen, H. J.; Wang, Y. L.; Qu, J. Y.; Dong, S. J., Self-Assembled Silver Nanoparticle Monolayer on Glassy Carbon: An Approach to Sers Substrate. *J Raman Spectrosc* **2007,** *38* (11), 1444-1448.
59. Peng, Z. Q.; Qu, X. H.; Dong, S. J., Immobilization of the Nanoparticle Monolayer onto Self-Assembled Monolayers by Combined Sterically Enhanced Hydrophobic and Electrophoretic Forces. *Langmuir : the ACS journal of surfaces and colloids* **2004,** *20* (1), 5-10.
60. Nakanishi, T.; Ohtani, B.; Uosaki, K., Fabrication and Characterization of Cds-Nanoparticle Mono- and Multilayers on a Self-Assembled Monolayer of Alkanedithiols on Gold. *J. Phys. Chem. B* **1998,** *102* (9), 1571-1577.
61. Freeman, R. G.; Grabar, K. C.; Allison, K. J.; Bright, R. M.; Davis, J. A.; Guthrie, A. P.; Hommer, M. B.; Jackson, M. A.; Smith, P. C.; Walter, D. G.; Natan, M. J., Self-Assembled Metal Colloid Monolayers - an Approach to Sers Substrates. *Science* **1995,** *267* (5204), 1629-1632.
62. He, P. L.; Hu, N. F.; Rusling, J. F., Driving Forces for Layer-by-Layer Self-Assembly of Films of Sio2 Nanoparticles and Heme Proteins. *Langmuir : the ACS journal of surfaces and colloids* **2004,** *20* (3), 722-729.
63. Zhou, Y. L.; Li, Z.; Hu, N. F.; Zeng, Y. H.; Rusling, J. F., Layer-by-Layer Assembly of Ultrathin Films of Hemoglobin and Clay Nanoparticles with Electrochemical and Catalytic Activity. *Langmuir : the ACS journal of surfaces and colloids* **2002,** *18* (22), 8573-8579.
64. Kim, J. Y.; DeRocher, J. P.; Mao, P.; Han, J.; Cohen, R. E.; Rubner, M. F., Formation of Nanoparticle-Containing Multilayers in Nanochannels Via Layer-by-Layer Assembly. *Chem. Mater.* **2010,** *22* (23), 6409-6415.

65. Bonk, S. M.; Lisdat, F., Layer-by-Layer Assembly of Electro-Active Gold Nanoparticle/Cytochrome C Multilayers. *Biosens. Bioelectron.* **2009,** *25* (4), 739-744.
66. Wang, F.; Peters, S.; Guzda, J.; Blunk, R. H.; Angelopoulos, A. P., Silica Nanoparticle Layer-by-Layer Assembly on Gold. *Langmuir : the ACS journal of surfaces and colloids* **2009,** *25* (8), 4384-4392.
67. Lu, C. H.; Donch, I.; Nolte, M.; Fery, A., Au Nanoparticle-Based Multilayer Ultrathin Films with Covalently Linked Nanostructures: Spraying Layer-by-Layer Assembly and Mechanical Property Characterization. *Chem. Mater.* **2006,** *18* (26), 6204-6210.
68. Mishchenko, M. I.; Travis, L. D.; Mackowski, D. W., T-Matrix Computations of Light Scattering by Nonspherical Particles: A Review. *J Quant Spectrosc Ra* **1996,** *55* (5), 535-575.
69. Frens, G., Controlled Nucleation for the Regulation of the Particle Size in Monodisperse Gold Suspensions. *Nature Physical Science* **1973,** *241*, 20-22.
70. Nath, N.; Chilkoti, A., A Colorimetric Gold Nanoparticle Sensor to Interrogate Biomolecular Interactions in Real Time on a Surface. *Anal Chem* **2002,** *74* (3), 504-9.
71. Scarpettini, A. F.; Bragas, A. V., Coverage and Aggregation of Gold Nanoparticles on Silanized Glasses. *Langmuir : the ACS journal of surfaces and colloids* **2010,** *26* (20), 15948-53.
72. Fujiwara, K.; Watarai, H.; Itoh, H.; Nakahama, E.; Ogawa, N., Measurement of Antibody Binding to Protein Immobilized on Gold Nanoparticles by Localized Surface Plasmon Spectroscopy. *Anal. Bioanal. Chem.* **2006,** *386* (3), 639-644.
73. Grabar, K. C.; Freeman, R. G.; Hommer, M. B.; Natan, M. J., Preparation and Characterization of Au Colloid Monolayers. *Anal. Chem.* **1995,** *67* (4), 735-743.
74. Palik, E. D., *Handbook of Optical Constants of Solids* Academic Press: Boston, 1998.
75. Bedeaux, D.; Vlieger, J., *Optical Properties of Surfaces*. 2nd ed.; Imperial College Press: 2004; p 450.
76. Wang, M.; Pan, N., Predictions of Effective Physical Properties of Complex Multiphase Materials. *Mat Sci Eng R* **2008,** *63* (1), 1-30.
77. Atay, T.; Song, J.-H.; Nurmikko, A. V., Strongly Interacting Plasmon Nanoparticle Pairs: From Dipole−Dipole Interaction to Conductively Coupled Regime. *Nano Lett.* **2004,** *4* (9), 1627-1631.
78. Bois, L.; Chassagneux, F.; Desroches, C. d.; Battie, Y.; Destouches, N.; Gilon, N.; Parola, S. p.; Stéphan, O., Electroless Growth of Silver Nanoparticles into Mesostructured Silica Block Copolymer Films. *Langmuir : the ACS journal of surfaces and colloids* **2010,** *26* (11), 8729-8736.
79. Jain, P. K.; Huang, W.; El-Sayed, M. A., On the Universal Scaling Behavior of the Distance Decay of Plasmon Coupling in Metal Nanoparticle Pairs: A Plasmon Ruler Equation. *Nano Lett.* **2007,** *7* (7), 2080-2088.
80. Willets, K. A.; Van Duyne, R. P., Localized Surface Plasmon Resonance Spectroscopy and Sensing. *Annu. Rev. Phys. Chem.* **2007,** *58*, 267-297.
81. Lee, M. H.; Gao, H. W.; Odom, T. W., Refractive Index Sensing Using Quasi One-Dimensional Nanoslit Arrays. *Nano Lett.* **2009,** *9* (7), 2584-2588.
82. McMahon, J. M.; Henzie, J.; Odom, T. W.; Schatz, G. C.; Gray, S. K., Tailoring the Sensing Capabilities of Nanohole Arrays in Gold Films with Rayleigh Anomaly-Surface Plasmon Polaritons. *Opt Express* **2007,** *15* (26), 18119-18129.
83. Malinsky, M. D.; Kelly, K. L.; Schatz, G. C.; Van Duyne, R. P., Chain Length Dependence and Sensing Capabilities of the Localized Surface Plasmon Resonance of Silver Nanoparticles

Chemically Modified with Alkanethiol Self-Assembled Monolayers. *J. Am. Chem. Soc.* **2001,** *123* (7), 1471-1482.
84. Sherry, L. J.; Chang, S. H.; Schatz, G. C.; Van Duyne, R. P.; Wiley, B. J.; Xia, Y. N., Localized Surface Plasmon Resonance Spectroscopy of Single Silver Nanocubes. *Nano Lett.* **2005,** *5* (10), 2034-2038.

Chapter Three :

Investigation of Temperature Dependent Photoluminescence Decay Kinetics in Quantum Dot – PNIPAM – Au Hybrid Nanocomplexes

3.1 Abstract

In this study, we demonstrated the synthesis, characterization and temperature dependent photoluminescence decay kinetics involving local stimuli responsive hybrid nano-assemblies consisting of the thermo-responsive polymer α-carboxy-ω-Thiol terminated Poly(N-isopropyl acrylamide) (PNIPAM), gold nanoparticle random arrays and CdTe/ZnTe core/shell quantum dots. The synergistic effect of plasmon-exciton coupling between Au NPs and QDs has been studied by exploiting the temperature dependent swelling/deswelling nature of PNIPAM polymer. The interparticle distance and therefore the extent of interaction between the Au NPs and QDs was effectively controlled by modulating the temperature of the hybrid system above and below lower critical solution temperature (LCST) of the polymer. Non-radiative energy transfer processes such as FRET are likely responsible for significant quenching of the photoluminescence emission of QDs in our system. The distance and interactions between the Au NPs and the QDs is controlled by the temperature, thus the variable contribution of the non-radiative energy transfer is also temperature-dependent.

3.2 Introduction

Localized surface plasmon resonance (LSPR) of nanoparticles can modify the fluorescence intensity and lifetime of molecules or quantum dots (QDs) when the particles are close together.[1-3] QDs are semiconductor nanocrystals that have unique size dependent optical properties[4-6]. Their

excitation spectra are very broad, and they have very narrow fluorescence emission spectra. QDs are used in many applications from tissue imaging and bio-detection, to nanoelectronics[7-9]. When placed next to gold nanoparticles, depending on the configuration of the system, the photoluminescence (PL) of the QDs can be either enhanced[10-12] or quenched[13-14], due to the interaction between the QD and the metal surface. The efficiency for non-radiative energy transfer increases as the QD gets closer to the gold.[9, 15-18] To control the interparticle distance, many types of dielectric spacers have been used, including silica[7, 17, 19-21], polymers[3, 22], DNA[14, 23-25], and antigen-antibody pairs[26]. Recently, thermo-responsive poly(N-isopropylacrylamide) (PNIPAM) shell has gained much attention for its excellent responsiveness to environmental temperatures, with many applications focusing on thermo-responsive microgels in solution.[15, 27-35] PNIPAM can undergo a sharp volume phase transition at a lower critical solution temperature (LCST) of about 32°C.[36-41] Below the critical transition, the PNIPAM is hydrophilic and disperses well in an aqueous solution. But above the LCST, it becomes more hydrophobic and the chains of the polymers collapse and shrink in aqueous solution[30, 42]. PNIPAM has been widely studied and applied in optical and electronic devices[43-45], responsive surfaces[46-49], drug delivery[30, 50], sensors[30, 51-53], biomedical applications[54-61], and many other areas[62-64].

In this work, the distance between the QD and Au NP is controlled by using α-carboxy-ω-Thiol terminated Poly(N-isopropyl acrylamide). The thiol group on the PNIPAM allows binding to gold. When the QD is adsorbed to the polymer, its distance from the Au NP should change based on the temperature of the solution. This will ultimately affect the luminescence of the QD and a temperature dependent change in the PL decay of the QD is observed.

3.3 Experimental Methods

3.3.1 Chemicals and Materials

Gold (III) chloride trihydrate ($HAuCl_4$), hydroxylamine hydrochloride ($NH_2OH{\cdot}HCl$), 3-aminopropyltriethoxysilane (APTES), cadmium perchlorate, zinc perchlorate, L-cysteine, tellurium powder, sodium hydroxide and sodium borohydride were purchased from Sigma-Aldrich. Sodium citrate, methanol, ethanol, hydrochloric acid, and glass coverslips (22x22mm, #2) were purchased from Fisher Scientific.

3.3.2 Methods

3.3.2.1 Synthesis of Gold Nanoparticles

The 120 nm Au NPs were synthesized by a two-step seed-mediated process according to previous work. The details can be found in the experimental methods section of chapter 2 (2.3.2.1).

3.3.2.2 Synthesis of Cadmium Telluride/Zinc Telluride Core/Shell Quantum Dots

The quantum dots (QD) were synthesized according to previous work[4]. The tellurium precursor, NaHTe, was prepared by adding 96 mg of tellurium powder and 58 mg of sodium borohydride in 10 mL of nitrogen saturation. The solution was placed in an ice bath and stirred for ~6 hours until it turned a light purple/pink color. The cadmium and zinc precursor was prepared by adding 0.50 g of cadmium perchlorate and 0.89 g of zinc perchlorate in 125 mL of nitrogen saturated DI water. L-cysteine was used as the capping agent and 0.42 g was added to the cadmium/zinc solution. This solution was brought to pH ~11 by the addition of NaOH drop by drop. The solution will turn a milky color, and NaOH is added until the solution is once again

clear. The solution is stirred for 3 hours. Once both precursors are ready, 5 mL of the NaHTe solution is injected into the Cd/Zn/cysteine solution under a reflux setup. The temperature is set to 95°C and as time proceeds, the QDs grow to larger sizes. The fluorescence color of the QDs will start at green, then turn to yellow, orange and finally red. When the desired size quantum dot is achieved, a sample is pulled from the solution for further use. After pulling out samples of green and yellow QDs, the temperature is r aised to 160°C to obtain the larger red QDs. The samples are put in the fridge overnight to allow contaminants to precipitate out. The QD solution is decanted off and further purified by centrifugation in ethanol.

3.3.2.3 Gold Nanoparticle Random Array Substrate Preparation

The gold nanoparticle random arrays are produced by adsorption of Au NPs to a silanized glass substrate. Details of the procedure for substrate preparation can be found in the experimental methods section of chapter 2 (2.3.2.2 and 2.3.2.3).

3.3.2.4 Adsorption of PNIPAM and CdTe/ZnTe Quantum Dots to the Au Nanoparticle Substrate

A 2 mg per mL solution of PNIPAM was prepared in DI water for attachment to Au NPs. The Au NP substrate was placed the PNIPAM solution for 1 hour, then rinsed lightly with DI water. The Au – PNIPAM substrate was kept in water to keep the polymer in its extended form. The CdTe/ZnTe QDs (400 uL) were drop coated onto the Au – PNIPAM substrate and left for 1 hour. After 1 hour, the substrate was rinsed with DI water to remove the free QDs, and placed in a 50 mL beaker with 20 mL of DI water.

3.3.2.5 Experimental design

A 120 nm Au NP random array immobilized on a silanized glass substrate was used as the gold source. The distance between the 120 nm Au NP and CdTe/ZnTe QDs was controlled by PNIPAM as shown in **Scheme 3.1**. PNIPAM will change from a swollen state at room temperature, to a collapsed state at temperatures higher than 33°C.

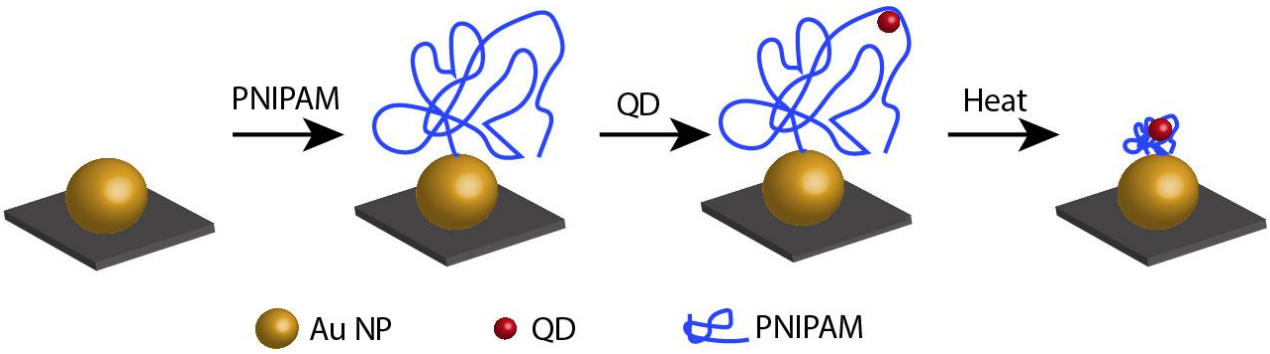

Scheme 3.1. Experimental design of QD – PNIPAM – Au hybrid nanocomplexes. 120 nm Au NPs are immobilized on a silanized glass substrate in a random array. PNIPAM is attached to the Au NP via thiol bond. The QD is then adsorbed to the polymer. At room temperature, the polymer is in its swollen state. Heat is applied at a temperature above the lower critical solution temperature of the polymer, causing the polymer to collapse on itself, thus bringing the QD closer to the Au NP. The ensemble PL lifetime at both temperatures is obtained to study the temperature dependent decay dynamics of the QD – PNIPAM – Au nanocomplex. Figures are not to scale.

3.3.2.6 Optical and Structural Characterization

A UV-vis spectrometer (Cary 60, Agilent Technologies) was used to determine the extinction spectrum of the gold nanoparticles in solution. A spectrofluorometer (FluoroMax Plus, Horiba Scientific) was used to obtain the solution ensemble emission spectra of the various sized

quantum dots dispersed in water. A home-built LSPR setup was used to measure the UV-vis extinction spectra of the immobilized Au NPs on the glass substrate, as well as the immobilized Au – PNIPAM and Au – PNIPAM – QD nanocomplex on the glass substrate. In this setup, a halogen light source was fiber coupled and focused with convex lens on the Au NPs to a spot of ~ 0.5 cm diameter. The transmitted light after passing through the Au NPs was focused onto a fiber coupled spectrometer (QE65 Pro, Ocean Optics). The substrates were placed in a home-built flow cell to allow incubation in water. The scanning electron microscopy (SEM) image of the Au NPs on glass was obtained with JEOL JSM-6330F.

All the optical measurements were performed using a home-built epifluorescence Nikon Ti-U microscope. The quantum dots were excited with a 405 nm pulsed laser (pulse width of 40 ps and repetition rate of 2.5 MHz, PicoQuant). The emission signal was collected through a 40x Nikon air-objective using an avalanche photodiode (τ-SPAD, PicoQuant) equipped with a 435 nm long-pass filter. The fluorescence decay was recorded using a time-dependent single photon counting module PicoHarp 300 (PicoQuant) with a timing resolution of 32 ps. The PL image of the sample was taken using a CCD camera (Pixis 1024, Princeton Instruments) coupled to a spectrometer (IsoPlane SCT 320).

3.4 Results and Discussion

3.4.1 Characterization of Au – PNIPAM – QD substrate

In this work, the temperature dependent photoluminescence decay kinetics of cadmium telluride/zinc telluride (CdTe/ZnTe) core/shell quantum dots (QD) is investigated when they were placed near gold nanoparticles (Au NPs) by using α-carboxy-ω-Thiol terminated Poly(N-isopropyl acrylamide) (PNIPAM) as a spacer between the two types of particles. Thermo-responsive

polymers, such as PNIPAM, contain both hydrophilic and hydrophobic moieties. At temperatures below the lower critical solution temperature (LCST), water is a good solvent and the polymer chains exits as coils. The substrate was kept in water throughout the experiment to keep the polymer in its extended state. PNIPAM was attached to the Au NPs via a strong thiol-gold bond and the polymer chains wrap randomly wrap around the Au NPs. After PNIPAM binding to the Au NP random array, a dilute sample of QDs was randomly distributed on the polymer, creating an Au – PNIPAM – QD nanocomplex. The localized surface plasmon resonance (LSPR) of the immobilized Au NP substrate was taken to ensure binding of the PNIPAM to the Au NPs by the observation of a peak wavelength shift (**Figure 3.1A**). Therefore, the LSPR of the Au NP random array substrate was also taken in water using the home built flow cell and LSPR setup. A 23 nm red shift of the Au NP random array LSPR peak wavelength in water was observed (**Figure 3.1A**, red dashed line) from that of the Au NP random array in air (**Figure 3.1A**, black solid line). After the addition of PNIPAM, the LSPR of the substrate was taken again in water and a small 5 nm red shift is observed (**Figure 3.1A**, blue dashed line) indicating the polymer was successfully bound to the Au NP. The LSPR after the addition of the QDs was also taken (data not show), but no observable shift occurred. It is believed the amount of QDs attaching is so minimal that the sensitivity of the setup is not high enough to detect their presence.

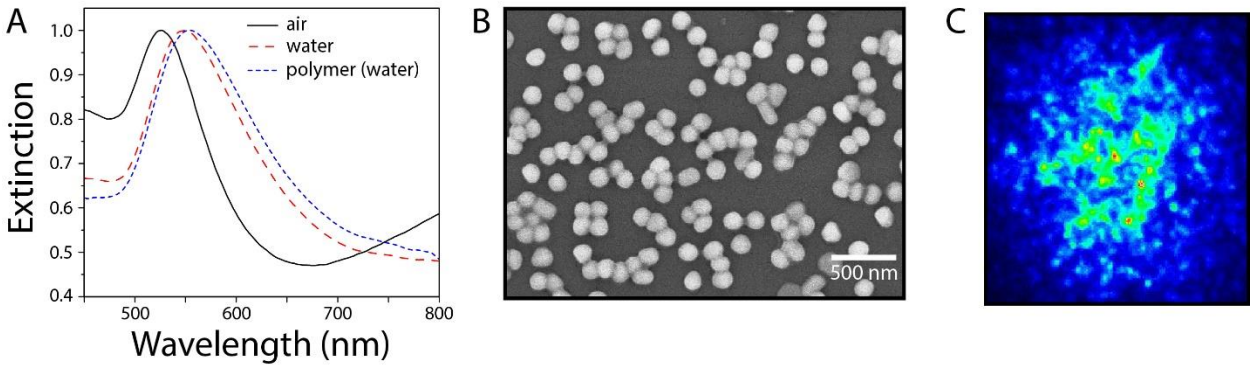

Figure 3.1. Characterization of polymer embedded Au NP substrates. (A) Extinction spectra of the Au NP random array in air (black solid line, λ_{max} = 526 nm), the Au NP random array with water as the solvent surrounding the Au NPs (red dashed line, λ_{max} = 549 nm) and the Au NP with PNIPAM random array with water as the solvent (blue dashed line, λ_{max} = 554 nm) The addition of water as the solvent creates a large red shift of the LSPR peak due to the dielectric environment change. After the addition of PNIPAM, the environment around the particles is changed slightly and this change can be observed in the small 5 nm red shift from the spectrum of just Au NPs on glass in water. The addition of QDs does not shift the Au – PNIPAM peak (data not shown). (B) SEM image of 120 nm Au – PNIPAM – QD nanocomplexes on glass substrate. The Au NPs are the white spheres. PNIPAM can be seen around the Au NPs as well as in between particles. (C) The wide-field image of photoluminescence of large batches of QDs. Observing green, yellow and red PL intensities shows QDs are present on the substrate.

The scanning electron microscopy (SEM) image of the Au – PNIPAM – QD substrate was obtained (**Figure 3.1B**) to further characterize the nanocomplex substrate. The polymer can be seen surrounding individual or clusters of Au NPs, as well as in between particles. The QDs are not visible in the image because, the characterization techniques used did not have high enough resolution to resolve the small QDs of less than 10 nm in size. To ensure the QDs were adsorbed

on the substrate, the PL image of the sample was taken (**Figure 3.1C**). It is evident from the image that the QDs were indeed adsorbed on the substrate.

3.4.2 Temperature-dependent PL decay

In our system, three different sized quantum dots are studied. There is good spectral overlap between the emission spectra of all three QDs and the extinction spectrum of the 120 nm Au NPs in solution (**Figure 3.2A**). The large spectral overlap will promote the plasmon-exciton interaction between the QDs and the Au NPs. The distance between the QDs and Au is controlled via temperature induced swelling and deswelling of PNIPAM layer. This change in the polymer layer in turn influences the PL decay rates of the QDs. The fluorescence color of the possible sized water-soluble QDs synthesized in our lab is shown in **Figure 3.3B**. Only red (λ_{em} = 620 nm), yellow (λ_{em} = 575 nm) and green (λ_{em} = 547 nm) QDs were used for lifetime measurements. The QDs are labeled in this work by the color of their fluorescence.

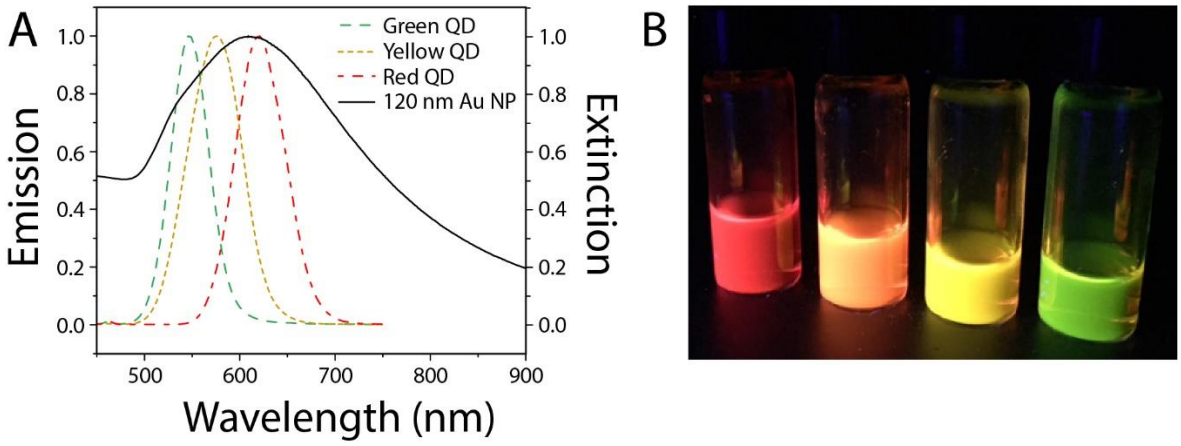

Figure 3.2. Emission of CdTe/ZnTe quantum dots and extinction of 120 nm gold nanoparticles. (A) The extinction spectra of 120 nm Au NPs (black solid line) in solution with an LSPR peak at 610 nm overlaps with the emission spectrum of all three of the different sized QDs (excited with a wavelength of 400 nm). The largest red QDs (red dashed line) have the greatest overlap with an emission peak at 620 nm, followed by the yellow QDs (yellow dashed line) with an emission peak at 575 nm, and the emission of the green QDs (green dashed line) with a peak at 547 nm. (B) An image of the various colors of QD solutions synthesized. The solutions are being excited by a UV-lamp with a wavelength of 365 nm. Only the green, yellow and red QDs were used for further studies.

The central focus of analysis in the hybrid Au – PNIPAM – QD platform was via temperature variation. PNIPAM has a lower critical solution temperature (LCST) of ~30-33°C. Below this temperature, the amide groups of the polymer are hydrogen bonding with the solvent making the polymer hydrophilic, and in a swollen state. When the solution is raised above the LCST of the polymer, the intra- and inter-molecular hydrogen bonding is stronger causing the polymer to collapse on itself, therefore condensing it's structure[65]. As the nanocomplex is heated,

the polymer collapses, moving the QDs closer to the Au NP than they are at room temperature (swollen state). Due to this temperature-dependent behavior of PNIPAM, the distance of the nanocrystals to the Au NP substrates can be controlled via temperature changes.

The decay kinetics of the nanocomplex was studied by collecting ensemble time-dependent PL on the nanocomplex substrate. Due to the randomness of the Au NP array and the QD adsorption, the QD to Au NP ratio was not well controlled. The temperature response on alteration the PL decay of the QDs was studied under hot and cold conditions. The temperature of the hybrid system was varied between 25-75^{0}C. The Au – PNIPAM – QD substrate was placed in a beaker with water. The beaker was then placed on a hot plate and heated to 75°C. Once at the desired temperature for at least 45 minutes, the beaker was moved from the hot plate to the microscope and the lifetime data was taken hot. The temperature dropped quickly off of heat, meaning the temperature was not well controlled and varied as the lifetime measurement was taking place. The temperature dropped to ~60°C by the end of the measurement, but was still well above the LCST of the PNIPAM. After taking the lifetime hot, the beaker was left to cool to room temperature. Once at room temperature for at least 45 minutes, the lifetime of the nanocomplex was taken cold (25°C).

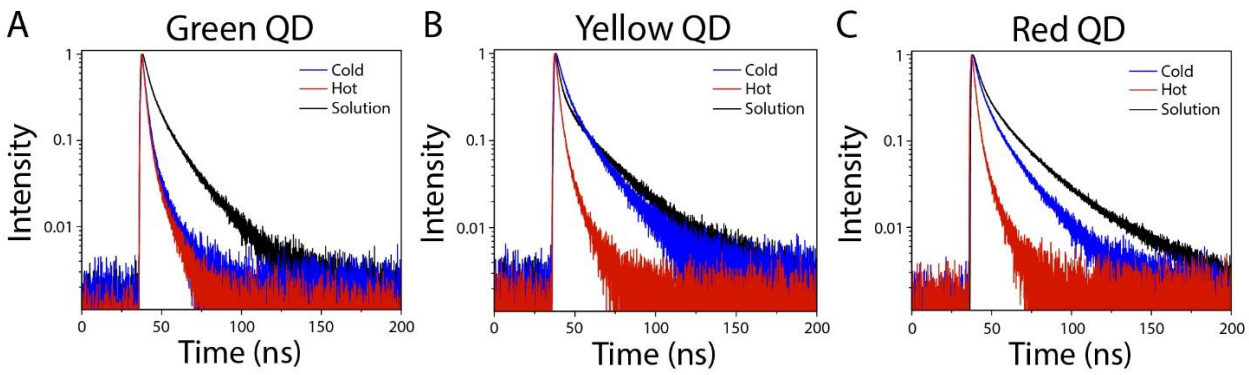

Figure 3.3. Time-dependent PL decay of CdTe/ZnTe quantum dots near Au – PNIPAM random array. (A) The hot (red line) and cold (blue line) PL lifetime data is shown on Au – PNIPAM substrates, along with the solution lifetime date (black line) with green (A), yellow (B) and red (C) QDs. The PL lifetime of all QDs on the Au – PNIPAM substrate are faster from their solution lifetimes. The lifetime of the red and yellow QDs is decreased when closer to the gold (hot) as seen in figure (B) and (C) red lines. This same phenomenon is not observed with the green QDs.

As observed in **Figure 3.3** from the PL decay curves of QDs adsorbed on Au-PNIPAM substrate, all the QDs exhibit faster decay when placed near the Au NP array (**Figure 3.3**, **blue and red lines**), than when they were in solution (**Figure 3.3**, **black lines**). The yellow (**Figure 3.3B**) and red (**Figure 3.3C**) QDs also show a faster decay when the temperature is increased above the LCST of the PNIPAM. The results of the red and yellow QDs follow our hypothesis of temperature dependent photoluminescence decay dynamics in a QD –PNIPAM – Au Hybrid nanocomplex. The green QDs, surprisingly, showed only small changes between the hot and cold measurements. It is believed that the experimental setup may have been a factor that leads to these results. The decay kinetics of the QDs was found to be temperature dependent in the QD – PNIPAM – Au Hybrid nanocomplex.

3.5 Conclusion

In conclusion, we have demonstrated in the successful creation of a thermo-responsive QD – PNIPAM – gold nanoparticle hybrid random array platform. We studied the temperature dependent photoluminescence decay kinetics of QDs when they are attached to a PNIPAM-coated gold nanoparticle random array. The interparticle distance, and therefore the extent of interaction between the Au NPs and QDs, was effectively controlled by modulating the temperature of the hybrid system above and below lower critical solution temperature (LCST) of the polymer. The rates of non-radiative processes radiative processes of QDs when placed near the Au NP random array, depend most likely on the interparticle distance. More control studies as well as an improved experimental design is needed in future work to reproduce the results of this work. The outcome of those studies will help in developing a PL based temperature sensor.

3.6 Acknowledgments

This work was funded by the UCONN start up fund. I would like to thank Dr. Swayandipta Dey for his help in obtaining the lifetime decay results, and Xudong Wang for the helpful discussions.

3.7 References

1. Pelton, M., Modified Spontaneous Emission in Nanophotonic Structures. *Nature Photonics* **2015,** *9* (7), 427-435.
2. Zhao, W.-W.; Yu, P.-P.; Shan, Y.; Wang, J.; Xu, J.-J.; Chen, H.-Y., Exciton-Plasmon Interactions between Cds Quantum Dots and Ag Nanoparticles in Photoelectrochemical System and Its Biosensing Application. *Anal. Chem.* **2012,** *84* (14), 5892-5897.
3. Chan, Y.-H.; Chen, J.; Wark, S. E.; Skiles, S. L.; Son, D. H.; Batteas, J. D., Using Patterned Arrays of Metal Nanoparticles to Probe Plasmon Enhanced Luminescence of Cdse Quantum Dots. *Acs Nano* **2009,** *3* (7), 1735-1744.
4. Law, W. C.; Yong, K. T.; Roy, I.; Ding, H.; Hu, R.; Zhao, W.; Prasad, P. N., Aqueous-Phase Synthesis of Highly Luminescent Cdte/Znte Core/Shell Quantum Dots Optimized for Targeted Bioimaging. *Small* **2009,** *5* (11), 1302-1310.
5. Medintz, I. L.; Uyeda, H. T.; Goldman, E. R.; Mattoussi, H., Quantum Dot Bioconjugates for Imaging, Labelling and Sensing. *Nat Mater* **2005,** *4* (6), 435-446.
6. Achermann, M., Exciton− Plasmon Interactions in Metal− Semiconductor Nanostructures. *The Journal of Physical Chemistry Letters* **2010,** *1* (19), 2837-2843.
7. Dey, S.; Zhou, Y.; Tian, X.; Jenkins, J. A.; Chen, O.; Zou, S.; Zhao, J., An Experimental and Theoretical Mechanistic Study of Biexciton Quantum Yield Enhancement in Single Quantum Dots near Gold Nanoparticles. *Nanoscale* **2015,** *7* (15), 6851-6858.
8. Alivisatos, P., The Use of Nanocrystals in Biological Detection. *Nat. Biotechnol.* **2004,** *22* (1), 47-52.
9. Ozel, T.; Hernandez-Martinez, P. L.; Mutlugun, E.; Akin, O.; Nizamoglu, S.; Ozel, I. O.; Zhang, Q.; Xiong, Q.; Demir, H. V., Observation of Selective Plasmon-Exciton Coupling in Nonradiative Energy Transfer: Donor-Selective Versus Acceptor-Selective Plexcitons. *Nano Lett.* **2013,** *13* (7), 3065-3072.
10. Kulakovich, O.; Strekal, N.; Yaroshevich, A.; Maskevich, S.; Gaponenko, S.; Nabiev, I.; Woggon, U.; Artemyev, M., Enhanced Luminescence of Cdse Quantum Dots on Gold Colloids. *Nano Lett.* **2002,** *2* (12), 1449-1452.
11. Paltiel, Y.; Aharoni, A.; Banin, U.; Neuman, O.; Naaman, R., Self-Assembling of Inas Nanocrystals on Gaas: The Effect of Electronic Coupling and Embedded Gold Nanoparticles on the Photoluminescence. *Appl. Phys. Lett.* **2006,** *89* (3), 033108.
12. Munechika, K.; Chen, Y.; Tillack, A. F.; Kulkarni, A. P.; Plante, I. J.-L.; Munro, A. M.; Ginger, D. S., Spectral Control of Plasmonic Emission Enhancement from Quantum Dots near Single Silver Nanoprisms. *Nano Lett.* **2010,** *10* (7), 2598-2603.
13. Govorov, A. O.; Bryant, G. W.; Zhang, W.; Skeini, T.; Lee, J.; Kotov, N. A.; Slocik, J. M.; Naik, R. R., Exciton− Plasmon Interaction and Hybrid Excitons in Semiconductor− Metal Nanoparticle Assemblies. *Nano Lett.* **2006,** *6* (5), 984-994.
14. Pons, T.; Medintz, I. L.; Sapsford, K. E.; Higashiya, S.; Grimes, A. F.; English, D. S.; Mattoussi, H., On the Quenching of Semiconductor Quantum Dot Photoluminescence by Proximal Gold Nanoparticles. *Nano Lett.* **2007,** *7* (10), 3157-3164.
15. Tagit, O.; Tomczak, N.; Benetti, E. M.; Cesa, Y.; Blum, C.; Subramaniam, V.; Herek, J. L.; Vancso, G. J., Temperature-Modulated Quenching of Quantum Dots Covalently Coupled to Chain Ends of Poly (N-Isopropyl Acrylamide) Brushes on Gold. *Nanotechnology* **2009,** *20* (18), 185501.

16. Dulkeith, E.; Ringler, M.; Klar, T.; Feldmann, J.; Munoz Javier, A.; Parak, W., Gold Nanoparticles Quench Fluorescence by Phase Induced Radiative Rate Suppression. *Nano Lett.* **2005,** *5* (4), 585-589.
17. Ma, X.; Fletcher, K.; Kipp, T.; Grzelczak, M. P.; Wang, Z.; Guerrero-Martínez, A.; Pastoriza-Santos, I.; Kornowski, A.; Liz-Marzán, L. M.; Mews, A., Photoluminescence of Individual Au/Cdse Nanocrystal Complexes with Variable Interparticle Distances. *The Journal of Physical Chemistry Letters* **2011,** *2* (19), 2466-2471.
18. Ratchford, D.; Shafiei, F.; Kim, S.; Gray, S. K.; Li, X., Manipulating Coupling between a Single Semiconductor Quantum Dot and Single Gold Nanoparticle. *Nano Lett.* **2011,** *11* (3), 1049-1054.
19. Reineck, P.; Gómez, D.; Ng, S. H.; Karg, M.; Bell, T.; Mulvaney, P.; Bach, U., Distance and Wavelength Dependent Quenching of Molecular Fluorescence by Au@ Sio2 Core–Shell Nanoparticles. *ACS nano* **2013,** *7* (8), 6636-6648.
20. Naiki, H.; Masuhara, A.; Masuo, S.; Onodera, T.; Kasai, H.; Oikawa, H., Highly Controlled Plasmonic Emission Enhancement from Metal-Semiconductor Quantum Dot Complex Nanostructures. *The Journal of Physical Chemistry C* **2012,** *117* (6), 2455-2459.
21. Liu, N.; Prall, B. S.; Klimov, V. I., Hybrid Gold/Silica/Nanocrystal-Quantum-Dot Superstructures: Synthesis and Analysis of Semiconductor− Metal Interactions. *J. Am. Chem. Soc.* **2006,** *128* (48), 15362-15363.
22. Ribeiro, T. n.; Prazeres, T.; Moffitt, M.; Farinha, J., Enhanced Photoluminescence from Micellar Assemblies of Cadmium Sulfide Quantum Dots and Gold Nanoparticles. *The Journal of Physical Chemistry C* **2013,** *117* (6), 3122-3133.
23. Cohen-Hoshen, E.; Bryant, G. W.; Pinkas, I.; Sperling, J.; Bar-Joseph, I., Exciton–Plasmon Interactions in Quantum Dot–Gold Nanoparticle Structures. *Nano Lett.* **2012,** *12* (8), 4260-4264.
24. Li, M.; Cushing, S. K.; Wang, Q.; Shi, X.; Hornak, L. A.; Hong, Z.; Wu, N., Size-Dependent Energy Transfer between Cdse/Zns Quantum Dots and Gold Nanoparticles. *The Journal of Physical Chemistry Letters* **2011,** *2* (17), 2125-2129.
25. Gueroui, Z.; Libchaber, A., Single-Molecule Measurements of Gold-Quenched Quantum Dots. *Phys. Rev. Lett.* **2004,** *93* (16), 166108.
26. Fu, Y.; Zhang, J.; Lakowicz, J. R., Silver-Enhanced Fluorescence Emission of Single Quantum Dot Nanocomposites. *Chem. Commun.* **2009,** (3), 313-315.
27. Lange, H.; Juárez, B. H.; Carl, A.; Richter, M.; Bastús, N. G.; Weller, H.; Thomsen, C.; von Klitzing, R.; Knorr, A., Tunable Plasmon Coupling in Distance-Controlled Gold Nanoparticles. *Langmuir* **2012,** *28* (24), 8862-8866.
28. Paek, K.; Yang, H.; Lee, J.; Park, J.; Kim, B. J., Efficient Colorimetric Ph Sensor Based on Responsive Polymer–Quantum Dot Integrated Graphene Oxide. *ACS nano* **2014,** *8* (3), 2848-2856.
29. Wongkongkatep, J.; Ladadat, R.; Lappermpunsap, W.; Wongkongkatep, P.; Phinyocheep, P.; Ojida, A.; Hamachi, I., Thermoresponsive Fluorescent Sensor Based on Core/Shell Nanocomposite Composed of Gold Nanoparticles and Poly (N-Isopropylacrylamide). *Chem. Lett.* **2010,** *39* (3), 184-185.
30. Tagit, O.; Jańczewski, D.; Tomczak, N.; Han, M. Y.; Herek, J. L.; Vancso, G. J., Nanostructured Thermoresponsive Quantum Dot/Pnipam Assemblies. *Eur. Polym. J.* **2010,** *46* (7), 1397-1403.

31. Pinaud, F.; Russo, L.; Pinet, S.; Gosse, I.; Ravaine, V. r.; Sojic, N., Enhanced Electrogenerated Chemiluminescence in Thermoresponsive Microgels. *J. Am. Chem. Soc.* **2013,** *135* (15), 5517-5520.
32. Dou, H.; Yang, W.; Tao, K.; Li, W.; Sun, K., Thermal Sensitive Microgels with Stable and Reversible Photoluminescence Based on Covalently Bonded Quantum Dots. *Langmuir* **2010,** *26* (7), 5022-5027.
33. Zhu, M.-Q.; Wang, L.-Q.; Exarhos, G. J.; Li, A. D. Q., Thermosensitive Gold Nanoparticles. *J. Am. Chem. Soc.* **2004,** *126* (9), 2656-2657.
34. Liu, T.-C.; Huang, Z.-L.; Wang, H.-Q.; Wang, J.-H.; Li, X.-Q.; Zhao, Y.-D.; Luo, Q.-M., Temperature-Dependent Photoluminescence of Water-Soluble Quantum Dots for a Bioprobe. *Anal. Chim. Acta* **2006,** *559* (1), 120-123.
35. Agrawal, M.; Rubio-Retama, J.; Zafeiropoulos, N.; Gaponik, N.; Gupta, S.; Cimrova, V.; Lesnyak, V.; López-Cabarcos, E.; Tzavalas, S.; Rojas-Reyna, R., Switchable Photoluminescence of Cdte Nanocrystals by Temperature-Responsive Microgels. *Langmuir* **2008,** *24* (17), 9820-9824.
36. Hong, S. W.; Kim, D. Y.; Lee, J. U.; Jo, W. H., Synthesis of Polymeric Temperature Sensor Based on Photophysical Property of Fullerene and Thermal Sensitivity of Poly (N-Isopropylacrylamide). *Macromolecules* **2009,** *42* (7), 2756-2761.
37. Hormeno, S.; Bastús, N. G.; Pietsch, A.; Weller, H.; Arias-Gonzalez, J.; Juárez, B. H., Plasmon-Exciton Interactions on Single Thermoresponsive Platforms Demonstrated by Optical Tweezers. *Nano Lett.* **2011,** *11* (11), 4742-4747.
38. Schild, H. G.; Tirrell, D. A., Microcalorimetric Detection of Lower Critical Solution Temperatures in Aqueous Polymer Solutions. *J. Phys. Chem.* **1990,** *94* (10), 4352-4356.
39. Ilmain, F.; Tanaka, T.; Kokufuta, E., Volume Transition in a Gel Driven by Hydrogen Bonding. *Nature* **1991,** *349* (6308), 400-401.
40. Yagi, Y.; Inomata, H.; Saito, S., Solubility Parameter of an N-Isopropylacrylamide Gel. *Macromolecules* **1992,** *25* (11), 2997-2998.
41. Ono, Y.; Shikata, T., Hydration and Dynamic Behavior of Poly (N-Isopropylacrylamide) S in Aqueous Solution: A Sharp Phase Transition at the Lower Critical Solution Temperature. *J. Am. Chem. Soc.* **2006,** *128* (31), 10030-10031.
42. Murphy, S.; Jaber, S.; Ritchie, C.; Karg, M.; Mulvaney, P., Laser Flash Photolysis of Au-Pnipam Core–Shell Nanoparticles: Dynamics of the Shell Response. *Langmuir* **2016,** *32* (47), 12497-12503.
43. Dong, L.; Agarwal, A. K.; Beebe, D. J.; Jiang, H., Adaptive Liquid Microlenses Activated by Stimuli-Responsive Hydrogels. *Nature* **2006,** *442* (7102), 551-554.
44. Weissman, J. M.; Sunkara, H. B.; Tse, A. S.; Asher, S. A. Thermally Switchable Periodicities and Diffraction from Novel Mesoscopically Ordered Materials; DTIC Document: 1996.
45. Sidorenko, A.; Krupenkin, T.; Taylor, A.; Fratzl, P.; Aizenberg, J., Reversible Switching of Hydrogel-Actuated Nanostructures into Complex Micropatterns. *Science* **2007,** *315* (5811), 487-490.
46. Koopmans, C.; Ritter, H., Color Change of N-Isopropylacrylamide Copolymer Bearing Reichardts Dye as Optical Sensor for Lower Critical Solution Temperature and for Host−Guest Interaction with B-Cyclodextrin. *J. Am. Chem. Soc.* **2007,** *129* (12), 3502-3503.
47. Yang, M.; Chu, L. Y.; Wang, H. D.; Xie, R.; Song, H.; Niu, C. H., A Thermoresponsive Membrane for Chiral Resolution. *Adv. Funct. Mater.* **2008,** *18* (4), 652-663.

48. Luzinov, I.; Minko, S.; Tsukruk, V. V., Adaptive and Responsive Surfaces through Controlled Reorganization of Interfacial Polymer Layers. *Prog. Polym. Sci.* **2004,** *29* (7), 635-698.
49. Chen, J.-K.; Chang, C.-J., Fabrications and Applications of Stimulus-Responsive Polymer Films and Patterns on Surfaces: A Review. *Materials* **2014,** *7* (2), 805.
50. Schmaljohann, D., Thermo-and Ph-Responsive Polymers in Drug Delivery. *Advanced drug delivery reviews* **2006,** *58* (15), 1655-1670.
51. Wu, K.; Shi, L.; Zhang, W.; An, Y.; Zhu, X. X., Adjustable Temperature Sensor with Double Thermoresponsiveness Based on the Aggregation Property of Binary Diblock Copolymers. *J. Appl. Polym. Sci.* **2006,** *102* (4), 3144-3148.
52. Hu, J.; Liu, S., Responsive Polymers for Detection and Sensing Applications: Current Status and Future Developments. *Macromolecules* **2010,** *43* (20), 8315-8330.
53. Liu, R.; Fraylich, M.; Saunders, B. R., Thermoresponsive Copolymers: From Fundamental Studies to Applications. *Colloid. Polym. Sci.* **2009,** *287* (6), 627-643.
54. Cheng, Z.; Liu, S.; Beines, P. W.; Ding, N.; Jakubowicz, P.; Knoll, W., Rapid and Highly Efficient Preparation of Water-Soluble Luminescent Quantum Dots Via Encapsulation by Thermo-and Redox-Responsive Hydrogels. *Chem. Mater.* **2008,** *20* (23), 7215-7219.
55. Kiser, P. F.; Wilson, G.; Needham, D., A Synthetic Mimic of the Secretory Granule for Drug Delivery. *Nature* **1998,** *394* (6692), 459-462.
56. Kim, J.; Nayak, S.; Lyon, L. A., Bioresponsive Hydrogel Microlenses. *J. Am. Chem. Soc.* **2005,** *127* (26), 9588-9592.
57. Murthy, N.; Xu, M.; Schuck, S.; Kunisawa, J.; Shastri, N.; Fréchet, J. M., A Macromolecular Delivery Vehicle for Protein-Based Vaccines: Acid-Degradable Protein-Loaded Microgels. *Proceedings of the National Academy of Sciences* **2003,** *100* (9), 4995-5000.
58. Zhang, Y.; Furyk, S.; Bergbreiter, D. E.; Cremer, P. S., Specific Ion Effects on the Water Solubility of Macromolecules: Pnipam and the Hofmeister Series. *J. Am. Chem. Soc.* **2005,** *127* (41), 14505-14510.
59. Li, Y.; Tang, Y.; Narain, R.; Lewis, A. L.; Armes, S. P., Biomimetic Stimulus-Responsive Star Diblock Gelators. *Langmuir* **2005,** *21* (22), 9946-9954.
60. Das, M.; Mardyani, S.; Chan, W. C.; Kumacheva, E., Biofunctionalized Ph-Responsive Microgels for Cancer Cell Targeting: Rational Design. *Adv. Mater.* **2006,** *18* (1), 80-83.
61. Guan, Y.; Zhang, Y., Pnipam Microgels for Biomedical Applications: From Dispersed Particles to 3d Assemblies. *Soft Matter* **2011,** *7* (14), 6375-6384.
62. Azzaroni, O., Polymer Brushes Here, There, and Everywhere: Recent Advances in Their Practical Applications and Emerging Opportunities in Multiple Research Fields. *J. Polym. Sci., Part A: Polym. Chem.* **2012,** *50* (16), 3225-3258.
63. Sierra-Martin, B.; Fernandez-Barbero, A., Inorganic/Polymer Hybrid Nanoparticles for Sensing Applications. *Adv. Colloid Interface Sci.* **2016,** *233*, 25-37.
64. Qiao, J.; Mu, X.; Qi, L., Construction of Fluorescent Polymeric Nano-Thermometers for Intracellular Temperature Imaging: A Review. *Biosens. Bioelectron.* **2016,** *85*, 403-413.
65. Gandhi, A.; Paul, A.; Sen, S. O.; Sen, K. K., Studies on Thermoresponsive Polymers: Phase Behaviour, Drug Delivery and Biomedical Applications. *Asian J. Pharm. Sci.* **2015,** *10* (2), 99-107.

Chapter Four :

A Polymer Hydrogel Modified Lateral Flow Sensing Platform

4.1 Abstract

In this work, a unique lateral flow immunochromatographic biosensing platform is introduced. The platform consists of a nitrocellulose membrane modified with a hydrogel "dam" to capture the detection probes, enabling direct visual detection. As a proof of concept, polyacrylamide and agarose hydrogel are incorporated into a nitrocellulose membrane to successfully separate and capture different nanoparticle probes (e.g. gold nanoparticles and quantum dots) in two distinct lines. This approach could potentially reduce the need for pre-printed biological probes at the test and control lines on the membrane, taking a step towards more universal detection strips as a sensing platform for lateral flow assays.

4.2 Introduction

Lateral flow immunochromatographic strips (LFIS) are among many inexpensive paper-based sensing devices, widely used as point-of-care (POC) diagnostic techniques to detect a large range of targets.[1-7] These targets could include anything from infectious disease and cancer biomarkers, to bio-toxins.[2-3, 6, 8-9] The most common and successful LFIS is the pregnancy stick, which detects the presence of human chorionic gonadotropin (hCG) in urine.[10] The fast response time, simplicity, and low cost of LFIS makes it an ideal choice for POC diagnostics. Personal healthcare has been revolutionized by the invention of LFIS[7]. The greatest advantage is its simplicity for the final user, albeit the complexity of the test design. A visual detection technique is what makes these devices so easy to use. Nanoparticle probes are often incorporated in these

devices to display color on the strip.[1-3] Current LFIS diagnostic devices require the pre-printing of biological elements (such as DNA or antibodies) at the test and control line to capture the nanoparticle-functionalized detection probes on the strip. These probes are highly specific to the analyte being detected,[1, 3] often requiring a new probe for every application and thus make streamlined production difficult.

This work focuses on the feasibility of incorporating polyacrylamide (PAA) and agarose hydrogel lines into the nitrocellulose membrane of the strip to capture the detection probes based on size exclusion and/or chemical interaction rather than using a conventional biological probe. Gold nanoparticles (Au NP) and quantum dots (QD) are used as model detection probes for proof of concept. Capturing these probes using a hydrogel "dam" eliminates the need for highly specific biologically functioning membrane. The capture is based on nanoparticle interaction with the hydrogel instead of immuno-recognition, introducing a more universal lateral flow strip.

4.2.1 Common Components of Lateral Flow Assays

In typical LFAs, the format consists of a sample being carried from the sample application pad, to the conjugate release pad, and then along the membrane to the absorbent pad. Each component has a specific duty to ensure proper device function. Understanding how current devices function is important in the development of new methods.

The membrane is the most important material in the lateral flow device. It must be able to accept the sample and labels (detection and recognition elements) from the sample/conjugate pad, wick them down the strip, as well capture the detection probes for visual detection[1]. The biological probes are pre-printed for detection probe capture and the most common material for the membrane is nitrocellulose.[1, 7] The advantages to using nitrocellulose is that is has good capillary flow characteristics, it is cheap, and has a high affinity for protein binding.[7] The sample pad is needed

to collect the sample, treat it for compatibility with the specific assay, and then release the analyte to the conjugate pad. Many samples, like blood, have a complex matrix and therefore need filtering before use in a sensing device. The sample pad is used as an in-line filtration step. Common material for the sample pad include cellulose, glass fiber, rayon or other materials that have filtering capabilities. The conjugate release pad is typically used for storing the labels, making sure the probes are kept stable over the entire shelf life of the device, and to finally release the conjugate when needed. Glass fibers is a common material for the conjugate pad, but polyesters and rayons are used as well.[7] The conjugate pad is where specific interactions between the analyte and labels begins to occur.[1] The absorbent pad helps wick the sample down the membrane. It is also used to collect the sample at the end of the membrane to prevent backflow. This step is vital in helping to reduce false positives. The absorbent pad typically consists of high-density cellulose. The detection probe (or label) consists of colored or fluorescent nanoparticles. The most commonly used particle for detection in LFAs is colloidal gold nanoparticles.[9] Latex particles coupled with detection reagents like colored or fluorescent dyes, or magnetic particles are also commercially available. Fluorescent nanoparticles, like quantum dots, have become more common in new developments of LFA devices.[1, 8] The type of detection probe used is highly dependent on the application. Is there a need for covalent attachment of a biomolecule? Does the application call for multiplexed detection? What level of sensitivity is required? The answers to these questions will affect which probe should be used for detection[7]. The recognition probe is used for specificity and is varied based on the target analyte. The sensitivity of the device relies heavily on the choice of recognition elements used. In a sandwich type assay, one recognition element is bound to the detection probe and typically consist of either antibodies or aptamers that can bind specifically and selectively to the analyte. There are also recognition elements printed on the membrane. The

molecule printed at the test line should bind specifically to the analyte as well.[1, 7] If the analyte is present, it will be sandwiched between the probe on the strip and the biological element attached to the detection probe, resulting in the required response. A molecule is also printed at the control line, and will selectively bind to the recognition element attached to the detection probe. There should always be a response at the control line if the test flowed properly. This helps to eliminate false negative results.

4.2.2 Polymer Hydrogels

4.2.2.1 Polyacrylamide

Polyacrylamide (PAA) is a polymer hydrogel commonly used to separate proteins in gel electrophoresis. The formation of PAA is a co-polymerization reaction between monomeric acrylamide and N,N'-methylene-bisacrylamide (bisacrylamide).[11-12] The reaction can be chemical or photo initiated. In our work, the well-known chemical initiated process using ammonium persulfate (APS) and tetramethylethylenediamene (TEMED) is used as shown in **Scheme 4.1**. The acrylamide monomer is activated by the persulfate free radicals that are formed when APS dissolves in water. The polymer chain is produced by activated monomers reacting with non-activated monomers. These chains are randomly cross-linked with bisacrylamide following the same mechanism. TEMED is a very good electron carrier and thus acts as a catalyst in the polymerization.

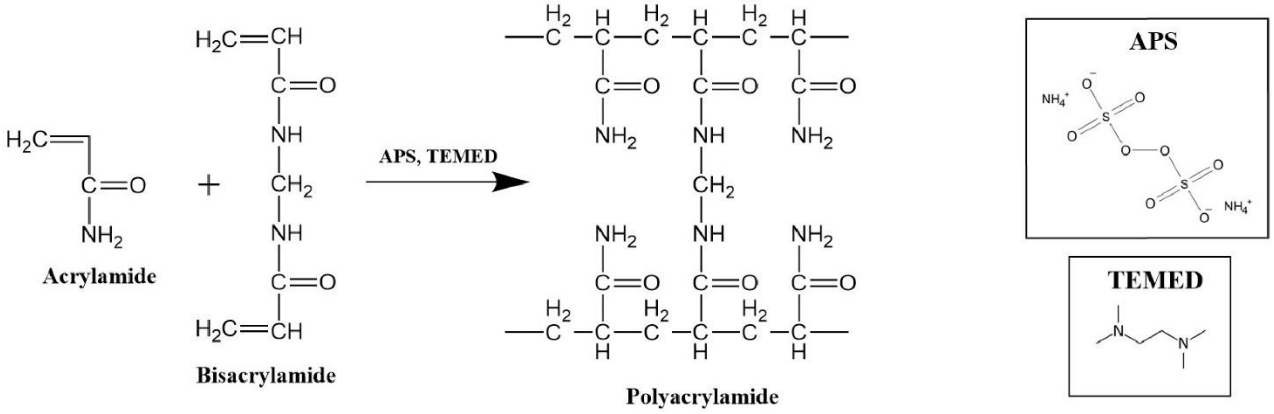

Scheme 4.1. Polymerization reaction of polyacrylamide hydrogel.

An important factor when synthesizing polyacrylamide is controlling the porosity of the gel. Certain applications require a specific pore size for separation. The concentration of acrylamide in the solution, as well as the degree of cross-linkage (amount of bisacrylamide) are the most important factors in determining pore size of the polyacrylamide hydrogel. The more bisacrylamide present, the smaller the pore size becomes until there is too much bisacrylamide and the polymer chains begin to cross-link with themselves creating large pockets of open space. The bisacrylamide forms the smallest pores at 5% of the total solution, and anything above that will begin to increase the effective pore size.[11]

The rate of polymerization will affect the porosity of the gel as well. If the hydrogel polymerizes faster, the pore size will be smaller and vice versa. There are many factors that can affect the polymerization of PAA as seen in **Table 4.1**. The rate of polymerization can be adjusted by varying the concentration of the initiators or monomer, by altering pH, or by changing temperature.[11] How these factors influence the polymerization can also be found in **Table 4.1**.

Table 4.1. Factors that influence polymerization of polyacrylamide.

Factor	Change	Effect on polymerization	Optimal Range
Concentration of initiator*	Increase Decrease	Faster Slower	N/A
Concentration of monomer**	Increase Decrease	Faster Slower	N/A
Ratio of cross-linker at 5%	Increase Decrease	Larger effective pore size Larger pore size	>5% for matrices with high porosity <5% for larger pores 5% for smallest pore
pH	Increase Decrease	Faster Slower	pH 7–10
Temperature	Increase Decrease	Faster Slower	23–25 °C
Rate of reaction	Increase Decrease	Less porous More porous	10–60 min
Oxygen	Increase Decrease	Inhibition of reaction Better reproducibility, Faster	No oxygen

*The best way to adjust rate of polymerization is to change the concentration of the initiator
**The best way to adjust the porosity is to change the concentration of the monomer/cross-linker

The porosity of the hydrogel was extremely important in development of this device so the concentration of the monomer was the polymerization parameter that was studied in this work. The concentration of initiators, pH and temperature were kept constant.

4.2.2.2 Agarose

Agarose is a polysaccharide that is extracted from marine red algae. It has repeating units of D-galactose and 3,6-anhydro-L-galactopyranose. Agarose forms a double helix structure and

the hydrogel forms through physical cross-linking and aggregation of these double-stranded α-helices.[13-16] The hydrogel is linked together by hydrogen bonds and therefore it undergoes gelation that is thermally reversible. The porosity of agarose is dependent on its concentration. As concentration is increase, the pore size decreases up until its gelation concentration is reached. After that point, a minimal difference in the stiffness of the hydrogel is observed[17]. The lack chemical reaction for polymerization makes this hydrogel easy to use, and much less toxic than polyacrylamide.[17]

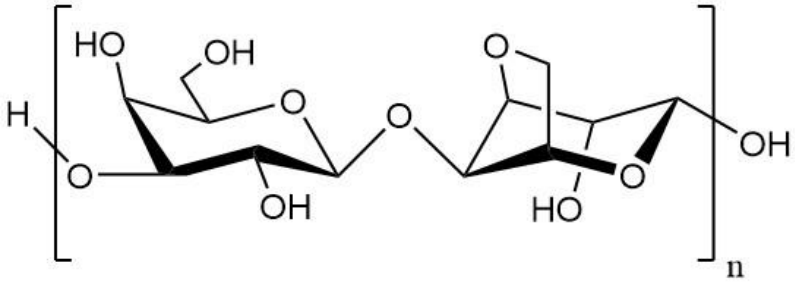

Figure 4.1. Structure of an agarose monomer.

4.3 Experimental Methods

4.3.1 Chemicals and Materials:

Gold (III) chloride trihydrate ($HAuCl_4$), hydroxylamine hydrochloride ($NH_2OH{\cdot}HCl$), cadmium perchlorate, zinc perchlorate, L-cysteine, tellurium powder, sodium hydroxide and sodium borohydride were purchased from Sigma-Aldrich. Sodium citrate, 40% (29:1) Acrylamide/bis acrylamide (AA), ammonium persulfate (APS), tetramethylethylenediamine (TEMED), and ethanol, were purchased from fisher scientific. The nitrocellulose membrane (180 seconds per 4 cm) and absorbent pads were purchased from EMD Millipore. All solutions were prepared using deionized (DI) water.

4.3.2 Polymer Hydrogel Preparation:

The PAA hydrogel modified nitrocellulose membranes were produced by first creating a PAA solution of desired concentration in water. The polyacrylamide (PAA) solution was prepared by chemical initiation of acrylamide/bis-acrylamide (29:1). The percentage of PAA was altered by varying the volume of as-received 40% acrylamide/bis-acrylamide monomer solution (w/w). The concentration of PAA was based on the total weight of acrylamide and bis-acrylamide combined. The hydrogel polymerization was initiated with a 10% (w/v) ammonium persulfate (APS) solution and tetramethylethylenediamine (TEMED). The amount of TEMED added was 0.1% of the total solution, and the amount of 10% APS added was 1% of the total solution. For example, to make 1 mL of 10 % PAA, 250 μL of AA was added to 740 μL of DI water. 1 μL of TEMED was added, followed by 10 μL of APS.

The agarose modified strips were produced by heating up a 2% agarose solution above its melting temperature. The agarose solution was then dropped on the nitrocellulose membrane and the strip was lyophilized before use.

4.3.3 Modification of Nitrocellulose Membrane:

Once all chemicals were mixed properly, the PAA solution was then immediately dropped onto a nitrocellulose membrane so the polymerization could occur on the strip. This solution will form a hydrogel fairly quickly, so it is imperative it's added to the nitrocellulose membrane immediately. Briefly, 10 μL of the PAA solution was dropped across the middle of a 5cm x 1 cm piece of a nitrocellulose membrane using a micro pipette. The solution spread out to form a ~1 cm length band (**Scheme 4.2**). The modified membrane was then immediately put into a freezer for 2

hours and lyophilized overnight. The hydrogel "dam" was located between 2 cm and 3 cm on the membrane as seen in **Figure 4.2**.

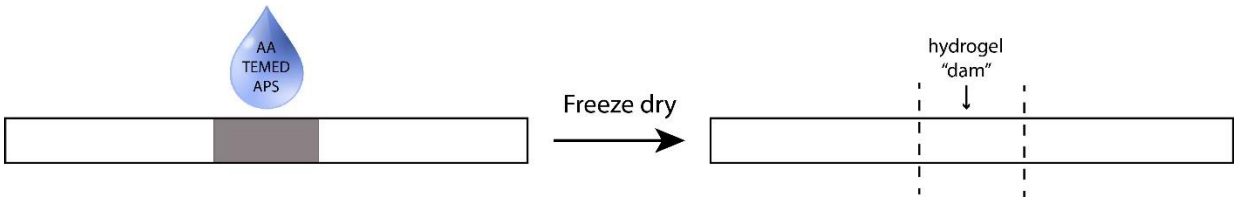

Scheme 4.2. Scheme of hydrogel dam formation on nitrocellulose membrane.

Once dried the strips were ready to be used. Each strip was cut in half the long way so their dimensions were 5cm x 0.5 cm. Each end of the strip was taped to transparency paper as a backing. The bottom of the strip was placed 2 mm below the 0 cm mark of a ruler (**Figure 4.2A**). The top of a 3 cm long absorbent (sample) pad was placed on the strip at the 0 cm mark (**Figure 4.2B**) and the bottom of a 2 cm long absorbent pad was placed on the strip at the 4.5 cm mark (**Figure 4.2C**). Based on this setup, the polymer hydrogel "dam" fell between the 1.8 cm and 2.8 cm mark of the ruler.

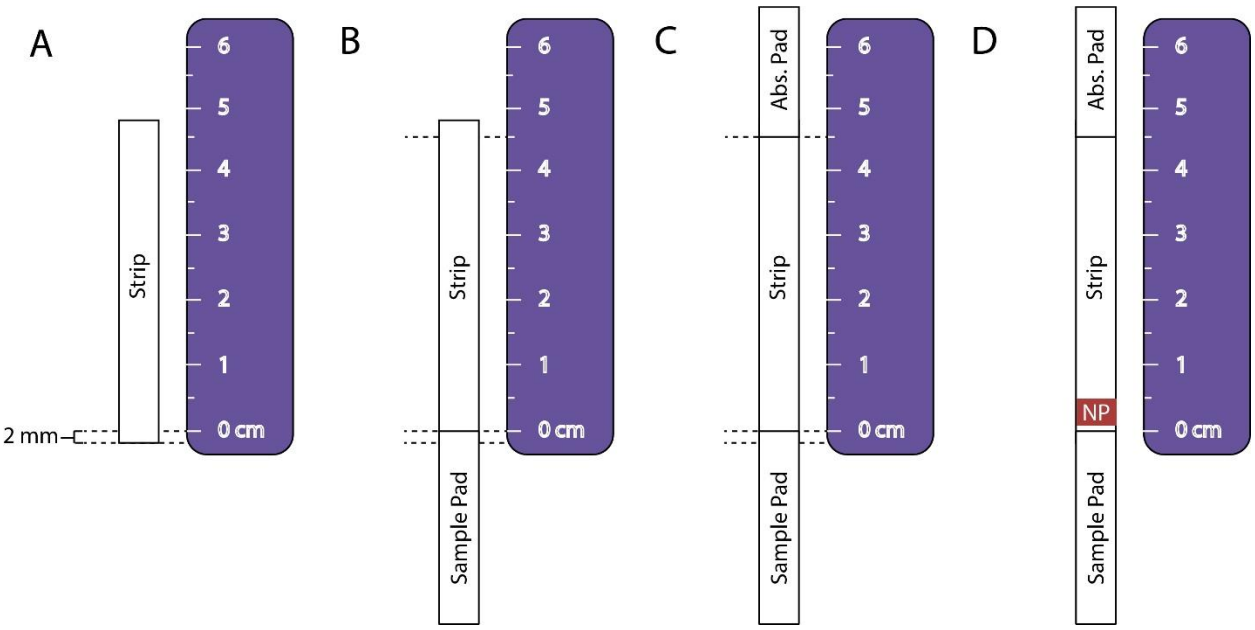

Figure 4.2. Setup for the lateral flow experiments. (A) Step 1, the bottom of the nitrocellulose strip was placed 2 mm below the 0 cm mark of the ruler. (B) Step 2, the top of the sample pad was placed at the 0 cm mark of the ruler. (C) Step 3, the bottom of the absorbent (Abs.) pad was placed at the 4.5 cm mark of the ruler. (D) Step 4, the nanoparticle (NP) sample was added to the nitrocellulose strip right above the bottom pad.

For each experiment, 200 μL of DI water was dropped on the sample pad. Due to the overlap of the absorbent pad with the strip, the water hit the strip and was pulled along the strip by capillary force. For gold nanoparticle and quantum dot studies, 2.5 μL to 5 μL of the Au NP solution is dropped onto the strip as close to the bottom pad as possible (**Figure 4.2D**), before the water is added to the sample pad.

4.3.4 Synthesis of Gold Nanoparticles

Four different size Au NPs were used in this work.

4.3.4.1 12 nm Au NP

The synthesis for 12 nm AuNPs follows the Frens' method.[18] Firstly, 4 mL of $HAuCl_4$ (0.0254 M) solution in 95 mL of DI water was brought to a boil while stirring. Once boiling, 1 mL sodium citrate (0.389 mM) was added. After 20 minutes, the solution was left to cool to room temperature.

4.3.4.2 25 nm Au NP

The Frens' method[18] was also used for the synthesis of 25 nm Au NPs. In this synthesis, 860 μL of HAuCl4 (0.0254 M) solution was stirred and brought to a boil in 99 mL of deionized (DI) water. Once boiling, 12 mL of sodium citrate solution (0.0388 M) was added to the boiling solution and continued heating for 20 minutes.

4.3.4.3 40 nm Au NP

The synthesis of 40 nm Au NPs is described in chapter 2, and follows the Frens' method as well.[18]

4.3.4.4 120 nm Au NP

A seed mediated growth method is used for the synthesis of 120 nm Au NPs and is described in the Experimental Methods section of Chapter 2.[19]

4.3.5 Quantum Dot Synthesis

The quantum dots are synthesized according to previous studies and the details can be found in the Experimental Methods section of Chapter 3 (3.3.2.2).

4.3.6 Instrumentation

The extinction spectra of the Au NPs were determined using A UV-vis spectrometer (Cary 60, Agilent Technologies). The fluorescence of the quantum dots was determined using a fluorometer (Fluoromax Plus, Horiba Scientific Inc.). The scanning electron microscopy (SEM) images were obtained using an FEI Nova NanoSEM 450. Micro computed tomography (micro CT) images were obtained using an Xradia microXCT-400. A home-made cell phone stand was built to video tape all experiments. The videos were taken using an iPhone 6.

4.4 Results and Discussion

4.4.1 Modification of Nitrocellulose Membrane

The modification of a nitrocellulose membrane with PAA hydrogel was confirmed using scanning electron microscopy (SEM) as shown in **Figure 4.3**. The cross-section of an as-received strip without modification (**Figure 4.3A**) is compared with the cross-section of a 5% PAA modified strip (**Figure 4.3B**). One can see that the PAA hydrogel formed around the fibers of the nitrocellulose membrane, thus resulting in less open space in the membrane and accordingly smaller pore size between the nitrocellulose fibers. Note that the SEM images were taken using the lyophilized sample, which maintained the actual structure of the membrane modified with PAA hydrogel in the wet state. In addition, PAA hydrogel itself consists of numerous nanopores though they are not visible by SEM. Therefore, the hydrogel will not only decrease the overall pore size of the fibers, but it also introduces smaller nanopores originating from the hydrogel itself. This overall hindering effect helps to capture or slow down the transport of the nanoparticle probes with different size and chemical properties.

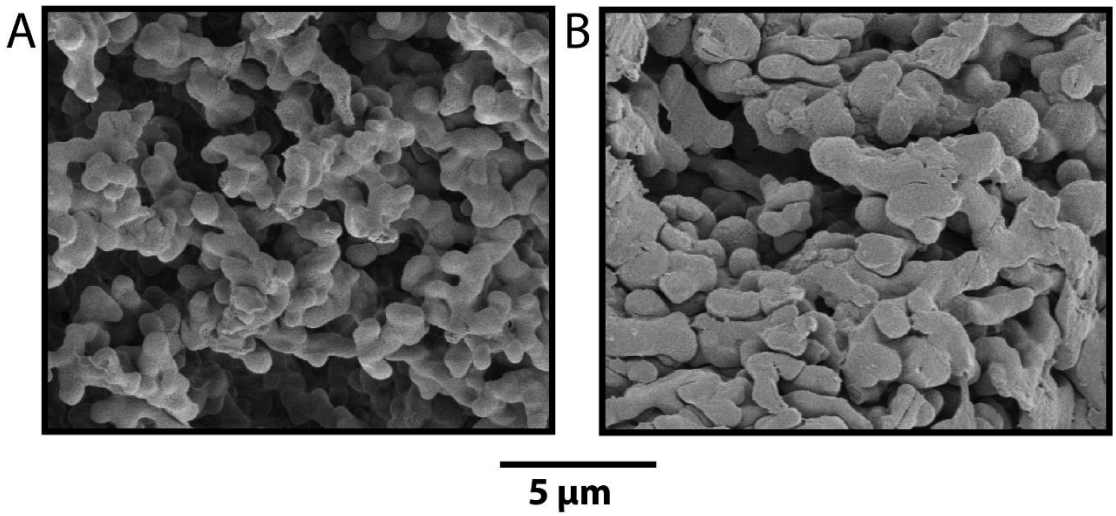

Figure 4.3. SEM images of the nitrocellulose membrane. (A) The cross section of a nitrocellulose membrane as received without modification. (B) The cross section of nitrocellulose membrane modified with 5% PAA hydrogel.

To further analyze the difference between nitrocellulose membranes with and without PAA modification, a volume analysis study was performed using micro-CT. In this study, the volume fraction refers to the occupied space of the system. This includes the nitrocellulose fibers as well as the PAA hydrogel. The volume fraction of the membrane without modification was determined to be 0.547156, and the volume fraction of the membrane modified with 10% PAA was determined to be 0.599594. This study confirms that a strip modified with 10% PAA has more occupied space than a strip without modification. We have shown that polymer formation on the nitrocellulose membrane has been achieved and that it does change the structure of the membrane.

4.4.2 Gold Nanoparticle Capture

Many commercially available lateral flow immunochromatographic strips use Au NPs as the color probe for the detection of a target molecule. Therefore, the ability to capture Au NPs in

a straight line is vital in the development of this device. In all experiments performed, the particles in water were dropped at one end of the strip, and water was added to the sample pad. The water flowed along the membrane due to capillary action,[4] pulling the particles with it through the tortuous and interconnected space. When 120 nm Au NPs were added to the membrane without a polymer hydrogel "dam", most Au NPs carried by the water flow passed through the entire as-received membrane and into the absorbent pad as seen in **Figure 4.4A**. The Au NP line is not as wide and concentrated at the end of the strip as the beginning. This is because the strip has a depth to it and the Au NPs are getting lost in the nitrocellulose fibers as they travel up the membrane.

It was also determined that lyophilizing the strip after dropping on PAA solution is critical for Au NP capture. If the strip was left to air dry, the Au NPs were not captured in a narrow line at the hydrogel "dam" (**Figure 4.4B)**. It is believed the polymer is collapsing on itself as the water dries during the air-dry process, altering the structure of the hydrogel and reducing its hindrance to the convective transport of Au NPs. Lyophilization helps to preserve the nano/micro structure of the hydrogel-modified membrane, which is necessary for Au NP capture. **Figure 4.4C** shows the lyophilized PAA modified nitrocellulose strips are able to capture the nanoparticles in a straight, narrow band.

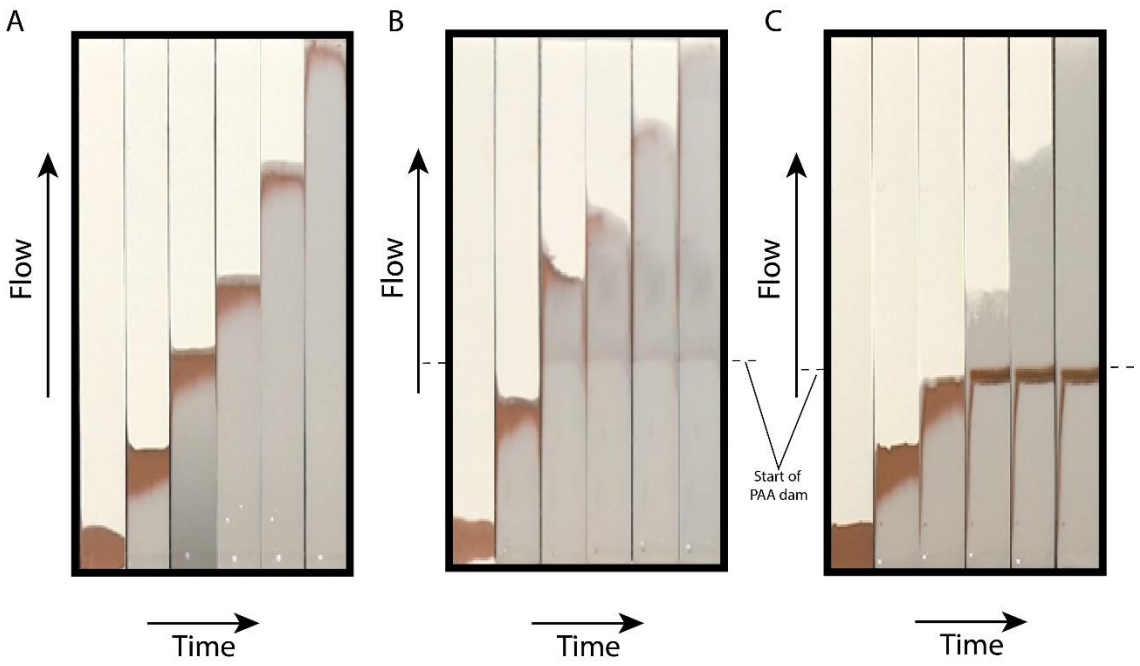

Figure 4.4. Sequential images showing 120 nm Au NPs flowed through the lateral flow strip within (A) as received, (B) 10% PAA air dried, and (C) 10% PAA lyophilized membranes. The beginning of the PAA "dam" is indicated by the black dashed line.

The porosity of the hydrogel depends on the conditions of polymerization as well as the initial monomer concentrations.[11] In every experiment, the initiator concentrations were kept constant. The PAA percentage was determined by the concentration of acrylamide/bis-acrylamide in the total solution (w/w). The PAA percentage was found to be very important for Au NP capture, as shown in **Figure 4.5**. 120 nm Au NPs in water were run through the nitrocellulose membrane modified with PAA concentrations of 0.1%, 0.5%, 1%, 5%, and 10% (**Figure 4.5A** a–e, respectively). The images in **Figure 4.5A** are screen shots at the end of each experiment. The 120 nm Au NPs stopped in the hydrogel formed with each percentage of PAA. As the PAA percentage increases, the particle band becomes narrower and more concentrated. Furthermore, at low PAA percentages, the Au NPs flowed into the polymer and a broader band was observed (**Figure 4.6**).

Using a PAA percentage higher than 5% is preferred in order to obtain a narrow band for detection. **Figure 4.5B** shows the SEM image of the cross-section of a nitrocellulose membrane modified with 5% PAA after flowing 120 nm Au NPs through the membrane. The strip was re-lyophilized after the flow and before the SEM image was taken. The image shows that dispersed Au NPs indeed were captured by the PAA modified nitrocellulose membrane. The successful capture of Au NPs was achieved without the need for printed biological probes on the membrane by simply modifying the membrane with a polyacrylamide hydrogel "dam".

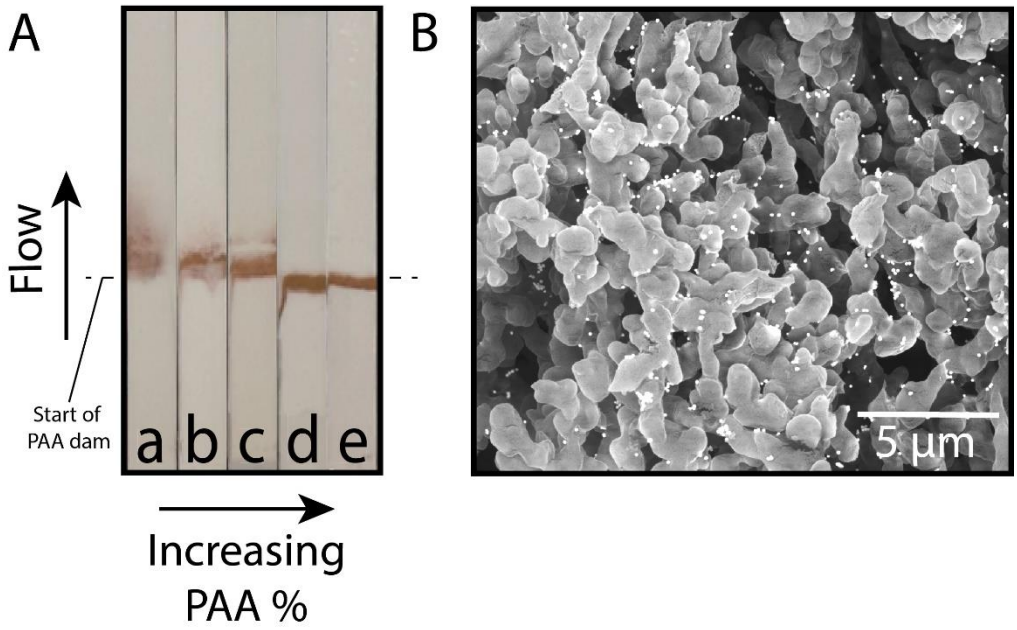

Figure 4.5. Comparison of modified nitrocellulose membranes with varying polymer percentages after 120 nm gold nanoparticles flowed through the membrane. (A) Pictures of the membranes with varying PAA percentages (increasing from left to right): (a) 0.1%, (b) 0.5%, (c) 1%, (d) 5%, and (e) 10% PAA at the end of the flow experiment. The approximate beginning of the PAA "dam" is indicated by the black dashed line. (B) A backscattering SEM image of the cross section of a nitrocellulose membrane modified with 5% PAA after 120 nm AuNP flowed through it. The Au NPs (white dots in the image) were captured by the membrane modified with PAA.

The distance versus color intensity studies were performed using Image J software (**Figure 4.6**). When analyzing the strips, the distance "0" refers to the top of the sample pad. Therefore, according to the setup up shown in **Figure 4.2**, the hydrogel "dam" falls between 1.8 and 2.8 cm. The gray scale spectra were obtained for the strips shown above. The gold nanoparticles were captured differently by varying the percentage of polyacrylamide. It is apparent that the 5% (**Figure 4.6**, green) and 10% (**Figure 4.6**, pink) PAA strips captured the nanoparticles in a narrow, more concentrated band than the lower percentage PAA strips. The front of the Au NP bands for

5% and 10% PAA was located right at 1.8 cm. According to the setup (**Figure 4.2**), 1.8 cm is where the start of the hydrogel "dam" band began. At higher PAA percentages, the Au NPs were stopped before entering the hydrogel, the lower PAA percentages allowed the Au NPs to travel into the hydrogel "dam" where they were eventually captured in a broader band. The polymer is not observed in the SEM image of the 120 nm Au NP band (**Figure 4.5B**) which confirms the observation that the Au NPs are stopped before the hydrogel "dam".

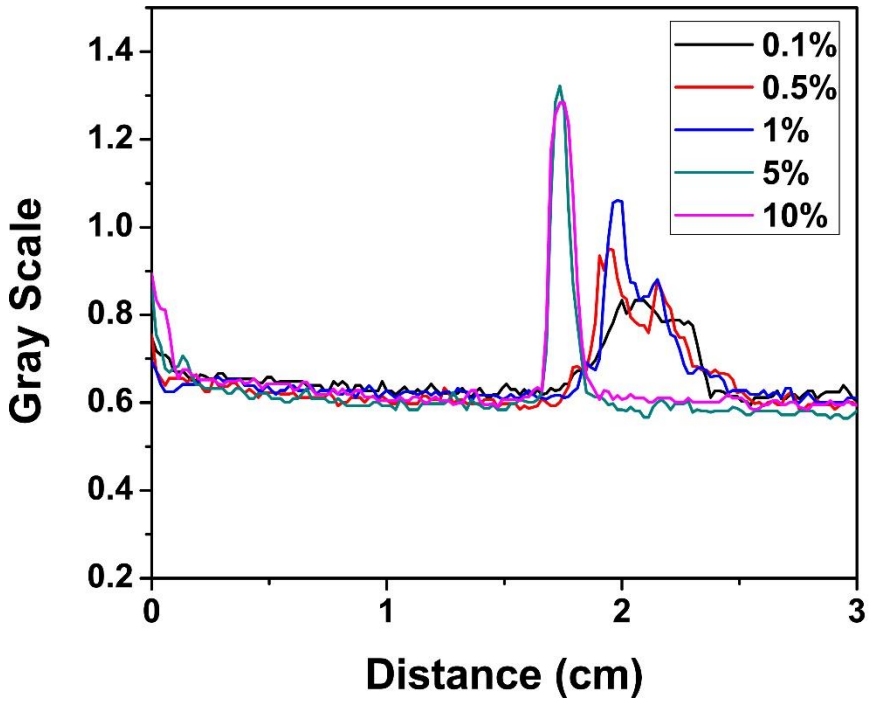

Figure 4.6. Concentration distributions of 120 nm gold nanoparticles on PAA modified nitrocellulose membranes. PAA percentages of 5% (green) and 10% (pink) clearly captured the nanoparticles in a narrow, concentrated band. At lower PAA percentages of 0.1% (black), 0.5% (red) and 1% (blue) the Au NPs traveled into the hydrogel "dam" and were stopped in a broader band.

For this device to be comparable to current lateral flow assay design, a test line and a control line are necessary. The device must be capable of separating the probes, so they can be captured individually depending on whether the target analyte is present or not, to form two distinct lines on the platform. This was not achievable with 120 nm Au NP probes by solely adjusting the PAA percentage of the modified membrane because the Au NPs were captured even at extremely low PAA percentages. This led to tests on smaller Au NPs sizes for size-dependent separation. To study the interaction of the polymer hydrogel "dam" with smaller Au NP sizes, three additional citrate capped Au NPs (12 nm, 25 nm and 40 nm) were synthesized. Au NPs of each size were run

through the hydrogel modified membranes with PAA percentages of 0.1%, 0.5%, 1%, 5% and 10% and the results are shown in **Figure 4.7**.

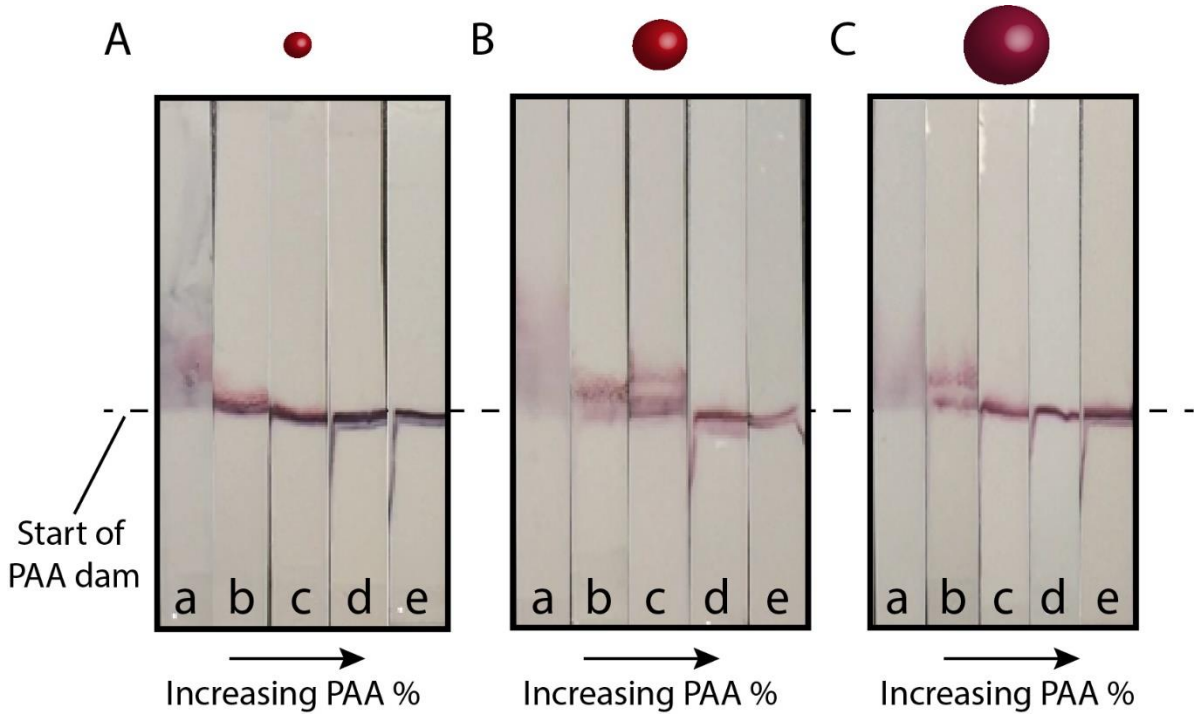

Figure 4.7. Comparison of PAA modified nitrocellulose run with different size gold nanoparticles. Varying PAA percentages (increasing from left to right), including (a) 0.1%, (b) 0.5%, (c) 1%, (d) 5%, and (e) 10% PAA, were shown at the end of the flow experiments. The water flow direction was from bottom to top. The approximate beginning of the PAA "dam" is indicated by the black dashed line. All sizes of Au NPs including (A) 12, (B) 25, and (C) 40 nm were captured using PAA hydrogel.

Similar to the 120 nm Au NPs, the 12 nm, 25 nm and 40 nm Au NPs (shown in **Figure 4.7A**, **Figure 4.7B**, and **Figure 4.7C**, respectively) were captured at the hydrogel for all the percentages tested. The higher percentage PAA strips stopped the Au NPs more efficiently in a

narrow band. We were able to capture Au NPs of different sizes and show they can all be used as probes in this device.

4.4.3 Separation and Capture of Gold Nanoparticles and Quantum Dots

Luminescent nanoparticles are another type of detection probe commonly used in lateral flow assays[1-2, 20]. Among them, quantum dots are often used[21]. Quantum dots are small semiconductor nanocrystals that are typically 2–10 nm in diameter. QDs have become more studied recently due to their size-tunable optical properties[22]. To examine whether QDs would be captured by the hydrogel "dam" modified membrane, two different sized aqueous phase L-cysteine capped cadmium Telluride/Zinc Telluride (CdTe/ZnTe) core-shell QDs were synthesized according to previous literature.[23] The smaller QD emits green light with a peak at 550 nm and the larger QD emits red light with a peak at 620 nm. The QDs were flowed through PAA modified nitrocellulose membranes with PAA concentration ranging from 5% to 40%. The PAA "dam" was unable to capture the larger red QDs even at 40% PAA concentration (**Figure 4.8A**). Multiple parameters in addition to monomer concentration were altered to attempt QD capture. Firstly, the size of the polymer dam was doubled from 10 μL to 20 μL (**Figure 4.8B**). The band of QDs broadens by making the dam bigger, but the QDs still were not captured by the PAA. Secondly, the entire strip was modified with varying percentages of PAA. The highest percentage achievable without curling of the paper based strip was 15% PAA as shown in **Figure 4.8C**. The QDs were captured, but not in a narrow band. Thirdly, the strips were modified with multiple layers of a 10% PAA dam as shown in **Figure 4.8D**. The strip was lyophilized after the addition of each layer. At 4 layers, most QDs were captured, but not in a narrow band. Finally, a concentration effect was attempted by layering multiple polymer "sheets," with the strip being lyophilized after the addition of each layer (**Figure 4.8E**). When 3 layers were used, the QDs were captured towards the

beginning of the strip, but in a jagged, large band. The "sheet" location was difficult to control due to the hydrophilicity of the nitrocellulose membrane, therefore optimization of the layering procedure needs to occur for PAA to successfully capture QDs in a narrow band.

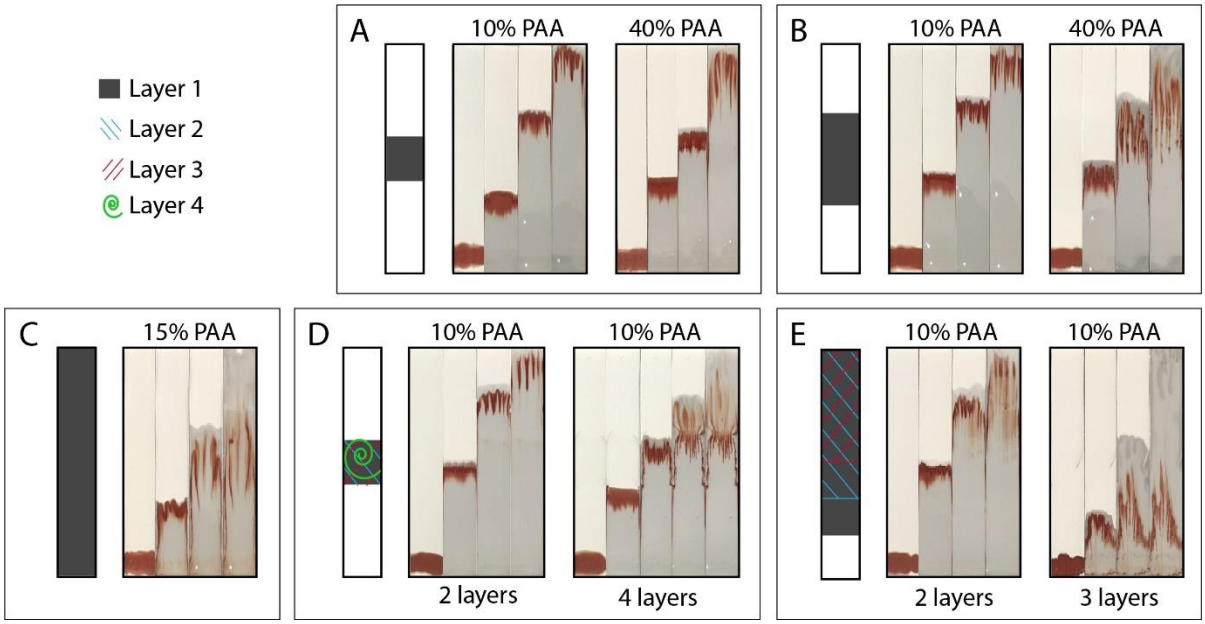

Figure 4.8. Images of CdTe/ZnTe quantum dots flowed through PAA modified membranes. (A) 10 uL PAA dam, (B) 20 uL PAA dam, (C) full PAA coverage, (D) multiple layers of 10 uL PAA dam, (E) multiple layers of PAA "sheets". In all cases, modifying the strip with PAA does not capture the QDs in a narrow band.

Since the PAA hydrogel "dam" can capture the citrate capped Au NPs but not the cysteine capped CdTe/ZnTe QDs, it ought to be able to separate the two types of particles. To examine if PAA hydrogel would capture Au NPs but let QDs go through when both the particles were present, QDs and Au NPs were mixed in water for the tests. When QDs were in close proximity with Au NPs in the mixture, and if there is good overlap between the emission spectrum of the QDs and the extinction spectrum of the Au NPs, the fluorescence of the QDs would be largely quenched due to Förster resonance energy transfer (FRET)[24] between the QDs and Au NPs. As shown in

Figure 4.9, the emission spectra of the green CdTe/ZnTe QDs (Figure 4A, dashed green line) overlaps well with the plasmon band of the 120 nm Au NPs (**Figure 4.9A**, solid orange line). Therefore, the fluorescence of the QDs is quenched in the mixture. The mixture was flowed through a 10% PAA modified strip (**Figure 4.9B**). The images in **Figure 4.9B** are screenshots with progression through the video from left to right. The experiment was run under UV light to observe the fluorescence of the QDs. The flow of the solution was from the bottom of the image to the top. Since the fluorescence of the QDs was partially quenched at the beginning of the video, a dark green band was observed in the leftmost image in **Figure 4.9B**. When the mixture hit the PAA "dam" (black dashed line), the Au NPs were captured (narrow black band), but the QDs continued to flow with water. The QDs were then separated from the Au NPs. In this case, FRET no longer happens because the distance between the QDs and Au NPs increases. The QD fluorescence was restored (bright neon green band in **Figure 4.9B**). Separation of QDs from Au NPs has been successfully achieved by the PAA modified nitrocellulose membrane.

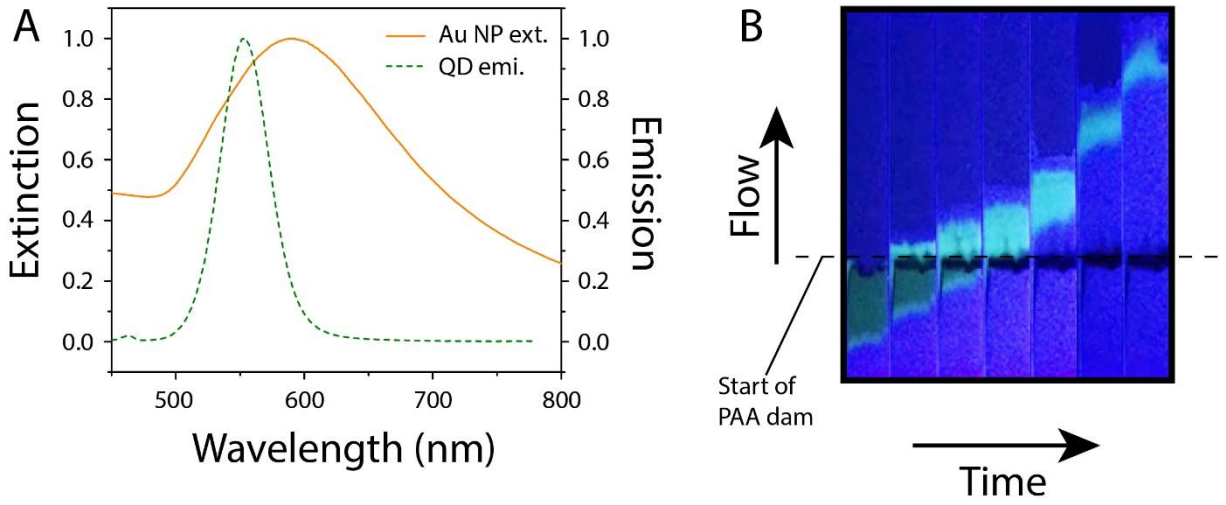

Figure 4.9. Separation of 120 nm gold nanoparticles from CdTe/ZnTe quantum dots. (A) The emission spectrum of the CdTe/ZnTe QDs (green dotted line) with a peak at 550 nm shows good overlap with the extinction spectrum of the 120 nm Au NPs (orange line) that has a broad peak at 590 nm. (B) Screenshot images taken under UV light of a mixture of 120 nm Au NPs with green CdTe/ZnTe QDs run on 10% PAA modified nitrocellulose membrane. The solution flow was from bottom to top and the experiment proceeded from left to right. The beginning of the PAA "dam" is indicated by the black dashed line. The QD fluorescence was originally largely quenched by the Au NPs due to Förster energy transfer between the QDs and the Au NPs (dark green band in first and second image). When the Au NPs were captured (black line) at the polymer "dam", the QDs continued to flow with the water line and separated from the Au NPs. Thus, fluorescence was recovered (bright green band).

Using the mixture of QDs and Au NPs as the color probes in lateral flow device was the next step in achieving the two or more distinct detection lines. However, since the PAA failed to capture the QDs after separation from the Au NPs, the nitrocellulose membrane is further modified by using a different polymer hydrogel that would capture the QDs. Agarose was used in the

following study. The SEM image of agarose modified nitrocellulose membrane (**Figure 4.10**) shows that it has a larger coverage of the void spaces in the nitrocellulose membrane than PAA. The feature pore size of the nitrocellulose membrane modified with agarose is significantly smaller than the strip modified with PAA. This affects the interaction between the NP probes and the polymer and allows for the capture of smaller CdTe/ZnTe particles.

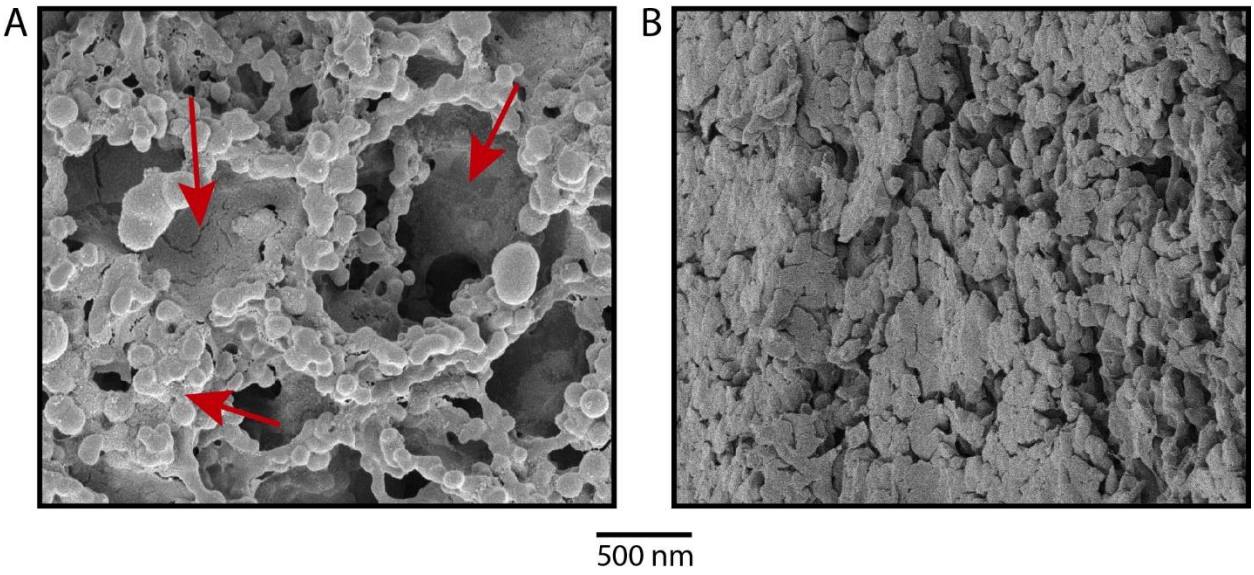

Figure 4.10. SEM of 2% agarose modified nitrocellulose membranes. (A) SEM image from the top of the strip. (B) SEM image of the cross-section of an agarose modified strip. The agarose fills the large voids of the nitrocellulose membrane better than PAA as pointed out by the red arrows. We hypothesize the larger coverage area of agarose amongst the nitrocellulose fibers creates smaller pore sizes in the strip. This leads to the successful size-dependent capture of small QDs by agarose. As explained in the text, possible chemical interactions between the nanoparticles and the different type of hydrogels cannot be ruled out as an influencing factor.

In order to capture both Au NPs and QDs simultaneously on one membrane, two polymer lines of PAA and agarose were drawn on a nitrocellulose membrane. The detection scheme can be

found in **Figure 4.11**. After addition of both polymers, the strip was lyophilized. A mixture of 12 nm Au NPs and red CdTe/ZnTe QDs was run on a 10% PAA/2% agarose modified strip and the results can be seen in **Figure 4.11C**. In the images, the time elapses from left to right, with flow from bottom to top. The solution hit the PAA "dam" first and the 12 nm Au NPs were captured. The red CdTe/ZnTe QDs continued to flow with the water until the solution reached the agarose "dam". At that time, the QDs were captured and the water continued to flow as seen in the rightmost image of **Figure 4.11C**. The two lines of Au NPs and QDs can be used as the test and control lines in a lateral flow device with further optimization of the procedure.

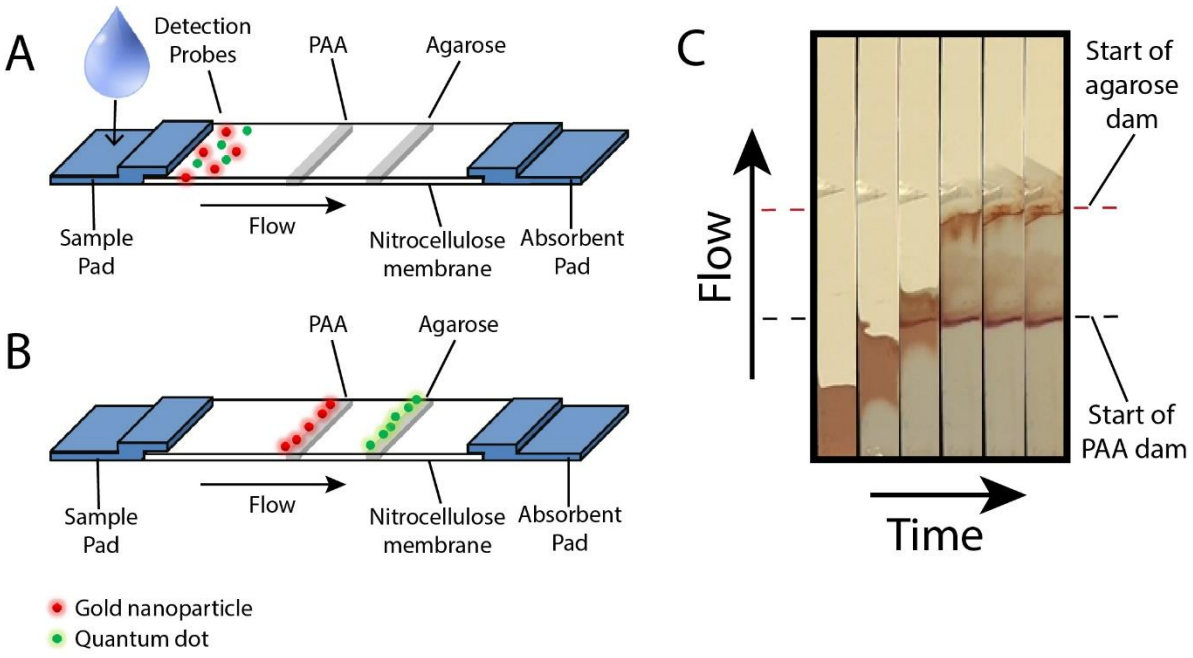

Figure 4.11. The separation and capture of gold nanoparticles and quantum dots in two distinct lines using two different polymer hydrogel "dams". (A) Scheme of nitrocellulose membrane modified with PAA and agarose before flow occurs. (B) Scheme of modified nitrocellulose after Au NPs and QDs are flowed through. The solution will interact with the PAA hydrogel "dam" first to capture the Au NPs, and will interact with the agarose "dam" second, capturing the QDs. (C) Screenshot images of experiment run with a mixture of 13 nm Au NPs and red CdTe/ZnTe quantum dots. The experiment proceeds from left to right with the first image being time 0. The beginning of the PAA "dam" (black dashed line) and agarose "dam" (red dashed line) are labelled. The 13 nm Au NPs were captured at the PAA hydrogel "dam" (red narrow band $\sim \frac{1}{3}$ of the way up the strip) and the QDs were captured at the agarose hydrogel "dam" (red narrow band $\sim \frac{2}{3}$ of the way up the strip).

While the mechanism of particle capture is not yet fully understood, a size dependent capture is hypothesized. We have shown that the polymer structure and porosity of the hydrogel are factors that play a critical role in successful size-dependent nanoparticle capture. All Au NPs used in our experiments were larger than the QDs. Although the difference between the smallest Au NP (12 nm) and the largest QD (red, ~8 nm) is quite minimal, the PAA was able to distinguish between the two and only capture the Au NPs (Figure 5C). In typical gel electrophoresis conditions, agarose is known to create larger pore sizes than PAA[25] so it is counterintuitive that it captures the smaller QDs at 2% polymer concentration when 40% PAA does not. We believe the polymerization of the acrylamide/bis-acrylamide system is affected by low temperature and the presence of nitrocellulose fibers and therefore cannot be directly compared to typical hydrogel formation. As seen in the SEM in **Figure 4.3B** the PAA hydrogel is mainly forming around the fibers and not in the void spaces. The agarose fills the voids more completely than PAA (**Figure 4.10**). The larger coverage of agarose amongst the nitrocellulose fibers likely creates much smaller pore sizes of the modified membrane. This leads to the successful size-dependent capture of small QDs by agarose. The polymer structure is also important and plays a role in porosity of the hydrogel. As stated previously, lyophilization of PAA is required for Au NP capture. It is believed that the nano/micro structure of the PAA-modified membrane is preserved when lyophilized, but it collapses when air dried. This collapse of the polymer creates larger pores, which allows a majority of the Au NPs to pass through, corroborated by our experimental results. Therefore, controlling the porosity and polymer structure will be crucial in the development of such devices.

Although a size-dependent particle capture is realized, possible chemical interactions between the nanoparticles and the hydrogel cannot be ruled out as an influencing factor. It is well documented that PAA and agarose are used in gel electrophoresis due to their inert properties when

interacting with proteins and DNA[26]. However, given the different nature of the hydrogels in the presence of nitrocellulose, it is worth studying their possible chemical interaction with nanoparticles. The Au NPs and QDs are made up of different materials, and have different capping ligands so they should interact differently with the hydrogel. Studies are being performed to help further understand these interactions. Furthermore, knowing the exact mechanisms of capture and the quantitative information of relevant capillary-driven flow and particle dynamics involved in the nitrocellulose-hydrogel porous material will allow for ease of development and optimization of specific detection applications. Future work will also include binding biological recognition elements to the detection probes and co-flowing them through the hydrogel modified nitrocellulose membrane as a necessary step for specific target detection. The addition of biological molecules to the device will further complicate particle capture, therefore optimization and pre-treatment of the strip may be needed[4]. This device shows promise for use in applications where Au NPs and QDs either attach or separate when the target analyte is present. This unique modification of current lateral flow strips provides an alternate method of capturing the nanoparticle probes and introduces many possibilities to enhance the design of conventional lateral flow devices.

4.5 Conclusion

In this work, a nitrocellulose membrane was successfully modified with polyacrylamide and agarose hydrogels. By modifying the nitrocellulose membrane with two different polymer hydrogels, the separation of gold nanoparticles from quantum dots was achieved and both particles were captured in distinct lines. We hypothesize the capturing of the nanoparticle probes is size-dependent, and also affected by the polymer type, concentration and how it was processed. Further understanding about the interactions between the particles and the hydrogel as well as the factors that influence their capture will aid in the design and further development of inexpensive,

lateral flow sensing devices in the future. This device introduces a new method for detection probe separation and capture in lateral flow strips. Further studies on how the addition of biological molecules to the detection probes affects their capture is required in order to apply the device for specific detection of desired targets.

4.6 Acknowledgments

This work was funded by the UCONN start up fund and the National Science Foundation EECS-1509216 grant. We would like to thank Joseph Favata and the CHASE lab at the University of Connecticut for their help with the volume studies. Thank you also to Dr. Jessica Rouge for her helpful discussions.

4.7 References

1. Posthuma-Trumpie, G. A.; Korf, J.; van Amerongen, A., Lateral Flow (Immuno) Assay: Its Strengths, Weaknesses, Opportunities and Threats. A Literature Survey. *Anal. Bioanal. Chem.* **2009,** *393* (2), 569-582.
2. Huang, X.; Aguilar, Z. P.; Xu, H.; Lai, W.; Xiong, Y., Membrane-Based Lateral Flow Immunochromatographic Strip with Nanoparticles as Reporters for Detection: A Review. *Biosens. Bioelectron.* **2016,** *75*, 166-180.
3. Ngom, B.; Guo, Y.; Wang, X.; Bi, D., Development and Application of Lateral Flow Test Strip Technology for Detection of Infectious Agents and Chemical Contaminants: A Review. *Anal. Bioanal. Chem.* **2010,** *397* (3), 1113-1135.
4. Krska, R.; Molinelli, A., Rapid Test Strips for Analysis of Mycotoxins in Food and Feed. *Anal. Bioanal. Chem.* **2009,** *393* (1), 67-71.
5. Dzantiev, B. B.; Byzova, N. A.; Urusov, A. E.; Zherdev, A. V., Immunochromatographic Methods in Food Analysis. *TrAC, Trends Anal. Chem.* **2014,** *55*, 81-93.
6. Chin, C. D.; Linder, V.; Sia, S. K., Commercialization of Microfluidic Point-of-Care Diagnostic Devices. *Lab Chip* **2012,** *12* (12), 2118-2134.
7. Wong, R.; Tse, H., *Lateral Flow Immunoassay*. Humana Press: New York, NY, 2009.
8. Li, X.; Lu, D.; Sheng, Z.; Chen, K.; Guo, X.; Jin, M.; Han, H., A Fast and Sensitive Immunoassay of Avian Influenza Virus Based on Label-Free Quantum Dot Probe and Lateral Flow Test Strip. *Talanta* **2012,** *100*, 1-6.
9. Li, Z.; Wang, Y.; Wang, J.; Tang, Z.; Pounds, J. G.; Lin, Y., Rapid and Sensitive Detection of Protein Biomarker Using a Portable Fluorescence Biosensor Based on Quantum Dots and a Lateral Flow Test Strip. *Anal. Chem.* **2010,** *82* (16), 7008-7014.
10. Leuvering, J. H.; Thal, P. J.; Van der Waart, M.; Schuurs, A. H., A Sol Particle Agglutination Assay for Human Chorionic Gonadotrophin. *J. Immunol. Methods* **1981,** *45* (2), 183-194.
11. Hames, B. D., Gel Electrophoresis of Proteins: A Practical Approach. OUP Oxford: 1998; Vol. 197.
12. Ahmed, E. M., Hydrogel: Preparation, Characterization, and Applications: A Review. *Journal of Advanced Research* **2015,** *6* (2), 105-121.
13. Lahaye, M.; Rochas, C. In *Chemical Structure and Physico-Chemical Properties of Agar*, International workshop on gelidium, Springer: 1991; pp 137-148.
14. Arnott, S.; Fulmer, A.; Scott, W.; Dea, I.; Moorhouse, R.; Rees, D., The Agarose Double Helix and Its Function in Agarose Gel Structure. *J. Mol. Biol.* **1974,** *90* (2), 269IN11273-272284.
15. Djabourov, M.; Clark, A.; Rowlands, D.; Ross-Murphy, S., Small-Angle X-Ray Scattering Characterization of Agarose Sols and Gels. *Macromolecules* **1989,** *22* (1), 180-188.
16. Rees, D. A., Structure, Conformation, and Mechanism in the Formation of Polysaccharide Gels and Networks. *Adv. Carbohydr. Chem. Biochem.* **1969,** *24*, 267-332.
17. Forget, A.; Christensen, J.; Lüdeke, S.; Kohler, E.; Tobias, S.; Matloubi, M.; Thomann, R.; Shastri, V. P., Polysaccharide Hydrogels with Tunable Stiffness and Provasculogenic Properties Via A-Helix to B-Sheet Switch in Secondary Structure. *Proceedings of the National Academy of Sciences* **2013,** *110* (32), 12887-12892.
18. Frens, G., Controlled Nucleation for the Regulation of the Particle Size in Monodisperse Gold Suspensions. *Nature* **1973,** *241* (105), 20-22.

19. Li, J. F.; Tian, X. D.; Li, S. B.; Anema, J. R.; Yang, Z. L.; Ding, Y.; Wu, Y. F.; Zeng, Y. M.; Chen, Q. Z.; Ren, B., Surface Analysis Using Shell-Isolated Nanoparticle-Enhanced Raman Spectroscopy. *Nat. Protoc.* **2013,** *8* (1), 52-65.
20. Paterson, A. S.; Raja, B.; Garvey, G.; Kolhatkar, A.; Hagström, A. E.; Kourentzi, K.; Lee, T. R.; Willson, R. C., Persistent Luminescence Strontium Aluminate Nanoparticles as Reporters in Lateral Flow Assays. *Anal. Chem.* **2014,** *86* (19), 9481-9488.
21. Taranova, N.; Berlina, A.; Zherdev, A.; Dzantiev, B., 'Traffic Light'immunochromatographic Test Based on Multicolor Quantum Dots for the Simultaneous Detection of Several Antibiotics in Milk. *Biosens. Bioelectron.* **2015,** *63*, 255-261.
22. Kairdolf, B. A.; Smith, A. M.; Stokes, T. H.; Wang, M. D.; Young, A. N.; Nie, S., Semiconductor Quantum Dots for Bioimaging and Biodiagnostic Applications. *Annu. Rev. Anal. Chem.* **2013,** *6*, 143-162.
23. Law, W. C.; Yong, K. T.; Roy, I.; Ding, H.; Hu, R.; Zhao, W.; Prasad, P. N., Aqueous-Phase Synthesis of Highly Luminescent Cdte/Znte Core/Shell Quantum Dots Optimized for Targeted Bioimaging. *Small* **2009,** *5* (11), 1302-1310.
24. Clapp, A. R.; Medintz, I. L.; Mattoussi, H., Förster Resonance Energy Transfer Investigations Using Quantum-Dot Fluorophores. *ChemPhysChem* **2006,** *7* (1), 47-57.
25. Serwer, P., Agarose Gels: Properties and Use for Electrophoresis. *Electrophoresis* **1983,** *4* (6), 375-382.
26. Freifelder, D., Physical Biochemistry: Applications to Biochemistry and Molecular Biology. Macmillan: 1982.

Appendix :

A Seed-Mediated Synthesis of Gold Nanoparticles of Controlled Sizes to Demonstrate the Impact of Size on Optical Properties

Reprinted and modified with permission from: J.A. Jenkins, T.J. Wax, and J. Zhao, Journal of Chemical Education, submitted for publication.

A.1 Abstract

Gold (Au) nanoparticles of varying sizes were synthesized during an Outreach Activity to introduce students to the size-dependent optical properties of nanomaterials. To fabricate Au nanoparticles of varying sizes, a seeded growth method was employed. In the first part of the Activity, students performed the Frens' method to obtain Au seeds. Students then used these seeds in the second part to conduct a seed-mediated synthesis, and obtained Au nanoparticles of a wide size range. The size differences in the particles were evident by eyesight due to color changes in the nanoparticle solutions. In addition to observations made about color, the nanoparticles were characterized using UV-vis spectroscopy, and a red-shift in the peak wavelength of the extinction spectra of the Au nanoparticles was observed when the nanoparticles were grown larger in size. This Activity demonstrates a straightforward approach to seed-mediated nanoparticle growth and is applicable to both high school and undergraduate students.

A.2 Introduction

Nanomaterials exhibit many unique features not observed on the bulk scale. Specifically, the properties of these materials are highly dependent on their size, shape, surface area, porosity,

structure, etc. This Activity showcases the interesting size-dependent optical characteristics of nanoscale materials to students via a seed-mediated synthesis of gold nanoparticles. In other words, students can visualize how the color of the nanoparticles changes with respect to particle size. By performing a seed-mediated synthesis, students are able to make two observations. First, students clearly observe a color change of the solution when the nanoparticle seeds grow bigger. Second, students also monitor a red-shift in the extinction spectra of bigger nanoparticles compared to smaller ones.

Gold (Au) nanoparticles have been utilized in a variety of applications, largely driven by their unique plasmonic features.[1-3] When the Au nanoparticles are excited by light of proper frequencies, the free electrons in the nanoparticle oscillate in unison, giving rise to the phenomenon of localized surface plasmon resonance (LSPR). The plasmon resonance frequency of the Au nanoparticles can be controlled through modification of the nanoparticle size.[4-5] The size of the nanoparticle is important for many applications, including sensing, drug delivery and bio-imaging.

Various methods exist to synthesize gold nanoparticles.[6-9] One of the most common and simplest syntheses is the Frens' method,[10] which uses sodium citrate to reduce $HAuCl_4$. Sodium citrate acts as both a reducing and capping agent in this synthesis. Despite the ubiquity of the Frens' method, various limitations exist that render this method ineffective when demonstrating the size dependent properties of nanomaterials to students. One such limitation of this method is that students are capable of synthesizing Au nanoparticles within a small size range (of similar colors) by adjusting the amount of sodium citrate. As larger size particles are synthesized using this method, it is difficult to obtain uniform and monodispersed particles.[11] Not only does the Frens' method result in limited size growth of Au seeds, the Frens' method is also a counter-

intuitive synthesis. Most students would have an easier time understanding that when more of a chemical is added to a nanoparticle solution, the nanoparticles would become larger in size. However in the Frens' method, when less of the chemical sodium citrate is added to the solution, the nanoparticles grow in size. The nanoparticle growth occurs due to there being less citrate ions available in solution to stabilize the smaller Au nanoparticles. As a result, the smaller Au nanoparticles begin to aggregate forming larger nanoparticles. Students may struggle to grasp why reducing the sodium citrate volume leads to larger size nanoparticles. Although students learn how to perform an Au nanoparticle synthesis, they may fail to fully understand how the particle size impacts both the optical and physical properties of the metal nanoparticles.

Unlike the Frens' method, seed-mediated growth synthesis introduces students to a more advanced nanofabrication technique.[11-12] First, students will synthesize gold nanoparticles using the Frens' method and then use the nanoparticles as seeds. In the second step, more precursors are added to the seed solution, growing the seeds to a larger size. A seed-mediated synthesis provides greater control over the particle size, and also allows the creation of more versatile nanomaterials, such as core/shell and bimetallic nanoparticles.[11, 13-14] The most significant difference between the Frens' method and seed-mediated technique, though, is that seed-mediated growth is a more straightforward approach for students to understand. When more of a reagent is added to a seed-mediated synthesis, the larger the nanoparticles become in size. The size impact on the color of nanoparticles can be directly observed by naked eye during the synthesis.

A.3 The Activity

A.3.1 Overview

In this Activity, students will synthesize spherical Au nanoparticles of various sizes ranging from 40 nm to 120 nm in diameter. Students will observe changes in the nanoparticle size indicated by the differences in the optical properties of the nanoparticles. Observations can be made in regards to visual color differences as well as changes in the extinction spectra of the gold nanoparticle solution. This has been executed by the authors as an Outreach Activity and details can be found in supporting information.

A.3.2 Hazards

All synthesis should be done wearing personal protective equipment such as gloves, safety goggles or glasses, and a lab coat. Skin can be stained by $HAuCl_4$ so it is important that gloves be worn while handling the chemicals. In order for the students to achieve the best results, aqua regia should be used clean all glassware and stir bars. [CAUTION: This solution is highly corrosive! and should only be used in a fume hood.] It is recommended that aqua regia be handled by the instructor only and the glassware cleaned before the activity. Aqua regia is made by carefully mixing nitric acid and hydrochloric acid at a 1:3 molar ratio. Once the Activity has been completed, the instructor should dispose of the aqua regia according to the standard operating procedures of their school/institution.

A.3.3 Implementation

12 teenage students partook in this Activity that was implemented during an outreach program aimed at high school students. Although the target audience for this specific outreach

program was high school students, this Activity is also applicable to undergraduates. The Activity was conducted in a research laboratory at the University of Connecticut. Students were divided into 4 groups, with each group having three students. In Part 1, groups 1-4 all followed the same synthesis procedure. In Part 2, each group synthesized only one size Au nanoparticle, and the size was different from group to group. All size particles were then used by the students for characterization. Experimental

A.3.4 Chemicals

All chemicals were used as received and all experiments were performed using deionized (DI) water. Stock solutions were prepared by the instructor in advance of the Activity. The stock solutions needed are the following: 0.025 M gold (III) chloride trihydrate ($HAuCl_4$, Sigma-Aldrich), 0.0388 M sodium citrate (Fisher Scientific), and 0.010 M hydroxylamine hydrochloride ($NH_2OH{\cdot}HCl$, Sigma-Aldrich).

The amount of stock solutions needed for the activity will vary with the number of participating students. Specifically, in this Activity, the $HAuCl_4$ solution was prepared by adding 1 gram of $HAuCl_4$ to 100 mL of DI water, and this solution can be used for up to one year. The sodium citrate stock solution was made by adding 1.14 grams of sodium citrate to 100 mL of DI water and must be made fresh each time. Lastly, 35 mg of $NH_2OH{\cdot}HCl$ was added to 50 mL of DI water to make the $NH_2OH{\cdot}HCl$ stock solution. As with the sodium citrate stock solution, the $NH_2OH{\cdot}HCl$ stock solution must also be freshly prepared before each Activity.

A.3.5 Synthesis Part 1: Au Nanoparticle Seeds

Gold nanoparticles were synthesized using the Frens' method. In this synthesis, $HAuCl_4$ is reduced by sodium citrate, which also acts as the capping agent. The synthesis of ~40 nm Au

nanoparticle seeds is done by first adding 99 mL of DI water to a 150 mL beaker with a stir bar. 1.0 mL of $HAuCl_4$ stock solution (0.025 M) is then added to the DI water. The heat and spin dials on the hot plate are turned to specified settings and a watch glass is placed on top of the beaker to limit heat and vapor loss. Once the stirring solution begins to boil, 1.0 mL of sodium citrate stock solution (0.0388 M) is added to the beaker. The solution will first turn a dark purple color, and then to wine red as shown in **Figure A.1A**. When the solution is wine red in color, it must still be heated and stirred for an additional 20 minutes. After 20 minutes, the solution can be removed from the hot plate and allowed to cool to room temperature. This solution will then be used as the seed solution to grow the particles to larger sizes.

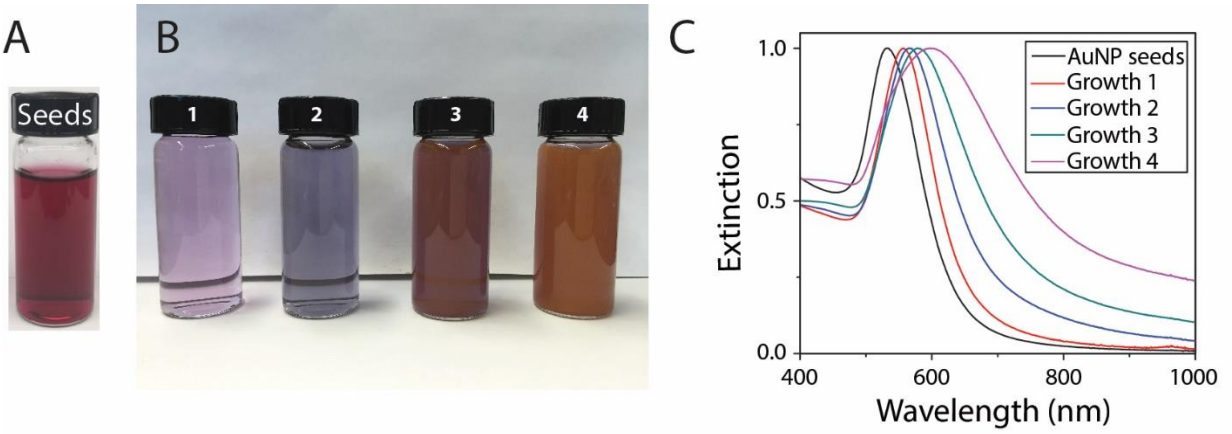

Figure A.1. Results of seed-mediated growth of varying sizes of spherical gold nanoparticles. (A) As made ~ 40 nm Au nanoparticles that will be used as seeds in the seed-mediated synthesis. (B) Images of nanoparticle growth after seed-mediated synthesis of group 1, group 2, group 3 and group 4. (C) The extinction spectra of Au nanoparticle seeds (black solid, λ_{max}: 530.6 ± 1.1 nm), group 1 (red, λ_{max}: 548.3 ± 4.1 nm), group 2 (blue, λ_{max}: 561.2 ± 6.1 nm), group 3 (green, λ_{max}: 576.9 ± 7.6 nm), and group 4 (purple, λ_{max}: 588.5 ± 10.0 nm). The standard deviations of λ_{max} are calculated based on 15 samples.

A.3.6 Synthesis Part 2: Seed-Mediated Growth of Au Nanoparticles

Once at room temperature the seeds can be used to grow the nanoparticles to various sizes. In this synthesis, $NH_2OH{\cdot}HCl$ is used as the reducing agent. The different sizes are achieved by varying the amount of $HAuCl_4$ and $NH_2OH{\cdot}HCl$. A previous synthesis method[12] was used as the foundation of this experimental design with modifications to allow for the seed-mediated synthesis of four different size nanoparticles. The specified chemical amounts for each can be found in **Table A.1**. The seed-mediated growth synthesis is done at room temperature. First, 52 mL DI water is added to a 150 mL beaker and placed on top of a stir plate. Next, 4.0 mL of Au nanoparticle seeds from the prior "seed" synthesis and 1.0 mL of sodium citrate stock solution are added to the beaker.

After 4 minutes, the $HAuCl_4$ stock solution is slowly added drop by drop to the stirring solution. Students must then wait 8 minutes before adding the final reagent. Once 8 minutes have passed, students can add drop by drop $NH_2OH{\cdot}HCl$ solution (0.010 M), waiting 10 seconds between each drop. A color change in the solution will be apparent within the first few minutes. Students must allow the solution to stir for 1 hour, so that the particle size can stabilize. To obtain better control of the size of the growth particles, we recommend that each group use Au seeds synthesized from the same batch.

Table A.1. The amount of chemicals used for seed-mediated growth. Each row in the table will produce Au nanoparticles of varying sizes.

Group	Sodium Citrate (mL)	$HAuCl_4$ (mL)	$NH_2OH{\cdot}HCl$ (mL)
1	1	0.08	0.11
2	1	0.23	0.34
3	1	0.50	0.75
4	1	0.90	1.40

A.4 Results and Discussion

A.4.1 Characterization of Nanoparticles

Upon completion of the seed-mediated growth synthesis, the gold nanoparticles are then characterized using UV-vis spectroscopy. This spectroscopic technique allows students to monitor the maximum peak wavelength (λ_{max}) of the nanoparticles, which is sensitive to changes in size and shape of the nanoparticles. At specific resonance wavelengths, Au nanoparticles are capable of absorbing and scattering light strongly; while at other wavelengths, light is transmitted through

the particles[15]. UV-vis spectroscopy is used to characterize the wavelength, or color, of white light that is absorbed and scattered by the Au nanoparticle solution. As the size of the Au nanoparticles increase, the λ_{max} of the nanoparticles will red shift as seen in **Figure A.1C**. This can also be observed by seeing a color change of the Au nanoparticles at varying sizes (**Figure A.1B**). There is a correlation between the color of the light absorbed and the color the naked eye observes. The wavelength of light that is transmitted through the particles and that humans see is the complimentary color to the wavelength of light that is being absorbed[15]. Depending on the educational level of the participants, the color wheel and visible spectrum can be used to help further explain the optical properties of the Au nanoparticles. When struck by white light (all the colors and wavelengths in the visible spectrum), the nanoparticles will absorb a certain wavelength, or color, of visible light based on their size and shape. Each wavelength of light in the visible spectrum corresponds to a certain color of light (**Figure A.2A**). The colors of light that are absorbed or scattered by the particle can be observed in the UV-vis spectra. The color of light that is transmitted through the particle is the color the human eye sees and is complementary to the color of light absorbed. Complementary colors are those viewed opposite of each other on the color wheel (**Figure A.2B**). For example, if green light is absorbed, a red color is seen by eye.

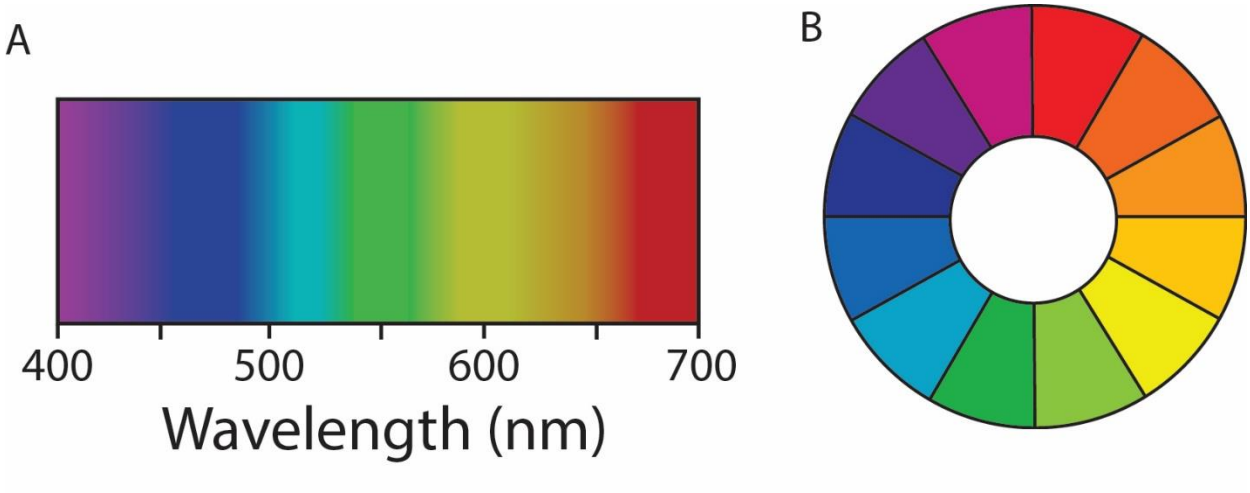

Figure A.2. The visible spectrum (A) and color wheel (B).

A.4.2 Hardships

One major problem that the instructors encountered while creating this outreach Activity was unclean glassware and stir bars. If the glassware and stir bars were left unclean, nanoparticle aggregation occurred, as evidenced by the incorrect color change in the nanoparticle solution. To circumvent the problem of dirty glassware, it is imperative that the instructors clean all glassware and stir bars with fresh aqua regia. (CAUTION: Aqua regia is extremely corrosive!)

A.4.3 Tips for Instructor

The experimental set up for both syntheses is shown in **Figure A.3**. The watch glass is not necessary for Part 2, but can be used. The first part of the Activity involved the Au nanoparticle seed synthesis. All four groups synthesized ~ 40 nm Au nanoparticles in the first segment of the Activity. Our participants set both the stir and heat settings to 7 using the hotplate in **Figure A.3**. The first part of the Activity should take ~ 45 - 60 min. However, cooling the seeds to room temperature could take up to two hours. The second part focused on the seed-mediated growth of

the Au nanoparticles. The synthesis was done at room temperature and the spin setting on the hot plate was set to 7. Each group was assigned specified amounts of reagents to add to the nanoparticle seeds, so that each group grew the nanoparticles to different sizes. Growing the nanoparticles to various sizes took the students ~30 - 45 minutes. In order for the nanoparticles to stabilize in size, the nanoparticle solutions for each group were then stirred for one hour. Characterization of the different size nanoparticles using UV-vis spectroscopy followed immediately after the seed-mediated synthesis. Throughout the Activity, students were asked multiple questions to assess their understanding of the experiments. Instructors also have the option to administer either a quiz or survey to their students to gauge their students' learning of the material.

Figure A.3. Image of the experimental setup for both syntheses completed during the Activity.

In addition to cleaning glassware, it is advised for each group to use ~ 40 nm Au nanoparticle seeds synthesized from the same batch when completing the seed-mediated growth. The Frens' synthesis will allow for approximately the same size seed from batch to batch but small variations could occur, as evident by the slight variance in λ_{max} of the seeds. The seed-mediated

method is a growth synthesis, so the final size is dependent on the original size of the seed. If the seed from one synthesis is smaller than the seed from the synthesis of a different group, their growth particles will be also be smaller. At the end of the synthesis portion of the Activity, all five nanoparticle sizes will be compared and it is possible the results could overlap if each group starts with a slightly different size seed. There are two ways to overcome this problem. The first approach is to choose an Au seed solution synthesized by one of the groups in the first part of the Activity to be used by all groups in the second part. It is highly recommended to choose particles that have a λ_{max} closest to 530 nm. The second way, as completed in this Activity, is to have the instructor prepare an Au seed sample in advance to be used for the seed-mediated synthesis in the second part of the Activity. If there is limited time available to carry out the Activity, the instructors can also prepare the seeds a day before so that the participants can begin Part 2 of the synthesis before their seed solution from Part 1 has cooled to room temperature. Another way to improve the synthesis of the the seeds is to use a reflux setup with a round bottom flask instead of beakers. Refluxing will not only help control the size of the original seed but will also keep the concentration of the seeds more consistent from synthesis to synthesis. This will help to reduce the discrepancies between results in the growth synthesis. It is also advised to use micropipettes, if available, as the measurement of the volume of chemicals will be more reliable.

An additional characterization technique that could be used in this activity is Dynamic Light Scattering (DLS). DLS is used to determine the hydrodynamic size of the particle. The size will include the Au nanoparticle as well as the ligand attached to it. Transmission Electron Microscopy (TEM) is a characterization technique that can also be used. TEM is done so that the students can see images of the nanoparticle size and shape. However, this technique can be both

timely and costly to use for just a day long Activity. It will be up to the instructor to decide whether he/she feels it is necessary to include another characterization technique.

A.5 Conclusion

In conclusion, gold nanoparticles of varying sizes were synthesized in this Activity. Two different synthesis methods were introduced to the students. The first synthesis involves the reduction of a gold salt, while the other approach entails a seed-mediated growth method. The size differences in the particles were characterized by eyesight as well as by UV-vis spectroscopy. Students were able to visually observe a color change in the solution of Au nanoparticles as the particle size increased, while UV-vis spectroscopy was used to determine the LSPR λ_{max} of the solution. A red shift of λ_{max} is observed as the size of the Au nanoparticle increases. This activity allows a hands-on and visual introduction to the size-dependent optical properties of materials at the nanoscale.

A.6 Acknowledgments

This work was funded by University of Connecticut startup fund and National Science Foundation CAREER grant (CHE 1554800). I would like to thank Kevin Organista for his help in developing the synthetic procedures.

A.7 References

1. Bai, J.; Flowers, K.; Benegal, S.; Calizo, M.; Patel, V.; Bishnoi, S. W., Using the Enzymatic Growth of Nanoparticles to Create a Biosensor. An Undergraduate Quantitative Analysis Experiment. *J. Chem. Educ.* **2009,** *86* (6), 712.
2. Choi, H.; Chen, Y.-S.; Stamplecoskie, K. G.; Kamat, P. V., Boosting the Photovoltage of Dye-Sensitized Solar Cells with Thiolated Gold Nanoclusters. *J. Phys. Chem. Lett.* **2014,** *6* (1), 217-223.
3. Yang, X.; Yang, M.; Pang, B.; Vara, M.; Xia, Y., Gold Nanomaterials at Work in Biomedicine. *Chem. Rev.* **2015,** *115* (19), 10410-10488.
4. Willets, K. A.; Van Duyne, R. P., Localized Surface Plasmon Resonance Spectroscopy and Sensing. *Annu. Rev. Phys. Chem.* **2007,** *58*, 267-297.
5. Mayer, K. M.; Hafner, J. H., Localized Surface Plasmon Resonance Sensors. *Chem. Rev.* **2011,** *111* (6), 3828-3857.
6. Turkevich, J.; Stevenson, P. C.; Hillier, J., A Study of the Nucleation and Growth Processes in the Synthesis of Colloidal Gold. *Discuss. Faraday Soc.* **1951,** *11*, 55-75.
7. Paluri, S. L.; Edwards, M. L.; Lam, N. H.; Williams, E. M.; Meyerhoefer, A.; Pavel Sizemore, I. E., Introducing "Green" and "Nongreen" Aspects of Noble Metal Nanoparticle Synthesis: An Inquiry-Based Laboratory Experiment for Chemistry and Engineering Students. *J. Chem. Educ* **2014,** *92* (2), 350-354.
8. Jenkins, S. V.; Gohman, T. D.; Miller, E. K.; Chen, J., Synthesis of Hollow Gold–Silver Alloyed Nanoparticles: A "Galvanic Replacement" Experiment for Chemistry and Engineering Students. *J. Chem. Educ.* **2015,** *92* (6), 1056-1060.
9. Sharma, R.; Gulati, S.; Mehta, S., Preparation of Gold Nanoparticles Using Tea: A Green Chemistry Experiment. *J. Chem. Educ* **2012,** *89* (10), 1316-1318.
10. Frens, G., Controlled Nucleation for the Regulation of the Particle Size in Monodisperse Gold Suspensions. *Nature* **1973,** *241* (105), 20-22.
11. Brown, K. R.; Natan, M. J., Hydroxylamine Seeding of Colloidal Au Nanoparticles in Solution and on Surfaces. *Langmuir* **1998,** *14* (4), 726-728.
12. Li, J. F.; Tian, X. D.; Li, S. B.; Anema, J. R.; Yang, Z. L.; Ding, Y.; Wu, Y. F.; Zeng, Y. M.; Chen, Q. Z.; Ren, B., Surface Analysis Using Shell-Isolated Nanoparticle-Enhanced Raman Spectroscopy. *Nat. Protoc.* **2013,** *8* (1), 52-65.
13. McGilvray, K. L.; Fasciani, C.; Bueno-Alejo, C. J.; Schwartz-Narbonne, R.; Scaiano, J. C., Photochemical Strategies for the Seed-Mediated Growth of Gold and Gold–Silver Nanoparticles. *Langmuir* **2012,** *28* (46), 16148-16155.
14. Cargnello, M.; Agarwal, R.; Klein, D. R.; Diroll, B. T.; Agarwal, R.; Murray, C. B., Uniform Bimetallic Nanocrystals by High-Temperature Seed-Mediated Colloidal Synthesis and Their Catalytic Properties for Semiconducting Nanowire Growth. *Chem. Mater.* **2015,** *27* (16), 5833-5838.
15. Harris, D. C., *Quantitative Chemical Analysis*. 8th ed.; Macmillan: New York, 2010; p 394-398.